

S T U D I A
UNIVERSITATIS BABEȘ – BOLYAI
CHEMIA

1

Editorial Office: 400015 – Cluj–Napoca Republicii no. 24, Phone: 0264-405352

CUPRINS – CONTENT – SOMMAIRE – INHALT

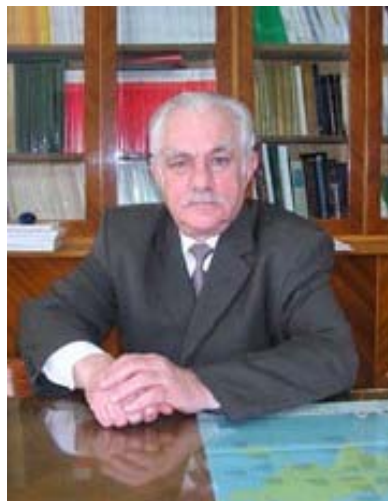
BIOGRAPHY IONEL HAIDUC	I
LIST OF PUBLICATIONS 2002-2007, IONEL HAIDUC	III
G. NEMES, I. SILAGHI-DUMITRESCU, P. M. PETRAR, R. SEPTLEAN, L. SILAGHI-DUMITRESCU, Secondary Interactions in Heteroallenic Systems with P=C-E Units	3
VASILICA LATES, DELIA GLIGOR, LIANA MURESAN, IONEL CATALIN POPESCU, RADU GROPEANU, ION GROSU, Graphite Electrodes Modified with 3,7-Di(<i>M</i> -Aminophenyl)-10-Ethyl-Phenothiazine	11
IOAN BALDEA, DANA - MARIA SABOU AND ALEXANDRA CSAVDARI, One-Plus Rate Equation, an Useful Tool to Elucidate the Reaction Mechanism.....	19
ALEXANDRA CSAVDARI AND IOAN BALDEA, Kinetics and Oxidation Mechanism of Lactic and Malic Acids by Permanganate in Acidic Media	35
RADU SILAGHI-DUMITRESCU, A Paradigm for O-O Bond Cleavage in Ferric-Hydroperoxo Complexes	47
M.M. VENTER, A. PASCUI, V.N. BERCEAN, AND S. CÎNTĂ PÎNZARU, New Group 2 Metal Salts of Monodeprotonated (3 <i>h</i> -2-thioxo-1,3,4-thiadiazol-2-yl)thioacetic Acid. Synthesis and Vibrational Characterization	55
FIRUTA GOGA, CRINA SUCIU, MIRELA ANDREI, MARCEL BENEĂ, MARIANA MOCEAN, Crystallized Glasses with Addition of Fly Ash.....	61

L.M. GHIZDAVU AND L.GHIZDAVU, New Metal Coordination Compounds of Sodium {2-[(2,6-dichlorophenyl)amino]phenyl}acetate	73
ADINA ROTAR, OVIDIU MOLDOVAN, SORIN I. FARCAS, RICHARD A. VARGA, CRISTIAN SILVESTRU AND ANCA SILVESTRU, New Copper(I) and Copper(II) Tetra-Organo-Dichalcogeno-Imidodiphosphinates. Crystal and Molecular Structure of the First Monothioimidodiphosphinato Copper(I) Complex, $Cu_4[(OPMe_2)(SPh_2)N]_4 \cdot 6CH_2Cl_2$	81
CRINA DAN, ELISABETH-JEANNE POPOVICI, FLORICA IMRE, EMIL INDREA, PETRE MĂRGINEAN AND IOAN SILAGHI-DUMITRESCU, Studies on Some Ozone Decomposition Catalysts Based on Nickel Oxide	91
OSSI HOROVIT, AURORA MOCANU, GHEORGHE TOMOAI, LIVIU BOBOS, DIANA DUBERT, IULIA DAIAN, TRAIANOS YUSANIS AND MARIA TOMOAI-COTISEL, Lysine Mediated Assembly of Gold Nanoparticles	97
CODRUTA VARODI, DELIA GLIGOR AND LIANA M. MURESAN, Carbon Paste Electrodes Incorporating Synthetic Zeolites and Methylene Blue for Amperometric Detection of Ascorbic Acid	109
ZENO GÂRBAN, GABRIELA GÂRBAN, ILIE VASILUȚĂ, LUDOVIC SAYTI, MIHAELA PUP, GEORGE-DANIEL GHIBU, Metallograms of Sialoconcrements with Metabolic and Nutritional Aspects Note I. Alkaline and Alkaline-Earth Metals	119

PROFESSOR IONEL HAIDUC BIOGRAPHY

This year **Professor IONEL HAIDUC**, Member of the Romanian Academy, celebrates his 70th birthday. Born in Cluj on May 9th, 1937, Ionel Haiduc graduated the Faculty of Chemistry of the University of Cluj in 1959.

In 1964, he obtained the equivalent of a PhD in chemistry at the M.V. Lomonosov Institute of Fine Chemicals Technology in Moscow under a guidance of the Academician K.A. Andrianov. From 1959 until the present time the scientific life of Acad. Ionel Haiduc was developed at the Faculty of Chemistry of the University of Cluj. Full professor at the age of 36, he completed his formation as a researcher, in U.S.A., between 1966 and 1972, during three postdoctoral stages. Between 1990 and 1993 he was the Rector of "Babes-Bolyai" University of Cluj-Napoca and the vice-president of National Conference of Rectors.



The passion for science in general and for chemistry in particular, the joy of sharing knowledge was appreciated by generations of students who often would have liked the courses to be never-ending stories. He is an outstanding professor and mentor recognized by the whole academic community.

The scientific areas covered by Professor Ionel Haiduc are coordination and organometallic chemistry of main group elements, supramolecular organometallic chemistry, inorganic rings, biologically active metal compounds (including those with antitumor activity), inorganic chemistry nomenclature and systematization.

The Faculty of Chemistry and Chemical Engineering of Babes-Bolyai University Cluj-Napoca has now a well known School of Organometallic Chemistry developed by Professor Ionel Haiduc starting the early 70's.

Professor Ionel Haiduc has been always connected to the different aspects of the chemists' community life. As a member of many academic bodies, he is involved in Science policy and management, as an active actor fighting for quality in the academic life and as author of publications.

The scientific work of Professor Ionel Haiduc is covered by 9 books (published in Romanian, Polish, English and Greek), 25 chapters in collective

BIOGRAPHY

volumes and more than 340 scientific and review articles (the following list presents only the publications from 2002 to 2007).

The most recent book published "Supramolecular Organometallic Chemistry" (co-authored by F. Edelmann), with the Foreword written by Jean-Marie Lehn, Nobel prize winner, describes not only a major field of chemistry, but also a vivid interface between chemistry, biology, physics, and materials science. The prestigious ACS journal *Crystal Growth & Design* quoted: "As a discrete field, supramolecular organometallic chemistry did not exist until the publication of Haiduc and Edelmann's book *Supramolecular Organometallic Chemistry*".

His brilliant career received a fully deserved recognition. The Romanian Academy offered him the "Gh. Spacu" prize in 1974 and elected him as corresponding member in 1990 and as full member in 1991. He was president of the Cluj-branch (1995-2006) and vice-president of the Romanian Academy (1998-2000). Starting 2006 he is the President of the Romanian Academy. Many other national and international awards and prizes mark the exceptional carrier of Ionel Haiduc. To name only a few of them: Humboldt Forschungsaufenthalt (1997), Gauss Professorship, Göttingen Academy (1998-1999), "Pro Colaboratione" Award, Hungarian Academy of Sciences, Debrecen Branch (1999), Honour Diploma, Presidium of the Moldavian Academy of Sciences (1999), Honorary Member of the Academy of Sciences of Moldova (2002), elected member of Academia Europaea (London) (2002), *Doctor honoris causa*, Technical University "Gh. Asachi", Iasi, Romania (2002) and Polytechnical University of Timisoara, Romania (2004), Prize of Romanian Chemical Society (2004), Nenitzescu-Criegee award of the Romanian and German Chemical Societies (2005).

He also was awarded by the Presidents of Romania with "*Star of Romania*" ["Steaua Romaniei"] (2000 – mare ofiter, 2006 "mare cruce") and in 2006 the "*Order of Honour*," by the President of Republic Moldova.

At his 70th anniversary, the Editorial Board of *Studia Universitatis Babes-Bolyai, Seria Chemia* presents to Professor Ionel Haiduc the very best wishes for a long healthy and fruitful life and many successes in the years to come.

Editorial Board

Prof. Ionel Haiduc

**LIST OF PUBLICATIONS
2002-2007**

ARTICLES and CHAPTERS IN BOOKS

2007

Ionel Haiduc

1,1-Dithiolato ligands and related selenium and tellurium compounds in vol. **Handbook of Chalcogen Chemistry. New Perspectives in Sulfur, Selenium and Tellurium** Edited by F.A. Devillanova, Royal Society of Chemistry, London, 2007, pag. 593-643.

2006

Marius Campian, Ionel Haiduc and Edward R. T. Tiekink
Bis(O-benzyl dithiocarbonato-S,S)bis(3-methylpyridine-N)nickel(II)
Acta Cryst. 2006, **E62**, m3516–m3517.

Ionel Haiduc, Hemant K. Sharma and Keith H. Pannell
Organolead Chemistry in vol. **Lead. Chemistry, analytical aspects, environmental impact and health effects**
Edited by José S. Casas and José Sordo, Elsevier Publ. Co., Amsterdam, 2006, pag. 100-157.

Ionel Haiduc, Gellert Mezei, Rodica Micu-Semeniuc, Frank T. Edelman, Axel Fischer
Differing Coordination Modes of (O-Alkyl)-p-Ethoxyphenyldithiophosphonato Ligands in Copper(I), Silver(I) and Gold(I) Triphenylphosphine Complexes **Z. anorg. Allg. Chem.** 2006, **632** (2) 295-300.

2005

Ionel Haiduc
Phosphorus-Nitrogen Compounds in vol. **Encyclopedia of Inorganic Chemistry-II, Edited by R.B. King**
J. Wiley & Sons, London, New York, Sept. 2005, pag. 4329-4355.

Ionel Haiduc
Inorganic Ring Systems
in vol. **Encyclopedia of Inorganic Chemistry-II, Edited by R.B. King**
J. Wiley & Sons, London, New York, Sept. 2005, pag. 2028-2055.

IONEL HAIDUC

Edward R.T. Tiekink, Ionel Haiduc

Stereochemical aspects of metal xanthate complexes. Molecular structures and supramolecular self-assembly in vol. **Progress in Inorganic Chemistry (Edited by K.D. Karlin)**, J.Wiley & Sons, London, New York, 2005, vol. **54**, Chapter 3, pp. 127-319.

Ramesh N. Kapoor, Paulette Guillory, Louis Schulte, Francisco Cervantes-Lee, Ionel Haiduc, László Párkányi and Keith H. Pannell

Di(*p-tert*-butylphenyl)-*N,N*-di-(*iso*-butyl)carbamoymethylphosphine oxide and its organotin and uranyl adducts: structural and spectroscopic characterization
Appl. Organomet. Chem. 2005, **19** (4), 510-517.

Hemant Sharma, Francisco Cervantes-Lee, Ionel Haiduc and Keith H. Pannell
Unprecedented self-assembled cyclic hexamer of ferrocenyldimethylsilanol,
[FcSiMe₂OH]₆

(Fc = η^5 -C₅H₅)Fe(η^5 -C₅H₄)

Appl. Organomet. Chem. 2005, **19** (4), 437-439.

Andrea Deák, Szilvia Kárpáti, György Vanko, Alajos Kálmán and Ionel Haiduc

Combining coordination chemistry with hydrogen bonds: perturbation of the structures by interaction of an organotin(IV) complex with O-donor solvent molecules

Inorg. Chim. Acta 2005, **358** (4) 1012-1018.

2004

Ionel Haiduc

Metals in medicine – a promising area of interdisciplinary research
in vol. **Metal Elements in Environment, Medicine and Biology**, Edited by Z. Garban and P. Dragan, Tome VI, Publishing House “Eurobit”, Tmsioara, 2004, p. 27-34

Ionel Haiduc, Rodica-Micu Semeniuc, Radu F. Semeniuc, Marius Campian, Axel Fischer and Frank T. Edelmann

Molecular structure and solid state supramolecular self-organization of nickel(II)di(methoxyethylxanthato) bi(pyridine) adduct, Ni(S₂COCH₂CH₂OCH₃)₂.2C₅H₅N
Rev. Roumaine Chim. 2004, 49 (3/4) 177-184.

Ionel Haiduc

Secondary bonding

in vol. **Encyclopedia of Supramolecular Chemistry**, Edited by J. Steed and J. Atwood, Marcel Dekker, Inc., New York, 2004, p. 1215-1224.

Ionel Haiduc

Silicone grease: a serendipitous reagent for the synthesis of exotic molecular and supramolecular compounds

Organometallics, 2004, **23** (1) 3-8.

2003

Ionel Haiduc, Radu F. Semeniuc, Marius Campian, Victor Ch. Kravtsov, Yurii A. Simonov and Janusz Lipkowski

The reaction of nickel(II) xanthates with tetraphenyldiphosphinoethane (dppe) revisited. Formation and crystal structures of $Ni_3S_2(S_2COR)_2(dppe)$ (R = Me, Et; dppe = $Ph_2PCH_2CH_2PPh_2$) at room temperature and of $Ni(S_2CO)(dppe)$ at 150 K
Polyhedron, 2003, 22 (21) 2895-2900.

Ionel Haiduc

1,1-Dithiolato Ligands

Comprehensive Coordination Chemistry II. From Biology to Nanotechnology, J.A. McCleverty, T.J. Meyer, Editors-in-Chief, Volume 1, Fundamentals, Edited by A.B.P. Lever, Elsevier, 2003, Chapter 1.15, pag. 349-376.

Ionel Haiduc

Dichalcogenoimidodiphosph(in)ate Ligands

Comprehensive Coordination Chemistry II. From Biology to Nanotechnology, J.A. McCleverty, T.J. Meyer, Editors-in-Chief, Volume 1, Fundamentals, Edited by A.B.P. Lever. Elsevier, 2003. Chapter 1.14, pag. 323-347.

Jose S. Casas, Alfonso Castineiras, Ionel Haiduc, Agustin Sánchez, Radu F. Semeniuc and Jose Sordo

Supramolecular Self-Assembly of $Ph_2TI(S_2COMe)$ Based on a Rare Coordination Mode of the Xanthate Ligand and Thallium· π -Phenyl Interactions

J. Mol. Struct. 2003, **656** (1/3) 225-230.

Herbert W. Roesky, Ionel Haiduc and Narayan Hosmane

Organometallic oxides of main group and transition elements downsizing inorganic solids to small molecular fragments.

Chem. Revs. 2003, **103** (7) 2579-2596.

Frank T. Edelman, Axel Fischer and Ionel Haiduc:

Two structurally differing (heterogeometric) mesityltellurium(II) phosphor-1,1-dithiolates: the first monomeric dicoordinate $MesTeS(S)PPh_2$ and a self-assembled tricoordinate $[MesTeS(S)P(OPr^i)_2]_x$

Inorg. Chem. Commun. 2003, **6** (7) 958-960.

Mary F. Mahon, Kieran C. Molloy, Monica M. Venter, Ionel Haiduc

Unsymmetrically-substituted 2,4,6-trimercaptotriazine: synthesis and reaction chemistry of $C_3N_3S_3H_2Na$, including the structures of $C_3N_3S_3H_2Na \cdot 3H_2O$ and $C_3N_3S_3H_2Cu(PPh_3)_2$

Inorganica Chimica Acta 2003, **348**, 75-81.

2002

Mircea D. Banciu, Alexandru T. Balaban, Constantin Draghici, Ionel Haiduc, Ovidiu Ivanciuc
Unexpected formation of 2,6,7-triphenylcyclopenta-[c]pyran from the reaction of
1,2-diphenylethanedione (benzil) with cyclopentadiene
Rev. Roum. Chim. 2002, 47 (8/9) 705-713 (pub. 2003)

Hemant K. Sharma, Ionel Haiduc, Keith H. Pannell
Transition metal complexes of germanium, tin and lead
in vol. "**The Chemistry of Organic Germanium, Tin and Lead Compounds**",
Editor: Zvi Rappoport
John Wiley & Sons, Ltd, Chichester, UK, 2002, Vol. 2 (Part 2), Chapter 17, pp. 1241-1332.

J. Zukerman-Schpector, I. Haiduc, M. J. Dabdoub, J. C. Biazotto, A.L. Braga, L.
Dornelles and I. Caracelli
Dichloro-bis(2-chloro-2-phenyl-vinyl)Te(IV) and dibromo-bis(2-bromo-2-phenyl-vinyl)Te(IV):
supramolecular self-assembly through different π -aryl interactions
Z. Kristallogr. 2002, **217**, 609-613.

Julio-Zukerman-Schpector, Ionel Haiduc, Robinson L. Camillo, João Comasseto,
Rodrigo Luiz Oliveira R. Cunha and Alvim George
Supramolecular self-assembly through tellurium halogen secondary bonds: A
hexagonal grid of Te₂Cl₂ and Te₆Cl₆ rings in the solid state structure of 1,1,3-
trichloro-2,4,5,6-tetrahydro-1*H*-1 λ^4 -benzo[b]tellurophene.
Can. J. Chem. 2002, **80** (11) 1530-1537

Lai Yoong Goh, Zhiqiang Weng, Weng Kee Leong, Jagadese J. Vittal, and Ionel Haiduc
An organometallic radical route to bis(phosphido)- and hydrido-phosphido-bridged
metal-metal-bonded complexes of cyclopentadienylchromium via desulfurization of
thiophosphinito ligands
Organometallics 2002, **21** (24) 5287-5291.

O. Cozar, Rodica Micu-Semeniuc, L. David and I. Haiduc
Local structure and metal-metal interaction in some Cr(III)-dithiophosphonate compounds
Modern Phys. Lett. B 2002, **16** (10&11) 401-407.

Julio-Zukerman-Schpector and Ionel Haiduc
Tellurium π -aryl interactions: a new bonding motif for supramolecular self-assembly
and crystal engineering
CrystEngComm 2002, **4** (33) 178-193.

Vasile Bercean, Crina Crainic, Ionel Haiduc, Mary F. Mahon, Kieran C. Molloy,
Monica M. Venter and Paul J. Wilson
The structural chemistry of organotin derivatives of 5-mercapto-3-phenyl-1,3,4-thiadiazoline-2-
thione: supramolecular structures involving intermolecular Sn S, N-H S or S S interactions
J. Chem. Soc., Dalton Trans., 2002, (6) 1036-1045.

LIST OF PUBLICATIONS 2002-2007

José S. Casas, Eduardo E. Castellano, Javier Ellena, Ionel Haiduc, Agustín Sánchez, Radu F. Semeniuc and José Sordo:
Supramolecular self-assembly in the crystal structures of methylmercury xanthates, MeHgS(S)COR, R = Et, ⁱPr and CH₂Ph
Inorganica Chimica Acta 2002, **329** (1) 71-78.

Ionel Haiduc and Lai Yoong Goh
Reactions of bis(thiophosphoryl)disulfanes and bis(thiophosphinyl)disulfanes with metal species: an alternative, convenient route to metal complex and organometallic dithiophosphates and dithiophosphinates
Coord. Chem. Rev. 2002, **224** (1/2) 151-170.

SCIENCE MANAGEMENT AND POLICY
(mostly in Romanian)

2005

Ionel Haiduc
Aspecte etice ale cercetării științifice în chimie, biologie și medicină
Revista de Politica Științei și Scientometrie 2005, 3(1) 37-42.

2002

Ionel Haiduc
Vizibilitatea internațională a cercetării românești. Rolul și efectele colaborării internaționale.
Comunicare prezentată la Simpozionul “Perspectiva Cercetării-Dezvoltării în Chimia Românească. Între Supraviețuire și Speranță” (Academia de Științe Tehnice din România, Secțiunea Inginerie Chimică), București, 20 iunie 2002.

Ionel Haiduc
Cercetarea științifică din România oglindită într-un recent raport american
Academica, Anul XII, Nr. 4, Iulie 2002, p. 55-60.
Republicat în: **Curierul de Fizică**, Anul XIII, Nr. 3 (42), Septembrie 2002, p. 14-16.
Revista de Politica Științei și Scientometrie, 2003, 1 (1) 18-24.

Ionel Haiduc
Cercetarea științifică din România în context internațional. Evoluții recente. Colaborări internaționale
Academica, Anul XII, Nr. 2-3, Mai-Iunie 2002, p. 56-59.
Republicat în: **Curierul de Fizică**, Anul XIII, Nr. 3 (42), Septembrie 2002, p. 16-17.
Revista de Politica Științei și Scientometrie, 2003, 1 (1) 33-7.

Ionel Haiduc
Ethical aspects of scientific research in chemistry, biology and medicine
In vol. **Metal Elements in Environment, Medicine and Biology**, Edited by Z. Garban, P. Dragan and G. Garban, Tome V, Publishing House “Eurobit” Timisoara, 2002, pp. 71-76.

IONEL HAIDUC

Other writings (in Romanian)

2003

Ionel Haiduc

Proiectul Rosia Montana - intre riscuri si beneficii [varianta scurta]

Academica, Anul XIII, Nr. 12, Martie 2003, p. 34-35.

Ionel Haiduc

Proiectul Rosia Montana - analiza raportului dintre riscuri si beneficii

Academica, Anul XIII, Nr. 13-14, Aprilie-Mai 2003, p. 77-80.

Ionel Haiduc

Proiectul Rosia Montana - intre riscuri si beneficii [varianta extinsa]

(a) in cotidianul **Curentul**, anul VIII, Nr. 118 (1699) joi 29 mai 2003, pag. 9.

(b) in cotidianul **Economistul**, anul XIII, Nr. 1382 (2408) marti, 17 iunie 2003, pag. 3.

(c) in saptamanalul **Flacara lui Adrian Paunescu**, anul III, nr. 47 (114) 20 Noiembrie 2003, p- 12-13 (varianta cu anexe)

(d) in volumul **Prezent si perspective de dezvoltare durabila a zonei Rosia Montana** (Colectia Biblioteca Economica, Seria Studii si Cercetari Economice, vol. 11-12), Academia Romana, Centrul de Informare si Documentare Economica, Buxcuresti 2003, pp. 25-29.

Ionel Haiduc

Originea unei cariere [despre experienta bursei Fulbright]

Revista 22, anul XIV, Nr. 693, Supliment PLUS Nr. 154 din 17 iunie 2003, pag. V.

Ionel Haiduc

Miracolul stiintei americane

Revista Româno-Americană (editata de Asociatia "Amicii Statelor Unite")
Decembrie 2003, Serie noua, Nr. VII-VIII, p. 16-20.

2004

Ionel Haiduc, Stefan Ragalie

Consideratii economice privind riscurile si oportunitatea investitiei de la Rosia Montana

Academica, 2004, Anul XIV, Nr. 26 (163) p. 66-69.

Stefan Ragalie, Ionel Haiduc

Riscuri si alternative de dezvoltare a zonei Rosia Montana

in volumul: **Fenomene si procese cu risc major la scara nationala**, Academia Romana, Coordonatori Florin G. Filip, Bogdan C. Simionescu, Editura Academiei Romane, Bucuresti, 2004, 381-391.

Ionel Haiduc

Riscurile de mediu ale proiectului Rosia Montana

ECO-TERRA, 2004, nr.1-2, p. 10.

VIII

LIST OF PUBLICATIONS 2002-2007

Ionel Haiduc

Migratia internationala a tinerilor cercetatori: cauze, efecte, solutii
in volumul: Institutul Cultural Roman, Conferinta Internationala **MIGRATIA TINERILOR
CERCETATORI ROMANI. PERFORMANTE si CAI DE INTOARCERE**, Sinaia, 14-18
octombrie 2004, pp.16-31.

Ionel Haiduc

Cinci decenii de calatorii prin chimia anorganica
Timisoara

2005

Ionel Haiduc and Iovanca Haiduc

COMMENTS ON A CONTROVERSIAL GOLD MINING PROJECT IN WESTERN
CARPATHIANS. ENVIRONMENTAL AND OTHER ASPECTS

In volumul **SUSTAINABILITY FOR HUMANITY & ENVIRONMENT IN THE
EXTENDED CONNECTION FIELD SCIENCE – ECONOMY - POLICY** , Editura
Politehnica, Timisoara 2005, pag. 53-60 (Scientific reunion of the special program
of the Alexander von Humboldt Foundation concerning the reconstruction of the
South Eastern Europe, Timisoara, 24-25 February 2005-02-27).

Ionel Haiduc

Aspecte etice ale cercetarii stiintifice in chimie, biologie si medicina
Revista de Politica Stiintei si Scientometrie 2005, 3(1) 37-42.

*Dedicated to Professor Ionel Haiduc,
President of The Romanian Academy at his 70th anniversary*

SECONDARY INTERACTIONS IN HETEROALLENIC SYSTEMS WITH P=C-E UNITS

G. NEMES, I. SILAGHI-DUMITRESCU*, P. M. PETRAR,
R. SEPTLEAN, L. SILAGHI-DUMITRESCU*

ABSTRACT. Intermolecular interactions of -CH \cdots O, -CH \cdots HC-, -CH \cdots F and -CH \cdots π types are responsible for the building of the crystal structure of *bis*-(phosphane oxide)methylene **3**, phosphinic acid derivative **4** and arsanyl-*bis*-(methylene)-phosphorane (**5**) as chains and layers.

Keywords: heteroallenes, intermolecular contacts, heterocumulenes, arsanylbis(methylene)phosphorane

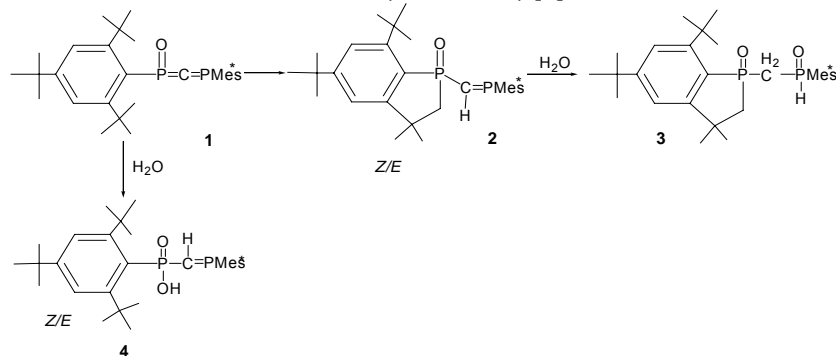
Introduction

Heteroallenic and heterocumulenic derivatives containing a group 14 and 15 heavy element have been in attention in the last years due to the novelty of the ways of the stabilization of the double bonds established between heavy elements [1, 2]. However the interest on such systems has been focused mainly on the core of the molecule and little attention has been paid on the role of the voluminous substituents - other than that of allowing for enough steric protection.

Substituted derivatives containing the Mes*P=C unit (Mes* = 2, 4, 6-tri-*tert*-butylphenyl) are of interest as precursors of phosphacumulenes of the type P=C=E and E'=P=C=E (E, E' = group 14 and 15 element), due to the steric protection afforded by the bulky supermesityl group [3]. In this respect, compound **1**, and **2** [4] bearing the sterically demanding substituents at phosphorus and at phosphorus and arsenic in **3** [5] have been synthesized and fully characterized in solid state by a single crystal X-ray diffraction. **1**, which is the first diphosphaallene featuring a $\lambda^5\sigma^3$ and a $\lambda^3\sigma^2$ phosphorus atom, the phosphavinylidene(oxo)phosphorane Mes*P(O)=C=PMes* (Mes* = 2,4,6-tri-*tert*-butylphenyl) has been synthesized in a one pot procedure starting from Mes*P=C(Cl)Li which reacts with Mes*P(O)Cl₂ [4]. The stabilizing effect of the substituents is revealed by the fact that **1** is stable for months at room temperature in the solid state but slowly rearranged in solution (about one day in THF and two days in pentane, toluene or chloroform) to afford in

* Facultatea de Chimie si Inginerie Chimica, Universitatea Babes-Bolyai, Mihail Kogalniceanu nr. 1, RO- 400084 Cluj-Napoca, Romania, e-mail: isi@chem.ubbcluj.ro

near quantitative yield the phosphaaalkenylphosphine oxide **2** in the form of two *Z/E* isomers in the ratio 85/15 (Scheme 1) [4].



Scheme 1

By addition of the difluoroarsane Mes^*AsF_2 to the supermesityl[bis(trimethylsilyl)methylene](lithiochloro-methylene)phosphorane, the first arsanylbis(methylene)phosphorane, $(\text{Me}_3\text{Si})_2\text{C}=\text{P}(\text{Mes}^*)=\text{C}(\text{Cl})\text{As}(\text{F})\text{Mes}^*$ **5** ($\text{Mes}^* = 2,4,6\text{-tri-}i\text{-tert-butylphenyl}$) has been synthesized [5].

The structures of **3**, **4** and **5**, unambiguously established by single crystal X-ray diffraction study, displays classical bond lengths and angles.

In this paper we discuss some secondary interactions leading to supramolecular associations shown by the crystal structures of **3**, **4** and **5**.

Results and discussion

Two $(\text{P}=\text{O})\cdots\text{H}(\text{Ar})$ intermolecular contacts are responsible for packing of **3** in chains (along the *a* axis) through the short bifurcated hydrogen bonds (Figure 1) of 2.65 Å (from O1 to H(Ar)) and 2.52 Å (from O1 to one of the methyl groups substituting the phospholene ring).

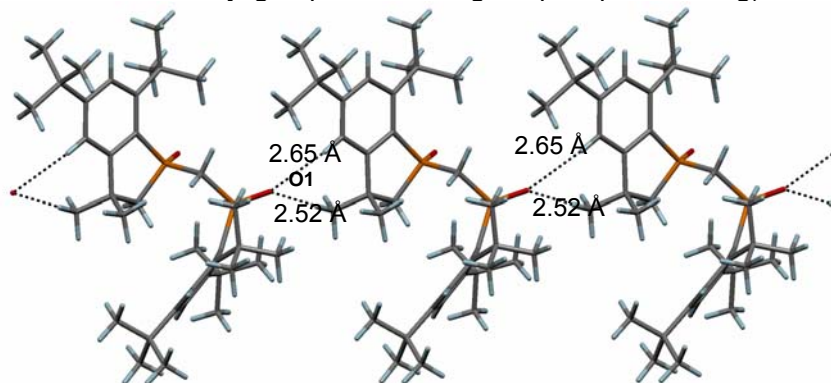


Figure 1. Crystal structure of **3** showing the short intermolecular contacts

SECONDARY INTERACTIONS IN HETEROALLENIC SYSTEMS WITH P=C-E UNITS

Such intermolecular $P=O \cdots H(C)$ contacts are quite common in the chemistry of organophosphorus (V) systems, and the Cambridge Data Base search displays 1484 from the total of 400977 entries registered in January 2007. [6]

Due to the presence of $P(O)OH$ groups, **4** displays in the crystal structure dimeric units formed through $O \cdots H$ contacts of 1.79 Å.

The $O \cdots O$ distances are of 2.564 Å, not very different from those found in bis(*p*-methylphenyl)-phosphoric acid dimer $O \cdots O$ 2.512 [7] or tetrakis(methylguanidinium) monohydrogen orthophosphate $O \cdots O$ 2.503 Å, 2.545 Å [8] showing that the overall organic environment of phosphorus does not change the properties of this fundamental unit (Figure 2).

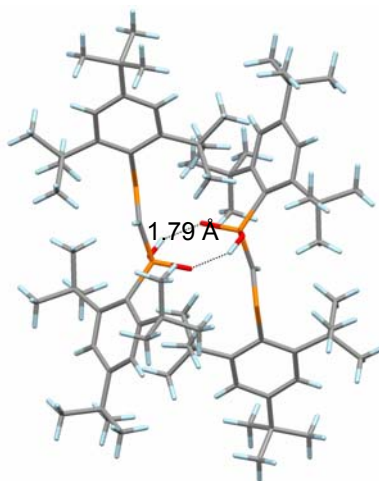


Figure 2. Dimeric units formed by short OHO contacts in the crystal structure of **4**.

These dimeric units exhibit further $CH \cdots HC$ contacts (of 2.38 Å) between the *o*-H-Mes* groups of neighbouring fragments leading to chair like polycycles (one is highlighted by CPK representation in Figure 3) displaying cavities of 5.6-5.8 Å diameter.

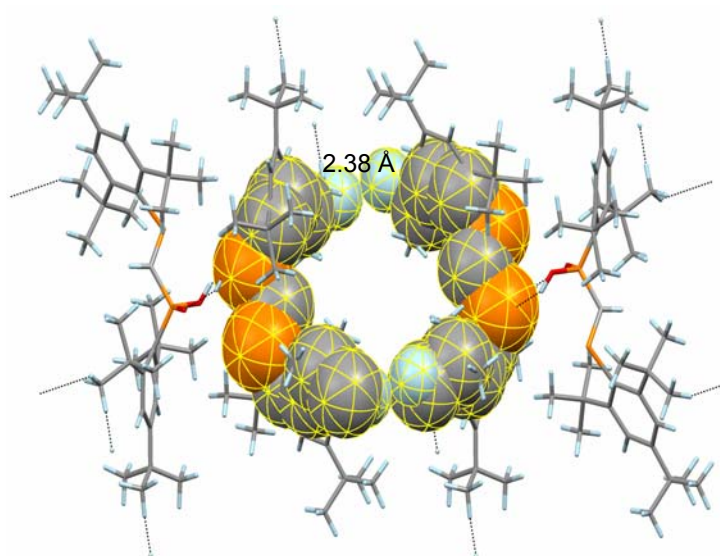


Figure 3. The chain arrangement of **4** is shown, highlighting the short HH contacts.

Close H...H contacts (2.289 Å) are also displayed in a 9-trimethylsilyl substituted fluorene derivative of germatrane [9] a finding which might be relevant in view of the increased interest paid in the last years to such interactions [10-13]. However, a systematic search in the Cambridge Database reveals that -CH...HC- contacts shorter than the sum of the van der Waals radii are quite common (we found 2051 entries from a set of 400977 data [6]).

The *p* H Mes* groups of **4** come also close, so that finally a layer is formed as shown in Figure 4,. Neighbouring cycles are in contact within distances of 2.32 Å (Figure 4) which are still shorter than the sum of the van der Waals radii of hydrogen (2.40 Å, [14]).

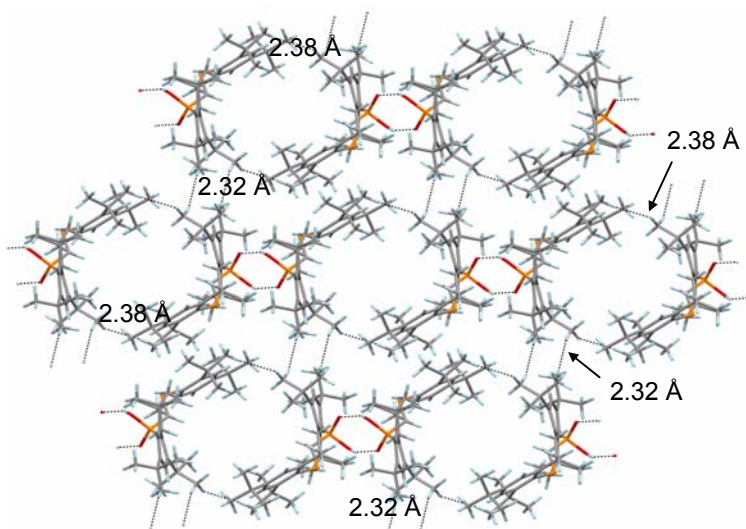


Figure 4. A top view of a layer formed by chair-like rings in **4**

In the case of arsanylbis(methylene)phosphorane (Me_3Si)₂C=P(Mes*)=C(Cl)-As(F)Mes* **5**, the main interactions in the crystal packing are the H···F bonds (2.59 Å) between the hydrogen atom from a Mes* and the fluorine from a neighbouring molecule leading to dimeric units (Figure 5). These dimers are supported also by CH··· π (2.97 Å) interactions between the H of one Mes* fragment and the aromatic ring from neighbour Mes* (Figure 5).

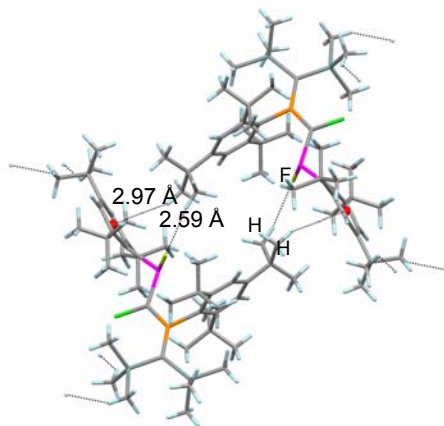


Figure 5. Dimeric units formed by CH π contacts found in the crystal structure of **5**

Further, the dimers are connected through H···H contacts (2.33 Å) and a zig-zag type chain is formed (Figure 6 a). These chains form a layer through H···H secondary interactions (2.36 Å), brought by the *t*-Bu groups of the supermesityl radicals (Figure 6 b).

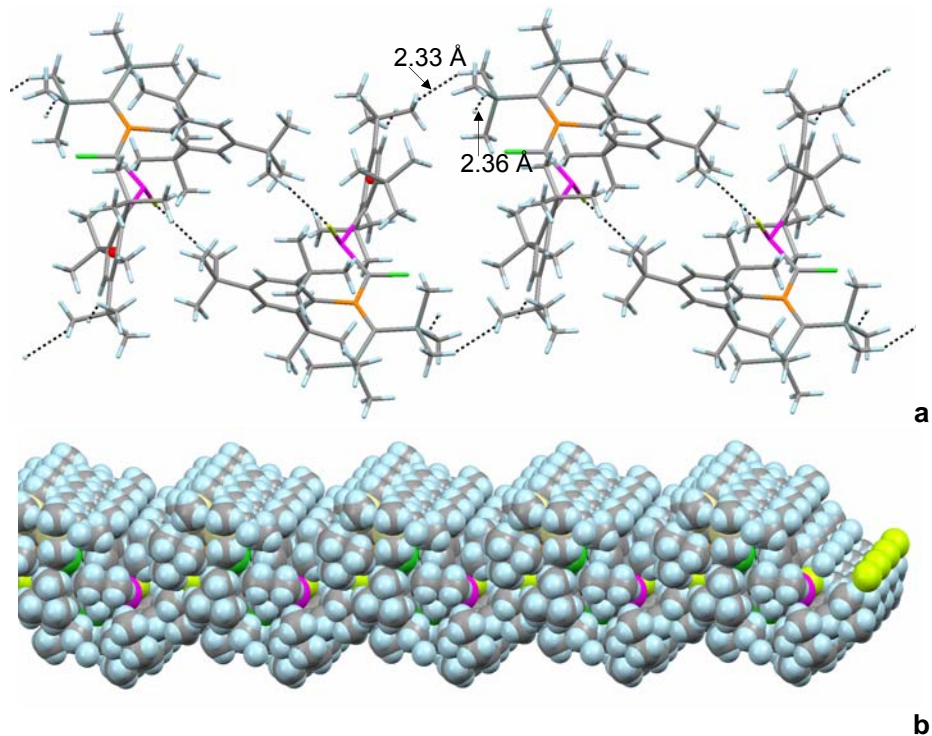


Figure 6. The crystal structure of 5 showing the chain arrangement (a) and the extension of these chains in a layer (b)

Conclusion

The voluminous substituents on the phosphallenic fragments responsible for the kinetic stabilization of the phosphorus carbon double bonds have also certain effects on the packing in the crystal structure and determine the formation of interesting supramolecular frameworks.

Acknowledgments

The authors are thankful for financial support from the Romanian Ministry of Education and Research (CEEX project). Dr. Jean Escudié from Paul Sabatier University Toulouse, is thanked for his hospitality and for useful discussion on this manuscript, as well as Dr. Heinz Gornitzka for collecting the X-Ray diffraction data.

REFERENCES

1. J. Escudie, H. Ranaivonjatovo, M. Bouslikhane, Y. El Harouch, L. Baiget, G. Cretiu Nemes, *Russian Chemical Bulletin, Int. Ed.* **2004**, 53, 1020.
2. J. Escudie, H. Ranaivonjatovo, L. Rigon, *Chem. Rev.* **2000**, 46, 1.
3. J. Escudie, H. Ranaivonjatovo, *Organometallics*, **2007**, 26, 1542.
4. R. Septelean, H. Ranaivonjatovo, G. Nemes, J. Escudié, I. Silaghi-Dumitrescu, H. Gornitzka, L. Silaghi-Dumitrescu, S. Massou, *Eur. J. Inorg. Chem.*, **2006**, 21, 4237.
5. P. M. Petrar, G. Nemes, L. Silaghi-Dumitrescu, I. Silaghi-Dumitrescu, J. Escudie, H. Gornitzka, H. Ranaivonjatovo, *Rev. Roum. Chim.*, **2007**, in press.
6. The Cambridge Structural Database System (CSDS), The Cambridge Crystallographic Data Centre, 12 Union Road, Cambridge, CB2 1EZ, UK.
7. E. Gebert, A. H. Reis Junior, S. W. Peterson, L. I. Katzin, G. W. Mason, D. F. Peppard, *J. Inorg. Nucl. Chem.*, **1981**, 43, 1451.
8. F. A. Cotton, V. W. Day, E. E. Hazen Junior, S. Larsen, S. T. K. Wong, *J. Am. Chem. Soc.*, **1974**, 96, 4471.
9. G. S. Zaitseva, S. S. Karlov, B. A. Siggelkow, E. V. Avtomonov, A. V. Churakov, J. A. K. Howard, J. Lorberth, *Z. Naturforsch.*, **1998**, B53, 1247.
10. M. J. Calhorda, *J. Chem. Soc., Chem. Commun.*, **2000**, 801.
11. C. F. Matta, J. Hernandez-Trujillo, T.-H. Tang, R. F. W. Bader, *Chem. Eur. J.*, **2003**, 9, 1940.
12. D. Braga, F. Grepioni, G. R. Desiraju, *Chem. Rev.* **1998**, 98, 1375.
13. G. Cretiu Nemes, L. Silaghi-Dumitrescu, I. Silaghi-Dumitrescu, J. Escudie, H. Ranaivonjatovo, K. C. Molloy, M. F. Mahon, J. Zukerman-Schpector, *Organometallics*, **2005**, 24(6), 1134.
14. M. Winter, WebElements, the periodic table on the Web, <http://w.w.w.webelements.com>.

G. NEMES, I. SILAGHI-DUMITRESCU, P. M. PETRAR, R. SEPTELEAN, L. SILAGHI-DUMITRESCU

*Dedicated to Professor Ionel Haiduc,
President of The Romanian Academy at his 70th anniversary*

GRAPHITE ELECTRODES MODIFIED WITH 3,7-di(*m*-AMINOPHENYL)-10-ETHYL-PHENOTHIAZINE

**VASILICA LATES^a, DELIA GLIGOR^a, LIANA MURESAN^a, IONEL
CATALIN POPESCU^{a*}, RADU GROPEANU^b, ION GROSU^b**

ABSTRACT. The electrochemical behavior of a new functionalized phenothiazine derivative 3,7-di(*m*-aminophenyl)-10-ethyl-phenothiazine, adsorbed on spectrographic graphite, has been investigated. From cyclic voltammetric measurements, performed in aqueous buffer solutions of different pH values and at different potential scan rates, the rate constant of the heterogeneous electron transfer and the transfer coefficient were estimated. The electrochemical parameters of the voltammetric response and the slope of the linear regressions between the formal standard potentials and pH suggest a quasi-reversible $1e/1H^+$ redox process, involving a surface confined redox couple. From the dependence of peak current on the cycling time, the electrochemical stability of the modified electrode was estimated. From cyclic voltammetry measurements performed at +150 mV vs. SCE, the electrocatalytic efficiency toward NADH oxidation was evaluated and it was found ~ 67 %, recommending the new synthesized compound as a promising mediator for NADH electrocatalytic oxidation.

Keywords: phenothiazine derivatives, NADH oxidation, modified electrodes.

Introduction

The detection of reduced β -nicotinamide adenin dinucleotide (β -NADH) is very important in enzyme assays, due to its participation in the enzymatic catalysis of more than 300 dehydrogenases, useful both in bioprocesses and in analytical applications [1,2]. The electrochemical oxidation of NADH has been studied intensively during the last two decades [3,4]. Unfortunately, the direct electrochemistry of this cofactor suffers from a high overvoltage at most solid electrodes which leads to the formation of an enzymatic inactive form of NAD^+ and of other side products, causing important interferences [5,6].

All these observations point to different solutions to overcome the problems of electrode fouling and overvoltage. One of the most

^a Department of Physical Chemistry

^b Department of Organic Chemistry, Babes-Bolyai University, 400028 Cluj-Napoca, ROMANIA

*e-mail address: cpopescu@chem.ubbcluj.ro

encountered solutions is the usage of chemically modified electrodes with surface adsorbed mediators.

It has been reported that several types of quinone derivatives, phenylenediamines, alkylphenazines and redox dyes, such as phenoxazine and phenothiazine derivatives, present catalytic activity towards NADH oxidation [7,8,9]. However, for various reasons, concerning the stability of the adsorbed mediator, fast heterogeneous electron transfer between the electrode and mediator, fast chemical redox reaction between adsorbed mediator and dissolved NADH etc., phenoxazine and phenothiazine mediators are often considered as being the most suitable in obtaining chemically modified electrodes for electrocatalytic oxidation of NADH [10]. A wide variety of these mediators was studied, including Nile Blue [11], Toluidine Blue [12], Methylene Green [13], Meldola Blue [14] and various derivatives of this parent structures.

In this paper, we report a detailed study on the electrochemical behavior of a new synthesized phenothiazine derivative: 3,7-di(meta-aminophenyl)-phenothiazine adsorbed on spectrographic graphite. Using cyclic voltammetry (CV) measurements, performed in different experimental conditions (scan rates and pH values), the rate constant (k_s) of the heterogeneous electron transfer and the transfer coefficient (α) were estimated as well as the electrocatalytic efficiency for NADH oxidation.

Experimental

Materials

The new functionalized phenothiazine namely 3,7-di(meta-aminophenyl)-10-ethyl-phenothiazine (DAPht) (Figure 1) was synthesized within the Organic Chemistry Department [15] and it was kindly given to us for research purpose.

β -Nicotinamide adenine dinucleotide, reduced form (NADH), was purchased from Sigma (St. Louis, MO, USA) as disodium salt. Phosphate buffer solutions were prepared using $K_2HPO_4 \cdot 3H_2O$ and KH_2PO_4 from Merck (Darmstadt, Germany). All other reagents were of analytical grade and used as received.

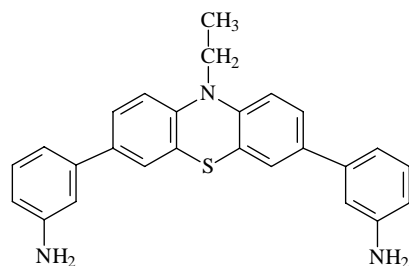


Figure 1. Structure of DAPht

The supporting electrolyte was a 0.1 M phosphate buffer solution and the pH value was adjusted using appropriate H_3PO_4 or NaOH solutions.

Electrode preparation

A spectrographic graphite rod (Ringsdorff-Werke, GmbH, Bonn-Bad Godesberg, Germany), of ~3 mm diameter, was wet polished on emery paper. Then, a graphite piece of suitable length was carefully press-fitted into a PTFE holder in order to obtain a graphite electrode, contacting the solution by means of flat circular surface of ~ 0.071 cm².

The modified graphite electrodes were obtained by spreading onto the electrode surface 2 μ l of 10 mM solution of DAPht in dimethylsulfoxide and keeping it over night at room temperature in order to evaporate the solvent.

Electrochemical measurements

CV measurements were carried out in a conventional three-electrode electrochemical cell. A saturated calomel electrode (SCE) and a coiled Pt wire served as reference and counter electrode, respectively. The cell was connected to a computer-controlled voltammetric analyzer (Autolab-PGSTAT10, Eco Chemie, Utrecht, The Netherlands).

Results and discussions

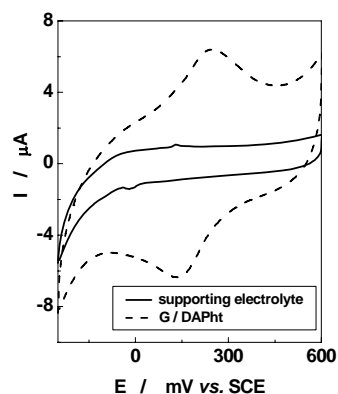


Figure 2. Cyclic voltammograms for DAPht adsorbed on spectrographic graphite. Experimental conditions: starting potential, -250 mV vs. SCE; scan rate, 10 mV s⁻¹; supporting electrolyte, 0.1 M phosphate buffer (pH 7); surface coverage, see Table 1.

1. Electrochemical behavior of the modified electrodes

The electrochemical behavior of DAPht adsorbed on spectrographic graphite was investigated in different working conditions using CV measurements. Figure 2 shows the electrochemical behavior of this compound. A well-defined peak pair with the formal potential around 200 mV vs. SCE (pH7) is observed (Table 1). The electrochemical parameters indicate a quasi-reversible redox process, taking into consideration the value of ΔE as criterion for the reversibility of the process. As the pH decreases the reversibility of the process decreases as well, suggesting that the reaction site is pH sensitive.

Table 1. Electrochemical parameters of voltammetric response for DAPht adsorbed on the spectrographic graphite. Experimental conditions: see Figure 2.

pH	E^0 (mV) vs. SCE	ΔE_{peak} (mV)	$I_{\text{pa}}/I_{\text{pc}}$	Γ (10^8 mol cm^{-2})
2	394	148	1.12	1.18
3	343	140	0.98	1.20
5	212	107	1.04	1.18
6	200	107	1.09	1.15
7	195	90	1.05	0.86

Cyclic voltammograms performed in a wide range of scan rates (5-1280 mV s^{-1}), showed a linear dependence of the current intensity on the scan rate (results not shown). Table 2 presents the parameters of the log-log linear regressions corresponding to the peak current dependence on the potential scan rate. The values of the slopes are dispersed around 1 for the reduction process suggesting that the reduced species are well adsorbed on the graphite surface. For the oxidation process, the values are smaller which leads to the assumption that the oxidized species are less adsorbed on the graphite surfaces. This can be explained by the repulsion existing between the positive charged species, generated on graphite electrode during the oxidation step.

Table 2. Parameters of the log-log linear regressions corresponding to the peak current dependencies on the potential scan rate (5 to 1280 mV s^{-1}) for DAPht adsorbed on graphite. Experimental conditions: supporting electrolyte, 0.1 M phosphate buffer.

pH	Slope ($\text{A} / \text{V s}^{-1}$)		R / no. of experimental points	
	Oxidation	Reduction	Oxidation	Reduction
3	0.49 ± 0.03	0.73 ± 0.04	0.996 / 4	0.993 / 8
5	0.69 ± 0.03	0.69 ± 0.01	0.993 / 10	0.999 / 10
7	0.54 ± 0.02	0.67 ± 0.02	0.990 / 12	0.996 / 8
9	0.57 ± 0.02	0.89 ± 0.03	0.991 / 15	0.996 / 8

Cyclic voltammograms were recorded also in a pH range from 1 to 8 with the scan rate of 5 mV s^{-1} . Figure 3 shows the linear dependence of the formal potential with the pH and the slope was close to 50.9 mV, suggesting a H^+/e^- ratio of 1. The influence of the pH on the electrochemical behavior of the compound is explained by the presence of the free primary amino groups in the compound structure (a similar behavior was reported for thionine [16]) which have the ability to bind a proton. The presence of a positive charge deactivates the phenothiazinic nucleus and, hence, the redox process is more difficult to realize.

The kinetic parameters of the redox process (the heterogeneous electron transfer rate constant, k_s and the transfer coefficient, α) were determined using

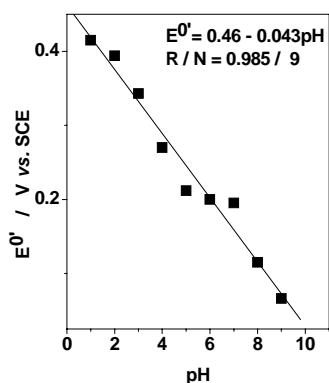


Figure 3. pH dependence of the formal potential of DAPht adsorbed on graphite. Experimental conditions: scan rate, 5 mV s⁻¹; supporting electrolyte, 0.1 M phosphate buffer.

Laviron's treatment [17] and they are shown in Table 3 for different pH values. It can be seen that the redox process is influenced by pH, which can be explained by the fact that the presence of a positive charge in the system makes the electron transfer at the electrode surface more difficult and hence, as the concentration of the hydrogen ions increases, the value of k_s decreases.

As compared to the value of k_s reported for phenothiazine (1,70 s⁻¹ at pH 7 [18]) a much lower value of k_s (0.73 s⁻¹, at pH 7) was observed for DAPht. This is due probably both to the presence of ethyl group on the phenothiazinic nitrogen atom and to the mesomeric effect of the two meta-aminophenyl substituents on the phenothiazinic nucleus.

Table 3. Kinetic parameters of the redox process for DAPht adsorbed on graphite.

pH	k_s (s ⁻¹)	α	R / no. of experimental points		Γ (10 ⁸ mol cm ⁻²)
			Oxidation	Reduction	
3	0.23	0.58	0.992 / 5	0.993 / 6	1.20
5	0.37	0.64	0.995 / 8	0.993 / 8	1.18
7	0.73	0.54	0.995 / 6	0.998 / 6	0.86
9	0.98	0.47	0.990 / 4	0.997 / 4	0.83

II. Electrochemical stability of the electrodes

The stability of the G/DAPht modified electrode was studied using repetitive CV measurements, by performing 25 consecutive scans at 50 mV s⁻¹. The dependence of peak current intensity on cycling time is shown in figure 4. It can be observed that the G/DAPht modified electrode presents a stable electrochemical response in time as the variation of peak current intensity on cycling time is almost constant both for cathodic and for anodic process.

III. Electrocatalytic activity for NADH oxidation

Taking into consideration the good electrochemical behavior of DAPht, its electrocatalytic activity for NADH oxidation was studied by cyclic voltammetry. Figure 5 presents the electrochemical behavior of DAPht

adsorbed on graphite, in the absence and in the presence of NADH dissolved in the buffer. The electrocatalytic efficiency for NADH oxidation estimated as $\frac{I_{[\text{NADH}] \neq 0} - I_{[\text{NADH}] = 0}}{I_{[\text{NADH}] = 0}}$ ratio, measured at a potential of 150 mV

vs. SCE, was found equal to 67 %. The electrocatalytic activity of the mediator is proved also by the decrease of the NADH electro-oxidation over potential with 400 mV, since at G/DAPht the catalytic peak was found at 150 mV vs. SCE while the uncatalyzed electro-oxidation of NADH at bare graphite electrodes was reported at 550 mV vs. SCE [5].

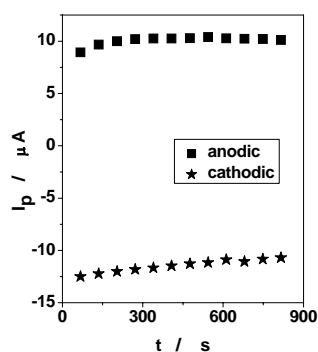


Figure 4. Time dependence of the peak current intensity for G/DAPht modified electrodes. Experimental conditions: scan rate, 50 mV s^{-1} ; potential range, -250 to 600 mV vs. SCE ; supporting electrolyte, 0.1 M phosphate buffer (pH 7).

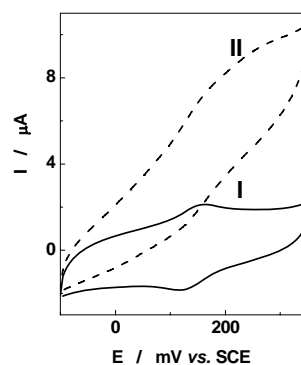


Figure 5. Electrocatalytic oxidation of NADH at G/DAPht modified electrode: (I) 0.1 M phosphate buffer (pH 7); (II) 0.1 M phosphate buffer containing 5 mM NADH. Experimental conditions: scan rate, 5 mV s^{-1} ; surface coverage, $\sim 3.5 \cdot 10^{-9} \text{ mol cm}^{-2}$; starting potential, -100 mV vs. SCE .

Conclusions

New modified electrodes were obtained by the adsorption of 3,7-di(*m*-aminophenyl)-10-ethyl-phenothiazine on spectrographic graphite.

The electrochemical studies indicate that the electron transfer process at the new modified electrodes is a quasi-reversible one and its reversibility decreases with the pH decrease.

The slope of the standard formal potential (E^0) linear regression vs. pH indicates a $1e^-/1H^+$ transfer during the redox process. The redox process is strongly influenced by pH, due to the presence in the mediator molecule of two primary amino groups.

The kinetic parameters, meaning the heterogeneous electron transfer rate constant (k_s) and the transfer coefficient (α), were determined. It was observed that k_s is affected by pH and by the presence of the ethyl group at the nitrogen atom, which is involved probably in the way in which the mediator binds to graphite.

The new modified electrodes present a good electrocatalytic activity for the NADH oxidation, with an electrocatalytic efficiency of 67%, hence recommending the new synthesized compound as a promising mediator for NADH electrocatalytic oxidation.

Acknowledgments

VL thanks UBB Cluj-Napoca for the research scholarship.

REFERENCES

1. G. T. R. Palmore, H. Bertschy, S. H. Bergens, G. M. Whiteside, *J. Electroanal. Chem.*, **1998**, *443*, 155-161.
2. Q. Gao, W. Wang, Y. Ma, X. Yang, *Talanta*, **2004**, *62*, 477-482.
3. I. Katakis, E. Dominguez, *Mikrochim. Acta*, **1997**, *126*, 11-32.
4. L. Gorton, E. Dominguez, *Encyclopedia of Electrochemistry*, Wilson, G. S, Wiley, New York, **2002**.
5. J. Moiroux, P. J. Elving, *Anal. Chem.*, **1978**, *50*, 1056-1062.
6. L. Bartalits, G. Nagy, E. Pungor, *Anal. Lett.*, **1984**, *17*, 13-41.
7. D. Dicu; L. Muresan, I. C. Popescu, C. Cristea, I. A. Silberg, P. Brouant, *Electrochim. Acta*, **2000**, *45*, 3951-3957.
8. N. S. Lawrence, J. Wang, *Electrochem. Comm.*, **2006**, *8*, 71-76.
9. A. R. Lovstad, *BioMetals*, **2006**, *19*, 1-5.
10. I. C. Popescu, E. Dominguez, A. Narvaez, V. Pavlov, J. *Electroanal. Chem.*, **1999**, *464*, 208-214.
11. A. Malinauskas, T. Ruzgas, L. Gorton, *J. Electroanal. Chem.*, **2000**, *484*, 55-63.
12. A. S. Santos, A. C. Pereira, L. T. Kubota, *J. Brazilian Chem. Soc.*, **2002**, *13*, 495-501.
13. D. Gligor, L. Muresan, A. Dumitru, I. C. Popescu, *J. App. Electrochem.*, **2007**, *37*, 261-267.
14. A. S. Santos, R. S. Freire, L. T. Kubota, *J. Electroanal. Chem.*, **2003**, *547*, 135-142.
15. R. Gropeanu, PhD Thesis, Babes-Bolyai University, Cluj Napoca, **2005**.
16. L. T. Kubota, L. Gorton, *Electroanalysis*, **1999**, *11*, 719-728.
17. E. Laviron, *J. Electroanal. Chem.*, **1979**, *101*, 19-28.
18. D. Gligor, PhD Thesis, Babes-Bolyai University, Cluj Napoca, **2002**.

VASILICA LATES, DELIA GLIGOR, ET AL.

*Dedicated to Professor Ionel Haiduc,
President of The Romanian Academy at his 70th anniversary*

ONE-PLUS RATE EQUATION, AN USEFUL TOOL TO ELUCIDATE THE REACTION MECHANISM

IOAN BALDEA, DANA - MARIA SABOU AND ALEXANDRA CSAVDARI*

ABSTRACT. One-plus rate equation rather than power rate equation is an useful tool in interpreting the reaction mechanism. Three systems, the oxidation of toluene and some substituted toluenes by Ce(IV), the oxidation of S-methylcysteine by chromate and the oxidation of thiamine by permanganate have been undertaken as kinetic studies and have been found to obey such type of rate laws. To suggest reaction mechanisms the inference of kinetic along with some extra-kinetic proofs were taken into consideration. The reactions start with the formation of intermediates made up from substrate and reactant as pre-equilibria, followed by electron-transfer processes. Various influence of hydrogen ion was deduced from the kinetic data.

The paper also discusses general and literature examples to clear up the concepts in connection with network elucidation.

Key Words: one-plus rate law, chromate, permanganate, Ce(IV), toluene, xylene, S-methylcysteine, thiamine.

Introduction

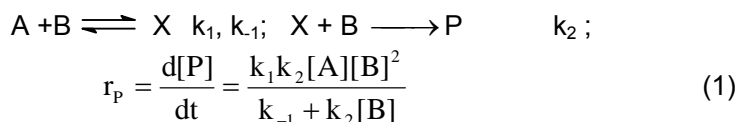
Guidelines have been proposed within which a kineticist works in developing a reaction mechanism on the basis of the rate law that can be deduced from the kinetic measurements¹⁻³. Extra-kinetic measurements as well as theoretical considerations will argue the postulated mechanism⁴⁻⁵.

The knowledge of how the changes of any molecular event are reflected in the observable kinetic behaviour is the very basis of chemical kinetics. Each kinetic study of a new reaction needs to measure reaction rates and compile *an empirical power-law rate equation* as complete as possible from extensive results over a wide range of experimental conditions. Most reactions of practical interest do not proceed by simple pathways. Therefore they do not obey always simple power-law rate equations and so have no exact and constant reaction orders. They are multistep reactions. The larger the network, the harder is its elucidation. Rate equation of a multistep reaction, especially with reverse steps is complex and contains more than one term in the denominator. The number of phenomenological rate coefficients can be reduced by one if numerator and denominator are divided by a term in the denominator. The outcome is an *one-*

* Babeș-Bolyai University, Faculty of Chemistry and Chemical Engineering. 11 Arany Janos Str. Cluj- Napoca, 400028 Romania. E-mail: ibaldea@chem.ubbcluj.ro

plus rate equation. The traditional power-law with empirical fractional exponents cannot be expected to result from combinations of elementary steps except for the case of simultaneous paths. In contrast, the one-plus rate equation can result from step combinations. It contains integer (or at most integer multiple of 1/2) exponents, being more likely to reflect the true mechanism, and plays a key role in the network elucidation⁵. The phenomenological rate coefficients are combinations of elementary steps in the network. This paper presents some results obtained in our laboratory as well as some literature examples to introduce the concepts concerning the elucidation of the reaction mechanism on the basis of one-plus rate law.

A straightforward example results from three elementary steps mechanism with X as an intermediate under steady-state conditions and an overall order between two and three^{3,5}:



Dividing the numerator and denominator by the first term in the denominator, the rate law of the one-plus type is obtained:

$$\frac{d[P]}{dt} = \frac{k_a [A] [B]^2}{1 + k_b [B]} \quad \text{with} \quad k_a = \frac{k_1 k_2}{k_{-1}} \quad \text{and} \quad k_b = \frac{k_2}{k_{-1}} \quad (2)$$

The number of rate coefficients has been reduced to two phenomenological ones (k_a and k_b). The linear form is:

$$\frac{[A][B]}{r_p} = \frac{k_b}{k_a} + \frac{1}{k_a} \frac{1}{[B]} \quad (3)$$

Even more complicated rate laws can be deduced for other systems, with fractional order with respect to two participants like (4):

$$\frac{d[P]}{dt} = \frac{k_a [A][B]}{1 + k_b [A] + k_c [B]} \quad (4)$$

Such a case needs some series of measurements with variable concentration of A at several constant concentration of B taken in large excess. In order to determine the phenomenological rate coefficients a nonlinear regression can be used or the equation can be brought into a linear form and tested by linear regression or plotting. The linear form is obtained when double reciprocal is taken.

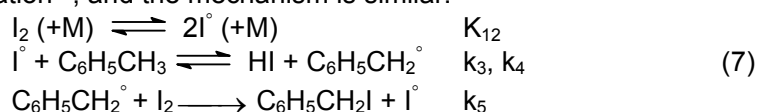
$$\frac{[B]}{r_p} = \frac{k_b}{k_a} + \frac{1 + k_c [B]}{k_a} \frac{1}{[A]}; \quad \text{Slope} = \frac{1 + k_c [B]}{k_a} \quad (5)$$

The first literature example with the order as an integer multiple of 1/2 is the gas phase reaction between iodine and various silanes⁶⁻¹⁰ and toluene¹¹ at 500-600K yielding iodinated compounds and HI. It obeys a

classical power rate law of 3/2 order, but the apparent $k_{3/2}$ depends upon the pressure and the reaction product HI. In the case of toluene¹¹, the rate law is of the form:

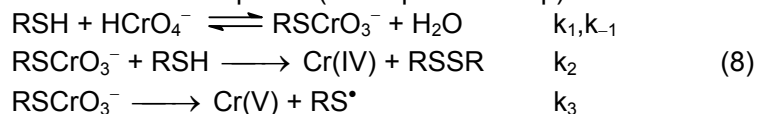
$$-\frac{d[I_2]}{dt} = k'[I_2]^{1/2}[C_6H_5CH_3]/(1 + k''[HI]/[I_2]) \quad (6)$$

Such kinetics offer strong support for an atomic abstraction chain mechanism. The rate law resembles the classical case of hydrogen bromide formation¹², and the mechanism is similar:

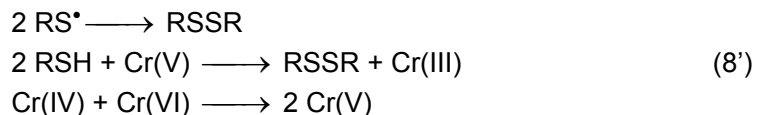


The one-plus rate law (6) can be deduced and the phenomenological rate coefficients are combinations of rate constants of the elementary steps in the above mechanism: $k' = k_3 K_{12}^{1/2}$ and $k'' = k_4 / k_5$. Here an inhibition process occurs (k_4). The rate-determining step is the one involving an iodine atom and toluene in transition state (k_3), and the dissociation pre-equilibrium (K_{12}) brings about the semi-integer overall order.

The second example, based on literature survey and experimental studies of our group, concerns the oxidation of inorganic^{13,14} or organic thio-derivatives¹⁵⁻²⁰ by chromate. A general mechanism for the reaction of chromium(VI) with a thiol involves the formation of a chromium(VI) - thioester followed by a redox decomposition of this intermediate or its redox reaction with a second molecule of thiocompound (a bi-equivalent step).



They are followed by several fast steps:



These steps were considered on the basis of extra-kinetic proofs (free-radical and Cr(V) identification)^{13,15,20} and to justify the reaction stoichiometry. The two-step mechanism involving thioester formation and its subsequent reaction with a second molecule of thiol is consistent with the observed rate law for thiosulphate, cysteine, cysteine methyl ester, cysteamine, glutathione, mercaptoethanol, thioglycolic and thiomalic acids. The apparent first-order rate coefficient depends on substrate concentration, having a fractional order between one and two with respect to the substrate. The uniequivalent electron transfer within the condensed

species RSCrO_3^- is extremely slow and negligible in the rate law. When thioester is formed rapidly and in significant concentration in a pre-equilibrium, as found in almost all the cases, the fraction of Cr(VI) as condensed compound is $[\text{RSCrO}_3^-]/[\text{Cr}^{\text{VI}}]_t = \text{K}[\text{RSH}]/(1 + \text{K}[\text{RSH}])$. The one-plus type rate law is accordingly:

$$-\frac{d[\text{Cr}^{\text{VI}}]}{dt} = \frac{(k_1/k_{-1})k_2[\text{RSH}]^2}{1 + (k_1/k_{-1})[\text{RSH}]}[\text{Cr}^{\text{VI}}] = \frac{k_2\text{K}[\text{RSH}]^2}{1 + \text{K}[\text{RSH}]}[\text{Cr}^{\text{VI}}] \quad (9)$$

In such cases substantial spectral evidence has been found for the thioester formation^{18,19}.

On the other hand, there are instances where the dependence of the apparent first order rate constant on substrate concentration exhibits a sub-unitary order. It is the case of benzene thiol and α -toluenethiol in acetic acid¹⁹. Here the uniequivalent step prevails. In such situations the rate law is of the one-plus form:

$$-\frac{d[\text{Cr}^{\text{VI}}]}{dt} = \frac{k_3\text{K}[\text{RSH}]}{1 + \text{K}[\text{RSH}]}[\text{Cr}^{\text{VI}}] \quad (10)$$

Similar behaviour has been found in the case of chromate oxidation of secondary alcohols to ketones²⁰ or DL-methionine to corresponding sulfoxide²¹.

Our experimental approach concerns the oxidation of xylene by Ce(IV), the oxidation of S-Methylcysteine by chromate and the oxidation of thiamine by permanganate in acidic media.

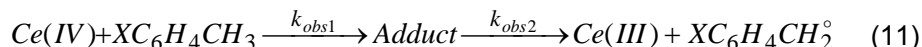
Experimental

The chemicals in the study were of guaranteed reagent grade purity, purchased from commercial sources (Merck, Aldrich, Fluka, Reanal Budapest) and used without further purification. Solutions were prepared in demineralised and four-distilled water.

The reactions were followed by spectrophotometrical means at appropriate wavelength, where the oxidant species exhibits a characteristic absorption band. A Jasco V-530 spectrophotometer (Japan), provided with a temperature jacket surrounding the cell holder and kinetic data acquisition has been used. Reactions were started directly in the spectrophotometer cell by injection of the reactant solution over the others, contained in the cell, and the absorbance was recorded as a function of time. The acidity and ionic strength were maintained constant by means of HClO_4 in excess and NaClO_4 . Temperature was controlled at a constant value by circulation of water from a Lauda M-20 thermostat through the cell-holder. Each reaction system has been studied in the presence of an excess of the organic substrate. The experimental details were presented elsewhere^{23,24}. At least three replicate runs were performed for each set of experimental conditions.

Oxidation of toluene and substituted toluenes by Ce(IV)

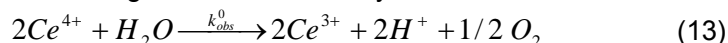
Preliminary investigations such as stoichiometric determination by spectrophotometrical titration²⁵ as well as spectra recorded immediately after mixing with solutions of increasing hydrocarbon concentration under conditions of very slow reaction, bring about arguments for the involvement of an intermediate. A small but systematic decrease of the intensity of Ce(IV) absorption band and the occurrence of an isosbestic point has been noticed (271, 275 and 276 nm in the case of toluene, *o*-xylene and *p*-xylene, respectively). Therefore, the reaction proceeds by consecutive steps, which under the excess concentration of substrate, is a first-order series



The further oxidation takes place and after hydrolysis the substituted benzyl alcohol is formed. The first stage could be attributed to the formation of an adduct between Ce(IV) and substituted toluene^{24,25}. The second stage is associated with the redox process consisting of an inner electron transfer within the complex, yielding a free radical and eventually the final products of the reaction. A first-order dependence on cerium has been found for both stages of the reaction. Indeed, the absorbance measurements ($A = f(t)$ curves) fitted a bi-exponential equation:

$$A - A_{\infty} = C_1 \exp(-k_{obs1}^0 \cdot t) + C_2 \exp(-k_{obs2}^0 \cdot t) \quad (12)$$

A and A_{∞} stand for the absorbance at actual time and at the end of the reaction respectively. The parameters C_1 and C_2 are constants including the molar absorptivities and Ce(IV) initial concentration and k_{obs1}^0 and k_{obs2}^0 are apparent rate constants of the two consecutive steps. The apparent first-order rate constants were determined by means of this non-linear fitting. Several data are collected in table 1. Parallel to the oxidation of aromatic hydrocarbons, oxidation of water by Ce(IV) takes place in perchlorate media, according to the stoichiometry:



The kinetics of this reaction obeys a first-order dependence on Ce(IV) for the whole duration of the reaction. It has been deduced by the same procedure as for the overall process, described before. We determined the influence of different parameters on the oxidation of water and both water and substrate. Because the literature stipulates²⁶ and we have also found^{24,25}, Ce(III) diminishes the rate of the water oxidation reaction. Therefore, we introduced Ce(III) into the reaction mixture from the beginning in a ratio 1:1 ([Ce(IV)]:[Ce(III)]). The experimental curves for the water oxidation reaction were determined by a fitting method with the equation:

$$A - A_{\infty} = C_3 \exp(-k_{obs}^0 \cdot t) \quad (14)$$

The data were published previously²⁴. Here we are interested in the oxidation stage of the reaction and present data concerning the second stage. Several rate constants are presented in table 1. Once we had all the first-order rate constants, we proceeded by subtracting the rate constant of the oxidation of water, which is a simultaneous process having a linear kinetics, from the rate constants of the overall reaction as follows

$$k_{\text{obs}2} = k_{\text{obs}2}^0 - k_{\text{obs}}^0 \quad (15)$$

where $k_{\text{obs}2}$ is the observed first-order rate constants of the aromatic hydrocarbon oxidation reaction allowing for the water oxidation reaction, under the same acidity or ionic strength conditions employed.

Table 1.
Apparent first-order rate coefficients of the oxidation reaction as a function of toluene, *ortho*- and *para*-xylene concentration: $[H^+] = 1.0 \text{ mole.L}^{-1}$, $[Ce(IV)] = 8.0 \cdot 10^{-5}$ and $\mu = 3.0$ and 40°C

Substrate S	$10^4[S]$	$10^4 k_{\text{obs}2} (\text{s}^{-1})$
$\text{C}_6\text{H}_5\text{CH}_3$	4.00	1.66
	6.00	2.32
	7.00	2.68
	8.00	2.92
	9.00	3.19
	10.00	3.42
<i>o</i> - $\text{CH}_3\text{C}_6\text{H}_4\text{CH}_3$	4.00	0.23
	6.00	0.60
	7.00	0.78
	8.00	0.98
	9.00	1.10
	10.00	1.18
<i>p</i> - $\text{CH}_3\text{C}_6\text{H}_4\text{CH}_3$	4.00	2.45
	6.00	3.22
	7.00	3.72
	8.00	4.01
	9.00	4.35
	10.00	4.64

The effect of aromatic hydrocarbon concentration, always in a large excess, upon the apparent rate constant at constant acidity is described with the best fit by equations:

$$r_2 = a \frac{[p\text{-xylene}]_0}{1 + b[p\text{-xylene}]_0} [Ce(IV)];$$

$$k_{\text{obs}2} = \frac{(13.8 \pm 0.5)[p\text{-xylene}]_0}{1 + (139 \pm 90)[p\text{-xylene}]_0} \quad (16)$$

$R^2 = 0.9800$, $\chi^2 = 7.50 \cdot 10^{-9}$ for $N = 18$. Similar equations have been deduced for toluene and *o*-xylene. We are interested here in the second stage that follows a one-plus pattern. It means an order between zero and one with respect to xylene and suggests also the involvement of an intermediate species. Even under high acid concentration, the hydrolysis of Ce(IV) ion takes place and complicates the kinetics. It is revealed from the influence of hydrogen ion concentration on the rate constant investigated in the limits presented in table 2.

Table 2.
Effect of hydrogen ion concentration on the apparent rate constant;
[Ce(IV)]= $8 \cdot 10^{-5}$ mol.L $^{-1}$; [Ce(III)]= $8 \cdot 10^{-5}$ mole.L $^{-1}$; [xylene]= $4.0 \cdot 10^{-4}$ mole. L $^{-1}$;
 $\mu = 3.0$ and temperature of 40°C

[H ⁺] (mole.L ⁻¹)	Toluene	10 ⁴ ·k _{obs2} (s ⁻¹)	
		<i>p</i> -Xylene	<i>o</i> -Xylene
0.25	0.19	1.46	0.15
0.5	0.38	2.28	0.28
1	0.63	3.16	0.56
1.5	0.96	4.07	0.77
2	1.26	5.08	1.03
2.5	1.51	5.98	1.25
3.0	1.78	6.15	1.43

The same behaviour was obtained with the other hydrocarbons. The data fit well with an equation of sub-unitary fractional order

$$k_{obs2} = \frac{a[H^+]}{b + c[H^+]} \quad (17)$$

The linear fit gave the slopes of 1.26, 1.64 and 0.141, the intercepts of 0.180, 0.177 and 0.136 with good correlation coefficients of 0.9982, 0.9993 and 0.9836 for toluene, *o*-xylene and *p*-xylene respectively.

The influence of ionic strength on the reaction rate suggests that like-charged species should be involved in the second stage of the reaction. In the case of *p*-xylene, for example:

$$\log k_{obs2} = -(5.68 \pm 0.06) + (3.43 \pm 0.12)(\sqrt{\mu}/(1 + \sqrt{\mu})) \quad (18)$$

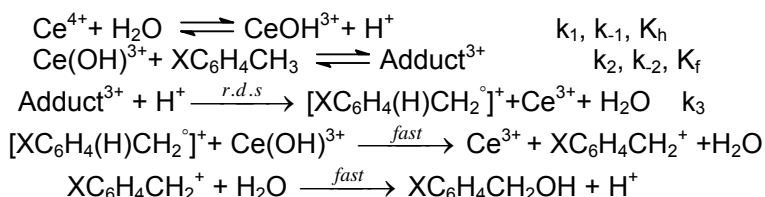
Activation parameters were determined for both stages of the reaction from the Arrhenius and from the Eyring plots. The values of activation energy and enthalpy for the first stage are quite small. The negative activation entropy is in agreement with the involvement of the adduct formation pre-equilibrium¹. Here we are interested in the second stage. Therefore, in table 3 we present the activation parameters. Activation enthalpy is greater for xylene oxidation as compared to toluene oxidation.

Table 3.
Activation parameters for the redox stage of the aromatic hydrocarbons oxidation.

Substrate	E_a (kJ/mole)	ΔH^\ddagger (kJ/mole)	ΔS^\ddagger (J/Kmole)	ΔG^\ddagger (kJ/mole)
Toluene	48.2±4.7	45.7±4.7	-170.1±6.2	99.0±6.8
p-xylene	73.2±5.6	70.64±5.7	-92.6±7.2	99.6±7.0
o-xylene	87.0±4.9	84.4±4.9	-55.6±3.8	101.8±6.2

The step of electron-transfer needs a little bit higher activation energy. The entropy modification in this stage is also negative, suggesting a bimolecular process, namely proton assisted formation of Ce(III) and uni-equivalent oxidized product. On the other hand, an isokinetic temperature seems to appear that is equivalent to a linear correlation between ΔH^\ddagger and ΔS^\ddagger (almost the same value of ΔG^\ddagger). This is a strong proof for a common oxidation mechanism of the three aromatic hydrocarbons.

A reaction mechanism can be suggested, based on kinetic and extra-kinetic data. It involves the formation of an adduct between toluene and the hydroxo-complex of Ce(IV), followed by the inner electron transfer. This rate-determining step also involves a proton, to stabilise the formed free radical. It is difficult to assign the position of this hydrogen ion. It can be bound either to the nucleus (π electron system conjugated with the free electron on methylene group), or to the side group²⁷. A proton stabilized free radical has been suggested by Baciocchi and co-workers²⁸. The subsequent steps - the oxidation to carbenium ion and its hydrolysis - are very rapid and leads finally to the major oxidation product, which is benzyl or methylbenzyl alcohol. It is presented in the scheme below:



The electron transfer takes place as proton assisted. To get more arguments to the suggested mechanism, we followed the oxidation reaction of substituted toluene, and checked whether a Hammett correlation holds. As presented before, the apparent first-order rate constant of the second stage (allowing for water oxidation) was calculated for nine compounds. Data are presented in table 4. The Hammett equation, by using the data in the table is

$$\lg \frac{k_{\text{obsd}2\text{X}}}{k_{\text{onsd}2\text{H}}} = -(0.06 \pm 0.1) - (1.25 \pm 0.05)\sigma \quad (19)$$

with $R = 0.9849$. It suggests a common mechanism. As the equation stipulates, the electron-releasing substituents increase the oxidation reaction rate, while the electron-withdrawing substituents have the opposite effect.

Table 4.

Observed first-order rate constants (allowing for water oxidation) for the oxidation process ($k_{\text{obs}2}$) and substituent constants at $[\text{Ce(IV)}]_0 = [\text{Ce(III)}]_0 = 8 \cdot 10^{-5} \text{ mole.L}^{-1}$; $[\text{p-xylene}] = 1.0 \cdot 10^{-3} \text{ mole.L}^{-1}$; $\mu = 2.0$ and temperature of 40°C ^{29,30}

Substrate	σ	$10^4 k_{\text{obs}2} (\text{s}^{-1})$
<i>p</i> -Xylene	-0.31	6.52
<i>m</i> -Xylene	-0.07	2.74
Toluene	0.0	3.32
<i>p</i> -Chloro-toluene	0.11	2.18
<i>p</i> -Bromo-toluene	0.15	2.04
<i>p</i> -Toluenesulphonic acid	0.32	0.85
<i>m</i> -Chloro-toluene	0.37	0.67
<i>m</i> -Nitrotoluene	0.71	0.39
<i>p</i> -Nitrotoluene	0.78	0.28

The rate determining step involves charge separation that may proceed easily with electron donating substituents on the aromatic ring. The reaction constant, negative and relative close to unity, suggests a free radical mechanism³¹. The $\rho = -1.25$ is in agreement with the one of the oxidation in acetic acid as solvent, with perchloric acid addition, of $\rho = -1.7$ ³². Here, because of lower dielectric constant as compared to water solution, the field effects are more important and a higher reaction constant value should be expected³¹.

Oxidation of *s*-methylcysteine by chromate

The stoichiometry of the reaction was found to be 1:1.5, corresponding to

$$2\text{HCrO}_4^- + 3\text{H}_3\text{C-S-CH}_2\text{-CH(NH}_2\text{)COOH} + 8\text{H}^+ \rightarrow 3\text{H}_3\text{C-SO-CH}_2\text{-CH(NH}_2\text{)COOH} + 2\text{Cr}^{3+} + 5\text{H}_2\text{O}.$$

This ratio has been established by colorimetric measurements at 350 nm. At excess concentrations of *S*-methylcysteine over 1.5 (abbreviated as MC) all amount of oxidizing agent Cr(VI) is completely consumed in the process and final absorbance remains small and constant. This implies that the oxidised product is the corresponding sulfoxide. Even with strong oxidizing agents such as peroxyanions, peroxydisulfate and peroxydihosphate, the oxidation product was sulfoxide in the case of alkyl aryl sulphide³³ or diphenylsulfide³⁴.

The kinetic measurements were made at various concentrations of *S*-methyl-cysteine always in large excesses, at constant acidity, and also at various HClO_4 concentrations (at constant excess of substrate). Under the pseudo-first-order conditions studied, apparent first-order kinetics has

been obtained. Plots of $\ln(A - A_\infty)$ versus time were linear over large degree of reaction with very good correlation coefficients (0.9900 - 0.9990), confirming the first-order dependence with respect to the oxidizing agent. Pseudo-first order rate coefficients were calculated from such plots.

The apparent first-order rate coefficient depends upon the substrate and mineral acid concentration. By increasing the concentration of the substrate at constant acidity, increased first-order rate constants were found with a slight tendency of levelling off, as depicted in figure 1.

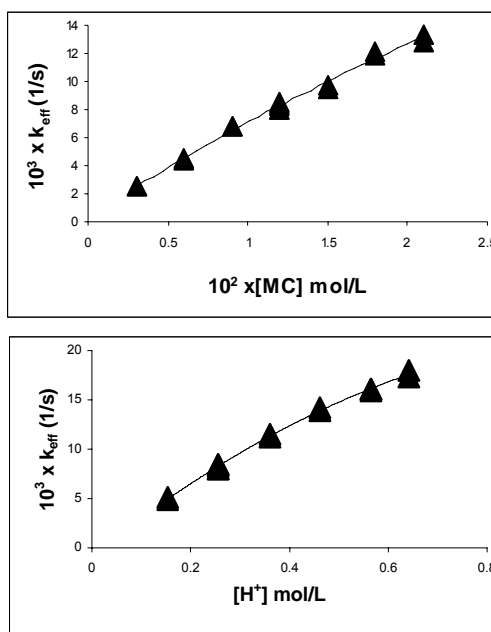


Figure1. Dependence of apparent first-order rate constant on S-methylcysteine ($[H^+] = 0.26$), and perchloric acid ($[MC]=0.012$) at 60°C and ionic strength of 0.7

This behaviour can be rationalised by the rate equation (similar to 10):

$$-\frac{d[Cr^{VI}]}{dt} = \frac{k_a[MC]}{1+k_b[MC]}[HCrO_4^-]; \quad \frac{1}{k_{obs}} = (1.62 \pm 0.34) + (1.47 \pm 0.05) \frac{1}{[MC]}$$

R=0.9976 (20)

$$-\frac{d[Cr^{VI}]}{dt} = \frac{k'_a[H^+]}{1+k'_b[H^+]}[HCrO_4^-]; \quad \frac{1}{k_{obs}} = (29.0 \pm 5.5) + (9.45 \pm 0.34) \frac{1}{[H^+]}$$

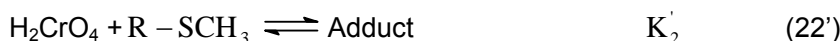
R=0.9960 (20')

which is of the one-plus form. The combined dependence on both the substrate and hydrogen ion concentration concerning the apparent first-order rate constant and its linear form are as follows:

$$k_{obs} = \frac{k_a''[MC][H^+]}{1 + k_b''[MC][H^+]} \quad \frac{1}{k_{obs}} = \frac{1}{k_a''} \frac{1}{[MC][H^+]} + \frac{k_b''}{k_a''} \quad (21)$$

By considering the inference of the kinetic behaviour, the following mechanism can be suggested:

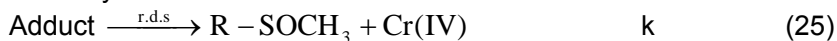
- The pre-equilibria involving the adduct intermediate could be either



We symbolize here S-methylcysteine by $\text{R} - \text{SCH}_3$ to show the two possibilities of protonation in forming the adduct intermediate. The two coupled equilibria can be written as an overall one, with $K = K_1' K_2'$ (or $K_1'' K_2''$).



- It is followed by the electron transfer and the formation of a S-O double bond



The process continues by rapid steps of the type (8), given in the literature cited example, with the formation of Cr(V). It also can oxidize S-methylcysteine to sulfoxide. The rate law deduced by this reaction scheme is of the form (21) in which third-order rate constant $k_a'' = kK = (2.8 \pm 0.1) \text{ L}^2\text{mole}^{-2}\text{s}^{-1}$ and $k_b'' = K = (29.0 \pm 7.5) \text{ L}^2\text{mole}^{-2}$ and first-order rate constant for electron transfer $k = (9.7 \pm 2.8) \cdot 10^{-2} \text{ s}^{-1}$ were computed.

The oxidation of thiamine (vitamin B 1) by permanganate

The anti-oxidant character of Vitamin B1 is well known. In order to set up a kinetic method of analysis for Vitamin B1, we have studied the kinetics of its oxidation by permanganate in acidic media³⁵. The stoichiometry of the process was determined at constant acidity of 0.2 mole.L^{-1} using various molar ratios. The remaining absorbance, after the reaction achieved completion, is presented in figure 2.

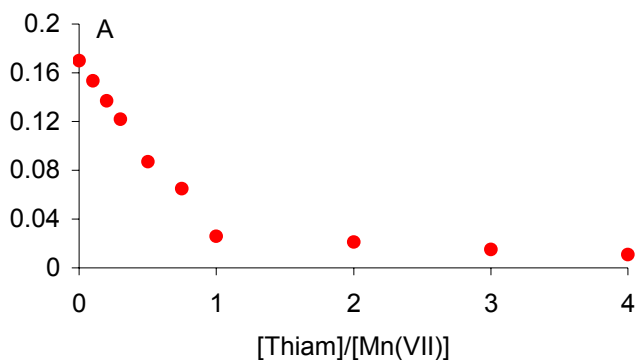
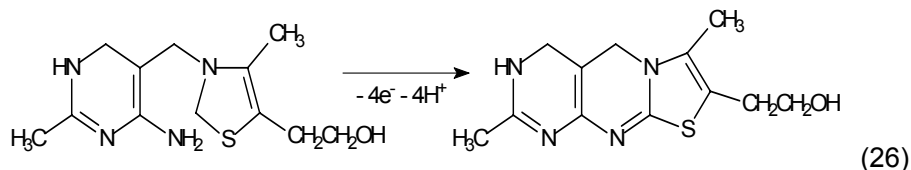


Figure 2. The left absorbance after the reaction has been accomplished at various molar ratios in the initial reaction mixture

It reveals an obvious change of the slope at the ratio 1.2 Thiamine:1 MnO_4^- confirming a process that involves four electrons. It corresponds to dehydrogenation and ring closure.



Kinetic measurements were made by spectrophotometrical means, following the absorbance of permanganate at 525 nm. The absorbance evolution can be described by an exponential, except for a small initial part where a salient decrease of it takes place. We have exploited the exponential dependence for the determination of first-order rate coefficient, as the slope of the line of $\ln(A - A_\infty)$ versus time. The results of at least three replicate runs are presented as means in table 5. The apparent first-order rate constants are dependent on both the substrate and the acid concentration. An increase of the rate coefficient has been found for the two influences but not strictly proportional. A slight tendency of levelling off appears in both cases. Indeed, if the initial rate as the decrease of absorbance against time was measured from the slope of the absorbance curve (within less than 5% of reaction) at various initial concentration of thiamine, the behaviour presented in figure 3 has been obtained.

ONE-PLUS RATE EQUATION, AN USEFUL TOOL TO ELUCIDATE THE REACTION MECHANISM

It can be described by an equation of the one-plus rate law form at constant HClO_4 concentration of 0.2:

$$r_0 = \frac{k_a[\text{Thiam}]}{1 + k_b[\text{Thiam}]}[\text{MnO}_4^-]; \quad r_0 = \frac{(25.9 \pm 1.1)[\text{Thiam}]}{1 + (181 \pm 13)[\text{Thiam}]}[\text{MnO}_4^-] \quad (27)$$

Table 5.

The effect of thiamine concentration at constant $[\text{H}^+] = 0.1$ and of the acid at constant $[\text{Thiam}] = 8.1 \cdot 10^{-3}$, at 25°C and ionic strength of 0.5

$10^3[\text{Thiam}] \text{ mol.L}^{-1}$	$10^2 k_{\text{obs}} (\text{s}^{-1})$	$[\text{H}^+] \text{ mol.L}^{-1}$	$10^2 k_{\text{obs}} (\text{s}^{-1})$
0.81	2.18	0.10	2.18
1.40	3.90	0.15	3.10
1.70	4.50	0.20	3.92
2.10	5.62	0.25	4.08
2.70	6.63	0.30	5.60
3.30	8.21	0.35	6.44
4.10	9.63	0.50	9.81
4.90	10.8		
5.30	11.5		
5.70	12.2		
6.20	13.0		

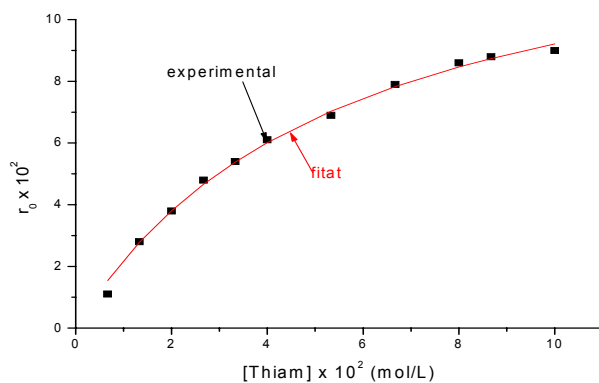


Figure 3. Dependence of the initial rate with thiamine concentration at 25°C and ionic strength of 2.00

The tendency of levelling off of the observed first- order rate coefficient in table 5 can be described by a linear double reciprocal plot with the equations:

a) at constant perchloric acid concentration:

$$k_{\text{obs}}^{-1} = (3.50 \pm 0.06) \cdot 10^{-2} [\text{Thiam}]^{-1} + (1.8 \pm 0.3); \quad R = 0.9988, \quad (28)$$

b) at constant thiamine concentration:

$$k_{\text{obs}}^{-1} = (4.36 \pm 0.13) \cdot [\text{H}^+]^{-1} + (3.0 \pm 0.7) \quad R = 0.9978 \quad (29)$$

The combined dependence on both the substrate and hydrogen ion concentration, concerning the apparent first-order rate constant, is of the one-plus form, which can be transposed into a linear equation.

$$k_{\text{obs}} = \frac{k_a' [\text{Thiam}] [\text{H}^+]}{1 + k_b' [\text{Thiam}] [\text{H}^+]} \quad \frac{1}{k_{\text{obs}}} = \frac{1}{k_a'} \frac{1}{[\text{Thiam}] [\text{H}^+]} + \frac{k_b'}{k_a'} \quad (30)$$

The line is presented in figure 4 and has a good correlation coefficient of $R = 0.9959$.

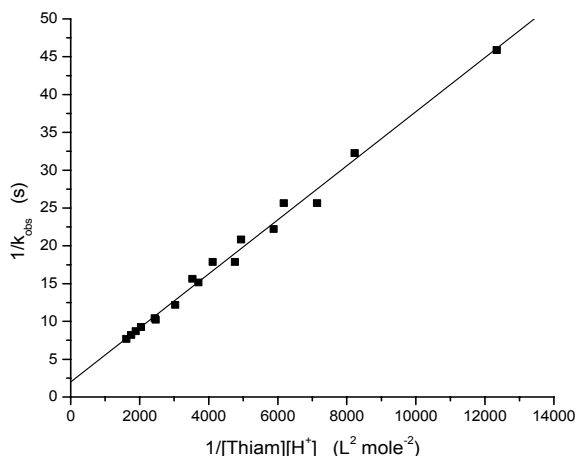
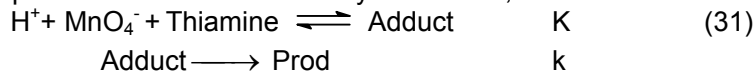


Figure 4. The double reciprocal plot of equation (30)

From the parameters of the line we obtained the following figures: $1/k_a' = (3.57 \pm 0.09) \cdot 10^{-3} \text{ mole}^2 \text{ L}^{-2} \text{ s}$ and $k_b' / k_a' = (2.0 \pm 0.5) \text{ s}$.

The steep decrease of the absorbance at 525 nm immediately after mixing as well as the rate law expression lead to the conclusion of a two step mechanism involving a pre-equilibrium followed by the rate determining step with the stoichiometry of transition state (1 Thiamine:1 MnO_4^- : 1 H^+). It is difficult to predict the change in oxidation state of manganese in this step. The reaction continues with complete reduction of the manganese intermediate valence states to Mn(II) in this strong acid medium, to respect the overall stoichiometry. Therefore,



From this two step mechanism, following the disappearance of the $[\text{Mn(VII)}]_t$, measured by the absorbance, the rate law deduced has the expression

$$k_{\text{obs}} = \frac{kK[\text{Thiam}][\text{H}^+]}{1 + K[\text{Thiam}][\text{H}^+]} \quad (32)$$

which is of the form (10). From the parameters of the linear equation (30), the rate constant of third order is $kK = (2.80 \pm 0.07) \cdot 10^2 \text{ L}^2 \cdot \text{mole}^{-2} \cdot \text{s}^{-1}$, $k = 0.50 \pm 0.16 \text{ s}^{-1}$ and $K = (5.6 \pm 1.6) \cdot 10^2 \text{ L}^{-2} \cdot \text{mole}^2$.

Conclusions

As presented for the studied reactions, the experimental kinetic data obey one-plus rate laws, with integer exponents. In each case a pre-equilibrium involving the oxidant and the organic substrate is present. In acidic media, the involvement of hydrogen ion is quite different for the three reactions approached. Phenomenological rate coefficients and some intermediate formation constants could be calculated. The data fit well with the rate law deduced from the reaction schemes of two steps, the pre-equilibrium and the rate determining electron transfer, thus supporting the suggested mechanisms. Extra kinetic proofs (stoichiometry, the absorbance evolution at the start of the processes) also account for the suggested reaction networks.

REFERENCES

- [1] R.G. Wilkins, *The study of kinetics and mechanism of reactions of transition metal complexes*, Allyn and Bacon Inc., Boston, **1974**, p.60-117
- [2] J.H. Espenson, *Chemical kinetics and reaction mechanisms*, McGraw-Hill Book Co., New-York, **1981**, p. 89-115
- [3] I. Baldea, *Cinetica chimica si mecanisme de reactie. Baze teoretice si aplicatii*, Presa Univ. Clujeana, Cluj-Napoca, **2002**, p. 358-379
- [4] J.W. Moore and R.G. Pearson, *Kinetics and Mechanisms*, 3-rd Ed., J. Wiley and Sons, New-York, **1981**, p.192-283
- [5] F.P. Helfferich, *Kinetics of multistep reactions*, 2-nd Ed., in *Comprehensive Chemical Kinetics*, Vol 40, N.J.B. Green, Elsevier, Amsterdam, **2004**, p.53-159; 178-206
- [6] M. Barber, A.M. Doncaster, R. Walsh, *Int. J. Chem. Kinet.* **1982**, *14*, 669
- [7] A.M. Doncaster, R. Walsh, *Int. J. Chem. Kinet.* **1981**, *13*, 99
- [8] A.M. Doncaster, R. Walsh, *J. Chem. Soc., Faraday Trans. 1*, **1979**, *75*, 1126
- [9] R. Walsh, J.M. Weller, *J. Chem. Soc., Faraday Trans. 1*, **1970**, *72*, 1212
- [10] R. Walsh, R.M. Golden, S.W. Benson, *J. Am. Chem. Soc.* **1966**, *88*, 650
- [11] A.M. Doncaster, R. Walsh, *Int. J. Chem. Kinet.* **1978**, *10*, 101
- [12] M. Bodenstein, S.C. Lind, *Z. Physik. Chem.* **1906**, *57*, 168
- [13] J.K. Beattie, G.P. Haight, *Progress in Inorg. Chem.* **1972**, *17(2)*, 93
- [14] I. Baldea, G. Niac, *Inorg. Chem.* **1970**, *9*, 110
- [15] P.H. Connett, K.E. Wetterhahn, *J. Am. Chem. Soc.* **1985**, *107*, 4282

- [16] D.A. Dixon, T.P. Dasgupta and N.P. Sadler, *Inorg. Reaction Mech.* **1** **1998**, 41
- [17] I. Baldea, G. Niac, *Studia Univ Babeş-Bolyai, Chem.* **1986**, 31(2), 41
- [18] I. Baldea, *Studia Univ Babeş-Bolyai, Chem.*, **1987**, 33(2)) 42
- [19] I. Baldea and Dana M. Sabou, *Rev. Roum. Chim.* **2000**, 45, 537
- [20] Dana M. Sabou, I. Baldea, *Studia Univ. Babeş-Bolyai, Chem.* **2001**, 45(1,2), 17.
- [21] K.B. Wiberg, H.Schafer, *J.Am.Chem. Soc.*, **1969**, 91, 927; *idem* 933: K.B. Wiberg, S.K. Mukherjee, *J.Am.Chem. Soc.*, **1971**, 93, 2543.
- [22] I. Baldea, Dana Maria Sabou, Alexandra Csavdari, *J. Serb. Chem. Soc.*, **2007**, 72 (to be published)
- [23] Alexandra Rustoiu-Csavdari, D. Mihai, I. Baldea, *Anal. Bioanal. Chem.* **2005**, 381, 1373
- [24] Gabriela C. Bucşa, I. Baldea, *Studia Univ. Babes-Bolyai, Chem.*, **2005**,50(1), 157
- [25] Gabriela C. Bucsa, Claudia G. Muresanu, I. Baldea, *Studia Univ. Babes-Bolyai, Chem.*, **2003**, 49(1), 125; Gabriela C. Bucsa, Claudia G. Muresanu, I. Baldea, *Studia Univ. Babes-Bolyai, Chem.*, **2002**, 48(1-2), 67
- [26] D. Kolp, H. C. Thomas, , *J. Am. Chem. Soc.*, **1949**, 71, 3047
- [27] G. Calvaruso, F. P. Cavasino, C. Sbriziolo, *Int. J. Chem. Kinet.*, **1981**, 13, 135
- [28] E. Baciocchi, C. Rol, G.V.Sebastiani, *J. Chem. Research (Symposis)* **1965**, 9, 232
- [29] H.C. Brown, Y. Okamoto, *J. Am. Chem. Soc.*, **1958**, 80, 4979
- [30] M. Charton, *Progr. Phys. Org. Chem.*, **1981**, 12, 119; H. Zollinger, *Helv. Chim. Acta.*, **1953**, 36, 1730
- [31] P.S. Radhakrishna, S.C. Pati, *Chem. Ind.*, **1967**, 17, 702
- [32] K. A. Connors, *Structure-Reactivity Relationships.in Chemical Kinetics. The study of Reaction Rates in Solution*; V. C. H. Publ. Inc., Weinheim, **1990**, p 311-380; C. D. Johnson, *The Hammett Equation*, Cambridge Univ. Press, Cambridge, **1973**
- [33] N. Arumugam, C. Srinivasan, P. Kuthalingam, *Indian J. Chem.* **1978** ,16A, 478; C. Srinivasan, P. Kuthalingam, N. Arumugam *Can. J. Chem.* **1978** , 56 3043; *idem*, *J. Chem. Soc. Perkin Trans. 2*, **1980**, 170; C. Srinivasan, P. Kuthalingam, N. Arumugam, *Int. J. Chem. Kinet.* **1982**, 14 , 1139
- [34] D. Kolp, H.C. Thomas, *J. Am. Chem. Soc.* **1949**, 71, 3047; G. Calvaruso, F.P. Cavasino, C. Sbriziolo, *Int. J. Chem. Kinet.* **1981**, 13, 135; V.K. Grover, S.K. Mishra, Y.K. Gupta, *J. Inorg. Nucl. Chem.* **1970**, 32, 2677
- [35] Simona Bungau, L. Copolovici, I. Baldea, Vasilica Merca, *Farmacia*, **2004**, 52 (1), 83

*Dedicated to Professor Ionel Haiduc,
President of The Romanian Academy at his 70th anniversary*

KINETICS AND OXIDATION MECHANISM OF LACTIC AND MALIC ACIDS BY PERMANGANATE IN ACIDIC MEDIA

ALEXANDRA CSAVDARI AND IOAN BALDEA*

ABSTRACT. Kinetic studies on the oxidation of malic and lactic acids by permanganate in acidic solutions have been carried out. In the presence of Mn(II) three ways of consumption of Mn(VII) are involved: a direct oxidation of the hydroxy acid, an oxidation of Mn(II) to Mn(III) and a catalytic route. The experimental rate law is quite complex. It involves a condensed esteric type compound for the direct oxidation by permanganate and two other parallel ways: one leading to a first-order and the other to a second order term with respect to Mn(II) as catalyst.

Key Words: Kinetics, reaction mechanism, lactic acid, malic acid, oxidation, permanganate, autocatalysis, catalysis.

Although the kinetic study of oxidation by permanganate has received considerable attention for well over a century, there are still unanswered questions concerning the mechanism of many processes [1]. The oxidation reactions in alkaline solutions [2] are better understood, but in acidic media they are usually multi-stage processes due to the ability of manganese to exist in a multitude of oxidation states.

Numerous permanganate oxidation reactions exhibit autocatalysis [3, 4]. Among these, the $\text{MnO}_4^- - \text{C}_2\text{O}_4^{2-}$ reaction has attracted much attention [5-7]. It is the base of a titration method, which involves autocatalysis. The overall reaction $2\text{MnO}_4^- + 5\text{C}_2\text{O}_4^{2-} + 16\text{H}^+ \rightarrow 2\text{Mn}^{2+} + 10\text{CO}_2 + 8\text{H}_2\text{O}$ can be split into two composite stoichiometric processes [8, 9]: the oxidation of Mn(II) to Mn(III) by MnO_4^- followed by the rapid formation of a Mn(III)-oxalate complex, that further undergoes a redox decomposition. The first process obeys a first-order law in MnO_4^- and a second-order in Mn(II) [10] in aqueous acidic solutions and exhibits various dependencies on hydrogen ion concentration [11-13]. Similar autocatalytic effect has been observed for the oxidation of malic acid [14]. The oxidation of α -hydroxy acids by various oxidizing agents will yield keto acids [15] or carbonyl compounds and CO_2 [16]. Transition metal ions exhibit

* "Babeș-Bolyai" University, Faculty of Chemistry and Chemical Engineering 11 Arany Janos Str., 400028 Cluj-Napoca, Romania E-mail: acsavdari@chem.ubbcluj.ro

catalytic effect in the oxidation by Cr(VI) or Mn(VII) [17]. Therefore some kinetic methods for analysis could be set off for traces of these metal ions [18].

This work has undertaken the study of the oxidation of the two title α -hydroxy acids as an attempt to determine the dependence of the rate on Mn(II) concentration as well as to establish a satisfactory mechanism.

Experimental

All chemicals employed in the study were of certified analytical reagent grade from commercial sources and therefore used without further purification. The solutions were prepared in twice distilled water. Stock solutions of HClO_4 and LiClO_4 were prepared and standardised by titration with a NaOH solution. Aliquots of the LiClO_4 solution were passed over a cationic resin Amberlite IR 122 in the H-form. The resulted acid was titrated. The solutions of reagents were freshly prepared and standardised before each set of runs.

The course of the reaction was followed spectrophotometrically at 525 nm by using a Jasco V-530 spectrophotometer interfaced to a computer and equipped with a cell holder connected to a Lauda M-12 recirculation bath. A 5-cm path length glass cell has been used. Three to seven replicate runs were performed for each set of experimental conditions, and calculated rate constants did not differ to more than $\pm 3\%$. The process was initiated by injecting permanganate solution, kept in the temperature bath, directly into the cell over the mixture of other reactants. Mixing time did not exceed 0.5 sec.

The stoichiometry of the process was determined by means of photometric titration. Various mixtures having known initial molar ratios were allowed to react to completion for at least ten half-lives at room temperature, constant acidity (0.32 mole/L) and ionic strength (0.75 mole/L). The final absorbance values were measured and compared to the one obtained with a solution containing the same mixture except for the hydroxy acid. In order to allow for potassium permanganate self decomposition or water oxidation, this solution was kept for the same period as the slowest reaction mixture [19].

Results and Discussion

Stoichiometry. Because Mn(II) has a contribution to the disappearance of Mn(VII) by means of reaction $\text{MnO}_4^- + 4 \text{Mn}^{2+} + 8\text{H}^+ \rightarrow 5 \text{Mn}^{3+} + 4 \text{H}_2\text{O}$, the stoichiometry of the oxidation process was determined in its absence in the starting reaction mixture. In acidic media, the stoichiometry corresponds to the oxidation to the oxo-acids: oxalylacetic and pyruvic acid, respectively.

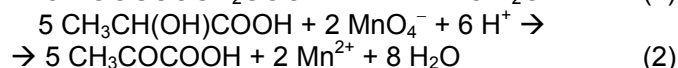
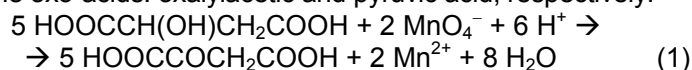


Figure 1 shows the dependence of the final absorbance values on the initial molar ratio in the case of DL-hydroxybutanedioic acid oxidation (symbolised by MA). A similar dependence has been found with lactic acid (LA) – results not shown. It is obvious that a clear intercept of the lines is obtained at the ratio 2.5, indicating consumption molar ratios as presented in equations (1) and (2). If hydroxy acids were oxidized by some Cu(II) permanganate complex, oxo acids were also obtained [20]. The oxidation of C–OH to carbonyl takes place even in some heterogeneous reactions [21]. The involvement of *free radicals* has been proved by the initiation of polymerisation. Polymer has been also isolated.

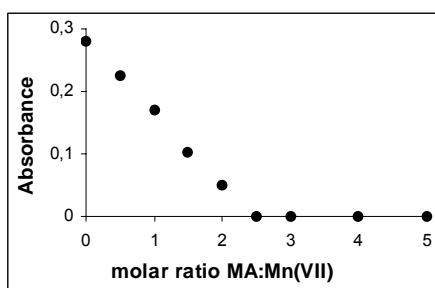
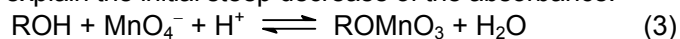


Figure 1. Absorbance measurements at the end of the reaction at various malic acid - permanganate initial molar ratios.

Reaction kinetics. The reaction starts for both hydroxy-acids, either in the presence or in the absence of initial Mn(II), with a steep decay of the colour within a short period of 10 to 15 sec. Afterwards the absorbance decreases quite slowly to its final value. This fast process involves only the hydroxy-acid and permanganate. Because of the lack of a stopped-flow device, we report here only the data for the slow stage. However, by analogy with permanganate oxidation of other substrates [22, 23], one can suppose that some rapid equilibrium yielding an ester takes place. This condensed compound has a smaller molar absorptivity as compared to that of permanganate ion at 525 nm. It can explain the initial steep decrease of the absorbance.



On the other hand, the oxidation of Mn(II) to Mn(III) by permanganate under the same acid concentration is slower than the oxidation of organic substrate itself (see table 1, where MA stands for malic acid and LA for lactic acid, respectively). When Mn(II) has not been added to the mixture, a sigmoid shape of the absorbance versus time plot has been noticed [14]. This is characteristic for reactions with an induction period. Intermediate valence states

of manganese are important oxidising entities [4]. The process went to completion more rapidly when Mn(II) was initially present in the reaction mixture.

Table 1.
Average values of the first-order rate coefficients at various concentrations of hydroxy acids; $[H^+] = 0.32$, $[Mn^{2+}] = 5.0 \times 10^{-2}$, $[MnO_4^-] = 1.0 \times 10^{-4}$, $\mu = 0.75$ and 297 K.

$10^3 [ROH]$ (mole/L)	$10^3 k_{obsd}$ (s ⁻¹) - MA	$10^3 k_{obsd}$ (s ⁻¹) - LA
0.00	1.48	1.48
1.66	3.91	2.53
2.50	4.62	2.93
3.33	5.44	3.53
4.16	6.27	3.73
5.00	7.13	4.23
5.83	7.67	4.60
6.66	8.13	4.98

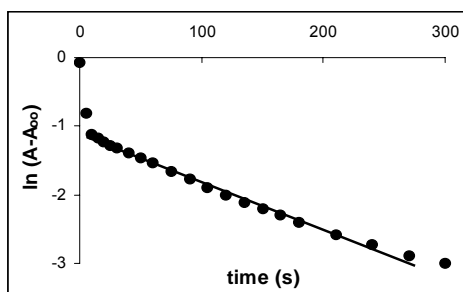


Figure 2. First-order plot for the oxidation of malic acid: $[MA] = 5.0 \times 10^{-3}$, $MnO_4^-] = 1.0 \times 10^{-4}$, $[Mn^{2+}] = 5.0 \times 10^{-2}$, $[HClO_4] = 0.32$, $\mu = 0.75$ and 290 K.

The oxidation process follows a first-order dependence on the coloured species. Figure 2 presents the linear semi-logarithmic plot. Linearity has been obeyed up to 90 % of reaction extent. Calculation of line parameters was carried out statistically. The first points (corresponding to the steep decay of the absorbance) and the last ones (close to the final value) were excluded. The rate coefficients depend upon the organic substrate concentration, $[Mn(II)]$, $[HClO_4]$, ionic strength and temperature.

The dependence of first-order rate constants on the hydroxy -acid concentration is presented in Table 1. It proves the existence of at least two parallel reaction paths consuming MnO_4^- during the slow stage. One that is independent of the substrate concentration may be assigned to the direct reduction of permanganate by Mn(II), while the other to the consumption of

Mn(VII) by DL-hydroxybutanedioic or 2-hydroxypropionic acid. Mn(II) catalyses the process.

By subtracting the contribution k_0 of the Mn(II)-Mn(VII) reaction, a non-linear dependence of Δk_{obsd} as a function of the organic substrate has been obtained. It is possible to make such difference because both processes follow a first-order dependence with respect to Mn(VII). A tendency of levelling off has been observed. It is more pronounced for malic acid.

Strictly speaking, the difference Δk_{obsd} should also contain the autocatalytic effect of generated Mn(II). Because Mn(II) has been used in large excess, the autocatalytic effect of produced Mn(II) is insignificant as compared to the catalytic one. At constant acidity the increment of observed rate coefficient on substrate concentration could be described by equation (4) where [ROH] stands for the concentration of the substrate. It is of the "one-plus" form of the rate law [24] and can be transposed into a linear form by making reciprocals (see equation 5). Such a rate law indicates the involvement of a pre-equilibrium [24].

$$\Delta k_{obsd} = \frac{a[ROH]}{1 + b[ROH]} \quad (4)$$

$$\frac{1}{\Delta k_{obsd}} = \frac{b}{a} + \frac{1}{a} \frac{1}{[ROH]} \quad (5)$$

As presented in figure 3, the plot of equation (5) has given straight lines with good correlation coefficients. In the case of malic acid oxidation $r = 0.9951$ and the parameters $b/a = 64.6 \pm 1.6$ (s) and $1/a = 0.60 \pm 0.06$ (mol.dm⁻³s). In the case of lactic acid the corresponding values were: $r = 0.9971$, $b/a = 69.0 \pm 5.0$ (s) and $1/a = 1.48 \pm 0.14$ (mol.dm⁻³s). The similar behaviour proves that both hydroxy acids react likewise.

Table 2.

The effect of HClO₄ concentration on the slow step; [Mn²⁺] = 5.0x10⁻², [MnO₄⁻] = 1.0x10⁻⁴, [ROH] = 5.0x10⁻³, $\mu = 0.75$ and 297 K.

[H ⁺] (mole/L)	0.08	0.16	0.32	0.48
10 ³ x k_{obsd} (s ⁻¹) - MA	9.39	8.35	7.13	6.26
10 ³ x k_{obsd} (s ⁻¹) - LA	4.35	4.27	4.23	4.20

The effect of hydrogen ion concentration on the rates is presented in table 2. It proves the slowing down of rate with increasing acid concentration. The inverse dependence on [H⁺] suggests some complex formation between Mn(II) and the α -hydroxy acids. Similar dependence on [H⁺] has already been established for oxalic acid oxidation [7, 8, 13].

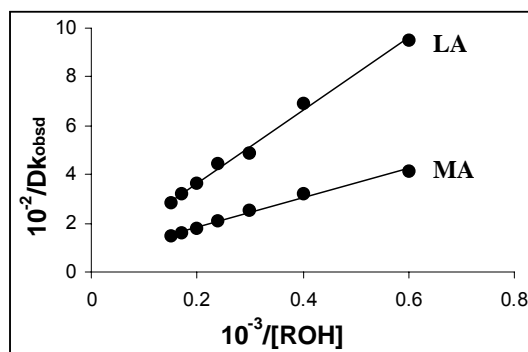


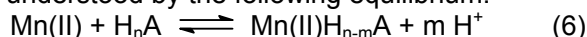
Figure 4. The plot of equation (5) for both malic and lactic acid under experimental conditions given in Table 1.

Table 2.

The effect of HClO₄ concentration on the slow step; [Mn²⁺] = 5.0x10⁻², [MnO₄⁻] = 1.0x10⁻⁴, [ROH] = 5.0x10⁻³, μ = 0.75 and 297 K.

[H ⁺] (mole/L)	0.08	0.16	0.32	0.48
10 ³ x k _{obsd} (s ⁻¹) - MA	9.39	8.35	7.13	6.26
10 ³ x k _{obsd} (s ⁻¹) - LA	4.35	4.27	4.23	4.20

The fact that malic acid is more influenced as compared to lactic acid could be understood by the following equilibrium:



In equation (6) m is greater for malic acid than for lactic acid. Autocatalysis by Mn(II) is caused by the involvement of the Mn(II)-hydroxy acid complex in the reduction of Mn(VII). Since Mn(II) is either an auto-catalyst if absent from the initial mixture or a catalyst if present at the beginning of run, it is essential to determine the order of the reaction with respect to it. Measurements have been made using various concentration of Mn(II). The observed first-order rate constants are given in table 3.

By plotting k_{obsd} versus the catalyst concentration, a parabolic dependence was obtained. Fitting of data leads to the relationships (7) and (8) for malic and lactic acid, respectively.

$$k_{\text{obsd}} = 0.0020 + 0.016 [\text{Mn(II)}] + 0.54 [\text{Mn(II)}]^2 \quad (\text{s}^{-1}) \quad (7)$$

$$k_{\text{obsd}} = 0.0022 + 0.014 [\text{Mn(II)}] + 0.49 [\text{Mn(II)}]^2 \quad (\text{s}^{-1}) \quad (8)$$

Correlation coefficients are 0.9948 and 0.9932, respectively. Equations (7) and (8) suggest the involvement of two reaction paths, one of first-order and the other of second-order with respect to Mn(II). These have comparable contributions to the overall rate.

Table 3.

The effect of Mn(II) concentration upon apparent first-order rate constants;
 $[H^+] = 0.32$, $[ROH] = 5.0 \times 10^{-3}$, $[MnO_4^-] = 1.0 \times 10^{-4}$ and $\mu = 0.75$.

[Mn(II)] (mole/L)	$10^3 k_{obsd} (s^{-1})$ - MA (at 290.5K)	$10^3 k_{obsd} (s^{-1})$ - LA (at 297 K)
0.00	2.01*	2.21*
1×10^{-4}	2.13	---
1×10^{-3}	2.25	2.66
1×10^{-2}	2.31	3.00
2×10^{-2}	2.52	---
3×10^{-2}	3.16	3.10
4×10^{-2}	3.38	---
5×10^{-2}	4.00	4.13
6×10^{-2}	4.53	---
7×10^{-2}	---	5.66
9×10^{-2}	---	7.20

*) measured after the induction period

The results can be explained in mechanistic terms by the involvement, beside MnO_4^- , of a monomeric and a dimeric Mn(II) – substrate complex, respectively. As presented in table 4, modification of ionic strength has some effect on the rates. $LiClO_4$ has been used to obtain the desired ionic strength. The effect is quite different for the two oxidised substrates: a decreasing effect on malic acid and a slight increasing effect on the lactic acid oxidation.

Table 4.

The effect of ionic strength on the first-order rate constant;
 $[ROH] = 5.0 \times 10^{-3}$, $[H^+] = 0.32$, $[Mn(II)] = 5.0 \times 10^{-2}$, $[MnO_4^-] = 1.0 \times 10^{-4}$ and 297 K.

μ (mole/L)	0.47	0.75	1.07	1.47
$10^3 k_{obsd} (s^{-1})$ - MA	8.33	7.13	6.95	6.51
$10^3 k_{obsd} (s^{-1})$ - LA	4.03	4.23	4.53	5.07

A plot of $\log k_{obsd}$ as a function of $\sqrt{\mu} / (1 + \sqrt{\mu})$ gave lines with opposite slopes: $-(0.89 \pm 0.10)$ for malic acid and $+(0.83 \pm 0.10)$ for lactic acid, respectively. The correlation coefficients were not very good: 0.9667 and 0.9631, respectively. This unusual behaviour cannot be interpreted only on the basis of the primary salt effect, but should take into consideration the effects of ionic strength on the equilibria involved.

Reaction mechanism. Presented data suggest that more complicate rate terms have to be considered to account for the disappearance of permanganate. At least three parallel paths are involved in bringing about the consumption of the oxidising species. These are:

- 1) The direct interaction between hydroxy acid and permanganate ion;
- 2) The reduction of permanganate by Mn(II) ion in acidic media and the formation of Mn(III) species that further oxidise the organic substrate to the products in fast steps;
- 3) The involvement of some Mn(II)-hydroxy acid complexes in reaction with Mn(VII).

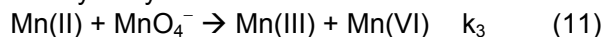
Such detailed reaction paths are consistent with experimental observations and literature data [13].

The formation of an ester by the condensation process (3) is a rapid pre-equilibrium followed by slower steps, yielding either a free radical and Mn(VI) in a mono-equivalent electron transfer process (step 9), or a keto-acid and Mn(V) in a di-equivalent electron transfer process (step 10).



Similar to the case of chromate esters [25-27], the permanganic ester has a smaller molar absorptivity at 525 nm as compared to that of MnO_4^- . This fact would explain the steep decrease of the absorbance immediately after mixing. Intermediate oxidation states of manganese are obviously involved in the reaction and will eventually generate Mn(II) in quite rapid steps in acidic media.

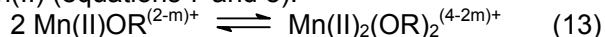
The direct reduction of permanganate by Mn(II) has been observed in the absence of hydroxy acid.



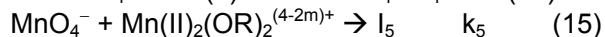
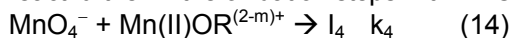
It yields Mn(III) that further interacts with the hydroxy acid to form a complex by binding the substrate as ligand. This complex undergoes an intramolecular electron transfer within a rapid step:



On the other hand, Mn(II) can also interact with the hydrox acid to form some complexes that further suffer the oxidation to Mn(III). The involvement of a dimeric species [28-30] explains the second order with respect to Mn(II) (equations 7 and 8).



These complexes react further in the oxidation steps with MnO_4^- [13], as follows:



The intermediates I_4 and I_5 , which might be some ion-pairs, will produce Mn(III) and eventually the oxidation products.

The above-suggested mechanism should lead to a rate law consistent with the experimental observations. By taking into account both

the rate-determining step for each of the paths and the equilibria involved, the disappearance of the coloured Mn(VII) species that contribute to the absorbance could be written as follows:

$$-\frac{d[Mn(VII)]}{dt} = \left\{ \frac{k_1 K_1 [ROH][H^+]}{1 + K_1 [ROH][H^+]} + k_3 [Mn(II)] + \frac{k_4 K_2 [Mn(II)][ROH]}{[H^+]^m} + \frac{k_5 K_2 K_3 [Mn(II)]^2 [ROH]^2}{[H^+]^{2m}} \right\} [MnO_4^-] \quad (16)$$

The pseudo-first-order rate constant is the expression in parenthesis in equation (16). Because there are no experimental means to discriminate between steps (9) and (10), only process (9) standing for the decomposition by electron-transfer of the permanganate ester has been considered. Anyhow, the formalism is the same. On the other hand, polymerisation experiments proved the presence of free radicals during the oxidation. The rate expression explains the negative dependence on the concentration of hydrogen ion as well as the different behaviour of the two substrates (because m has different values for malic and lactic acids).

When Mn(II) is not added to the reaction mixture, the last two terms in equation (16) explain the autocatalysis. When it is present from the beginning of the run and also has a relatively high concentration, the terms on Mn(II) dominate in the sum and the contribution of Mn(II) as reaction product is insignificant as compared to the added Mn(II). It explains the influence of hydrogen ion on the rate. If we subtract from the pseudo-first-order rate constant its value in the absence of the substrate, the second and the third term in the first order apparent rate coefficient (equation 17) will disappear:

$$\Delta k_{obsd} = \left\{ \frac{k_1 K_1 [ROH][H^+]}{1 + K_1 [ROH][H^+]} + \frac{k_4 K_2 [Mn(II)][ROH]}{[H^+]^m} + \frac{k_5 K_2 K_3 [Mn(II)]^2 [ROH]^2}{[H^+]^{2m}} \right\} \quad (17)$$

In the absence of Mn(II) and at the beginning of the process the first term prevails, hence:

$$\Delta k_{obsd} = \frac{k_1 K_1 [ROH][H^+]}{1 + K_1 [ROH][H^+]} \quad (18)$$

This expression accounts for the direct interaction between HMnO₄ [31] and the hydroxy acid. It is of the form of equation (6). Hence, one can calculate k_1 (or the sum $k_1 + k_2$) as well as K_1 from the values $1/a$ and b/a obtained from the experimental rate constants. The results at 297 K are $k_1 = (1.55 \pm 0.04) \times 10^{-2}$ (s⁻¹) and $K_1 = 335 \pm 41$ (M⁻¹) in the case of malic acid and $k_1 = (1.45 \pm 0.10) \times 10^{-2}$ (s⁻¹) and $K_1 = 146 \pm 25$ (M⁻¹) in the case of lactic acid, respectively.

The decomposition of the ester condensed compound to form free radicals and some intermediate oxidation states of manganese proceeds at

about the same rate for both substrates. The esters formation constants are different but quite large for both hydroxy acids to provide an important fraction of permanganate condensed to these. The value of the ratio

$$\frac{[ROMnO_4^-]}{[Mn(VII)]_t} = \frac{K_1[ROH][H^+]}{1 + K_1[ROH][H^+]}$$

suggests that the reaction takes place with an important fraction of the product *via* direct interaction between substrate and permanganate.

In conclusion, the oxidation of both malic and lactic acid by permanganate occurs in acidic media by means of a rather complicated mechanism. This involves at least three parallel reaction paths that compete to the consumption of the coloured species. The proposed detailed reaction paths are consistent with the experimental observations, the autocatalytic behaviour as well as with the literature data.

Acknowledgements

The authors gratefully acknowledge the financial support of Romanian Government, Ministry of Education and Research, Council for Scientific Research in Universities (CNCSIS), grant No. A/337/2006.

REFERENCES

1. R. Stewart, "Oxidation in Organic Chemistry", K. B. Wiberg Ed., Acad. Press New York 1965, 1-30; D. Benson, "Mechanisms of Oxidation by Metal Ions", Elsevier, Amsterdam, 1976, 149.
2. A.Y. Drummond, W.A. Waters, *J. Chem. Soc.*, **1953**, 2, 435; R.G. Panari, R.B. Chougale, S.T. Nandibewoor, *J. Phys. Org. Chem.*, **1988**, 11, 448.
3. V. Pimienta, D. Lavabre, G. Levy, J.C. Micheau, *J. Phys. Chem.*, **1994**, 98, 3294.
4. J.W. Ladbury, C.F. Cullis, *Chem. Rev.*, **1958**, 58, 403; M.J. Insuasti, F. Mata-Perez, M.P. Alvarez-Macho, *Collect. Czech. Chem. Commun.*, **1994**, 59, 28; *idem*, **1996**, 61, 232; *idem*, *Int. J. Chem. Kinet.*, **1995**, 27, 507; *idem*, *An. Quim.*, **1991**, 87, 877.
5. R.M. Noyes, *Trans. New York Acad. Sci., Ser. II*, **1951**, 13, 314.
6. J. M. Malcolm, R.M. Noyes, *J. Am Chem. Soc.*, **1952**, 74, 2769.
7. S.J. Adler R.M. Noyes, *J. Am. Chem. Soc.*, **1955**, 77, 2036.
8. T.J. Jones, R.M. Noyes, *J. Phys. Chem.*, **1983**, 87, 4686.
9. M. Ganapathisumbramanian, *J. Phys. Chem.*, **1988**, 92, 414.
10. D.R. Rosseinsky, M.J. Nicol, *Trans. Faraday Soc.*, **1965**, 61, 2718.
11. J.T. Morrow, S. Perlman, *Inorg. Chem.*, **1973**, 12, 2453.
12. T. Ernst, M. Wawrzenczyk, M. Wronska, *Z. Physik. Chem. (Leipzig)*, **1980**, 261, 306.

13. R.T. Powell, T. Oskin, M. Ganapathisubramanian, *J. Phys. Chem.*, **1989**, *93*, 2718.
14. A. Rustoiu-Csavdari, I. Baldea, M.C Pasc, *Proceedings of the 13-th International Congress of Chemical and Process Engineering, CHISA'98*, Praha, Czech Republic, 23-28 August, **1998**, 7122.
15. C.S. Reddy, *Oxid. Commun.*, **1988**, *12*, 33.
16. V. Sharma, P.K. Sharma, V. Mishra, *Oxid. Commun.*, **1988**, *11*, 275.
17. M.M.I. Montegui, M.P. Alvarez-Macho, *Anal. Quim.*, **1990**, *86*, 146.
18. I. Baldea, C. Calin, *Rev. Chim.*, **1998**, *49*, 665; S. Bungau, I. Baldea L. Copolovici, *Rev. Chim.*, **2003**, *54*, 213.
19. M.C.R. Symons, *J. Chem. Soc.*, **1953**, 3956.
20. B.K. Satsangi, S. Kothari, *J. Ind. Chem. Soc.*, **1977**, *74*, 16.
21. A. Shaabani, A. Bazgir, D.G. Lee, *Synth. Commun.*, **2005**, *35*, 571; A. Shaabani, F. Tavasoli-Rad, *Synth. Commun.*, **2004**, *34*, 3595.
22. S. Vivekanandan, K. Venkatarao, M. Santappa, *Indian J. Chem.*, **1980**, *19A*, 364.
23. F. Freeman, C.O. Fuselier, C.R. Armsted, C.E. Dalton, P.A. Davidson, E.M. Karchesfski, D.E. Krochman, M.N. Johnson, N. Jones, *J. Am. Chem. Soc.*, **1981**, *103*, 1154; F. Freeman, D. Lynn Bond, S.M. Chernow, P.A. Davison E.M. Karchefsky, *Int. J. Chem. Kinet.*, **1978**, *10*, 911.
24. F.P. Helfferich, "Kinetics of Multistep Reactions", 2-nd Ed. Elsevier, Amsterdam 2004, in "Comprehensive Chemical Kinetics", N.J.B. Green Ed., Vol. 40. (Chapt. 3 and Chapt. 7).
25. R. Asopa, V. Sharma, P.K. Sharma, K.K. Banerji, *J. Chem. Res. Synap*, **1990**, 252.
26. M. COHEN, P.S. Westheimer, *J. Am. Chem. Soc.*, **1952**, *74*, 4387.
27. U. Klänig, M.C.R. Symons, *J. Chem. Soc.*, **1961**, 3204.
28. G. Davies, *Coordin. Chem. Rev.*, **1969**, *4*, 199.
29. M.I. Hussain, F. Ahmad, *Transition Met. Chem.*, **1990**, *15*, 185.
30. A. McAuley, *Coordin. Chem. Rev.*, **1970**, *5*, 245.
31. N. Bailey, A. Carrington, K.A.K. Lott, M.C.R. Symons, *J. Chem. Soc.*, **1960**, 290; K.W. Hicks, J.K. Sutter, *J. Phys. Chem.*, **1971**, *75*, 1107.

ALEXANDRA CSAVDARI AND IOAN BALDEA

*Dedicated to Professor Ionel Haiduc,
President of The Romanian Academy at his 70th anniversary*

A PARADIGM FOR O-O BOND CLEAVAGE IN FERRIC-HYDROPEROXO COMPLEXES

RADU SILAGHI-DUMITRESCU*

ABSTRACT. Using density functional (DFT) calculations, heterolytic oxygen-oxygen bond cleavage is found to be extremely facile in heme and non-heme ferric-hydrogen peroxide complexes, Fe(III)-OH-OH. These findings question the need to invoke double protonation of the “distal” oxygen atom in Fe(III)-O-OH complexes as the universal mechanism of O-O bond cleavage in biological systems.

Introduction

Controlled activation of oxygen-oxygen bonds in hemoproteins has been at the heart of breakthrough moments in the development of modern science, both in terms of concepts and in terms of methodology. [1-10] In heme and non-heme iron complexes, O-O bond cleavage is generally accepted to occur via $[\text{Fe(III)-O-OH}]^{2+}$ intermediates, in processes of vast biological significance.[1-12] In biological systems, this decay of Fe(III)-O-OH species is heterolytic; this is presumably due to proton donors placed strategically at enzyme active sites, leading to a doubly-protonated $[\text{Fe(III)-O-OH}_2]^{3+}$ (oxy-water) state which decomposes to water and a high-valent $[\text{FeO}]^{3+}$ species (formally Fe(V)).[12-15] Alternatively, when such proton donors are not available (e.g., in synthetic model compounds), homolytic decay of $[\text{Fe(III)-O-OH}]^{2+}$ to $[\text{FeO}]^{2+}$ (formally Fe(IV)) and hydroxyl radical, $\bullet\text{OH}$, has been reported; the extraordinary toxicity of $\bullet\text{OH}$ would justify the choice of a heterolytic mechanism in biological systems.[6,11,16-19] Related to the double-protonation heterolytic mechanism, it is generally believed that alteration of proton delivery, leading to a doubly-protonated $[\text{Fe(III)-OH-OH}]^{3+}$ species rather than to “oxy-water”, is responsible for “uncoupling” processes, whereby the peroxide substrate leaves the active site as H_2O_2 , rather than undergo O-O bond cleavage.[8] Reported here are density functional calculations challenging these assumptions, and pointing to $[\text{Fe(III)-OH-OH}]^{3+}$ species as competent substrates for O-O heterolytic O-O bond cleavage in biological systems.

Results and discussion

Non-heme iron. Activated bleomycin (ABLM) has been characterized as a non-heme Fe(III)-O-OH (ferric-hydroperoxo) complex.[11,19] ABLM oxidatively

* Department of Chemistry, “Babeș,-Bolyai” University, Cluj-Napoca RO-400028, Romania

A PARADIGM FOR O-O BOND CLEAVAGE IN FERRIC-HYDROPEROXO COMPLEXES

damages nucleic acids, in a process thought responsible for bleomycin's therapeutic action. Although an initial hypothesis was that ABLM's oxidative action was due to cleavage of the O-OH bond and transient formation of a strongly-oxidizing $[\text{FeO}]^{2+}$ or $[\text{FeO}]^{3+}$ species, it is now known that O-O bond cleavage is energetically unfavourable in Fe(III)-O-OH ABLM.[16,19] By contrast, Figure 1 shows that elongation and cleavage of the O-O bond in a Fe(III)-OH-OH bleomycin model (i.e., a protonated version of the classical ABLM ferric-hydroperoxide) is intrinsically extremely facile.[20] The final products of this O-O bond cleavage reaction are a water molecule and a $[\text{FeO}]^{3+}$ (formally Fe(V)) bleomycin adduct, which is expected to be a strong oxidant and may account for bleomycin's therapeutic action. It may be speculated that O-O bond cleavage in ABLM is in fact triggered by specific proton donation upon binding to the substrate, DNA. These findings on O-O bond cleavage in protonated ABLM are strongly reminiscent to those recently reported for another non-heme Fe-OH-OH complex, where initial homolytic dissociation of the HO-OH bond was accompanied by a subsequent hydrogen atom abstraction by the leaving OH radical, leading to an iron-oxo moiety and water as the final products.[21]

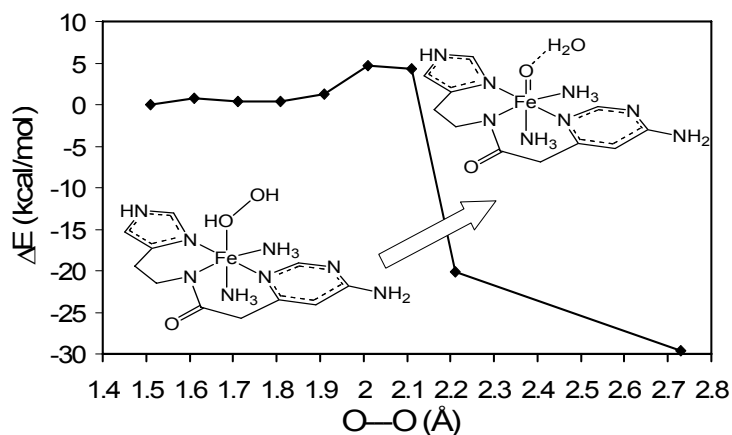


Figure 1. Potential energy surface, following O-O bond elongation in a bleomycin Fe(III)-OH-OH model (structure shown in inset, left lower corner). Geometries were optimized with the HO-OH distance constrained to values indicated in the plots, starting from the equilibrium value of 1.51 Å. Energy differences are plotted for each model, with the energy of the equilibrium structure (far left side of the plot) taken as reference for each model. At an O-O distance of 2.2 Å, both protons originating from the HOOH ligand were found on the leaving oxygen atom, yielding the structure depicted in the inset, upper right corner. Further optimization without any geometry constraints led to a final O-O distance of ~2.7 Å (rightmost data point in the plot).

Heme iron. Fe(III)-O-OH complexes are a common point in the mechanisms of all oxygen and peroxide-activating heme enzymes, including peroxidases and heme oxygenase. [1-10] In peroxidases, addition of a second proton to lead to the doubly-protonated $[\text{Fe(III)-O-OH}_2]^{3+}$ (oxy-water) state is accepted as the dominant mechanism of O-O bond cleavage.[2,12] By contrast, in heme oxygenase proton donation is thought to occur at the iron-bound oxygen atom of a Fe(III)-O-OH intermediate, assisting the departing OH group as it attacks the meso carbon on the porphyrin ring.[22] Figure 2 shows that, similar to the ABLM case, a heme Fe(III)-OH-OH complex is catalytically competent in the heme oxygenase reaction, in line with an independent recent report by Shaik and co-workers.[23] The even more remarkable observation is that, along the reaction coordinate for the heme oxygenase reaction, i.e., as the FeO(H)OH---meso carbon distance is decreased, O-O bond cleavage occurs before any significant interaction between oxygen and carbon develops.

Indeed, as shown in Figure 3, at an oxygen-carbon distance of 2.3 Å the O-O bond is already broken. This implies that the O-O bond in heme $[\text{Fe(III)-OH-OH}]^{3+}$ systems is *intrinsically weak*. Lifting any geometrical constraints from the model initially optimized with an O---C distance of 2.3 Å leads, as in the case of the $[\text{Fe(III)-OH-OH}]^{3+}$ doubly-protonated ABLM model, to hydrogen abstraction by the departing OH moiety, yielding a water molecule and a non-protonated $[\text{FeO}]^{3+}$ moiety as the final products (cf. Figure 3).

The catalytic competence of a Fe(III)-OH-OH intermediate is in agreement with the well-established “peroxide shunt” notion for P450 monooxygenases, i.e. that reaction of ferric P450 with H_2O_2 (presumably via Fe(III)-OH-OH intermediate) and with a hydrocarbon does indeed generate the same product as the “normal” catalytic cycle.[24] Site-directed mutagenesis studies aimed at disturbing the proton delivery network in P450 had the effect of decreasing the enzyme efficiency via H_2O_2 liberation (“uncoupling”) and were interpreted as evidence for increased formation of the Fe(III)-OH-OH tautomer, which, unlike “Fe(III)-O-OH₂” tautomer, would release H_2O_2 rather than hydroxylate the substrate.[8,12] However, the effects of these mutations can be alternatively interpreted as affecting the polarity and/or sterics at the active site, which in turn are known to affect the reduction potentials and/or spin state of the heme.[25] The calculations reported herein assume an $S = 1/2$ state for the Fe(III)-OH-OH state. Indeed, coordination of water (a ligand similar to H_2O_2) to P450 is enough to change the spin state from $S=5/2$ (pentacoordinate) to $S=1/2$ (aqua).[8] The iron-oxygen bond in $S=1/2$ Fe(III)-OH-OH is relatively short, apparently allowing sufficient interaction between iron and peroxide orbitals to facilitate O-O bond cleavage. Such orbital interactions would be drastically

diminished in a high-spin state, where a distinctly longer Fe-O bond is predicted.[26] Thus, formation of a certain percentage of *high spin* state for Fe(III)-OH-OH may be the cause of experimentally observed[8] uncoupling in P450. Related to P450 uncoupling, the catalytic cycle of superoxide reductases (SOR)[27-30] involves liberation of H₂O₂ from a ferric-peroxo intermediate. The SOR active site contains a ferric ion with an axial cysteine ligand and four equatorial nitrogen ligands, similar to P450.[31] Unlike the buried porphyrin in P450, the SOR nitrogen ligands belong to neutral imidazoles, and the iron is solvent-exposed.[31] The combination of these structural features appears to result in a distinct preference of the SOR ferric site for high-spin states: even with a carboxylate coordinated to its sixth position, the octahedral SOR site is still high-spin (S=5/2).[32] This preference for high-spin states is presumably essential for SOR in avoiding O-O bond cleavage at the *Fe(III)-OH-OH* stage (which, in light of the results reported herein, may be the state where the SOR site must make efforts to avoid O-O bond cleavage, as opposed to previous proposal involving Fe(III)-O-OH as the critical step[28,30,32]).

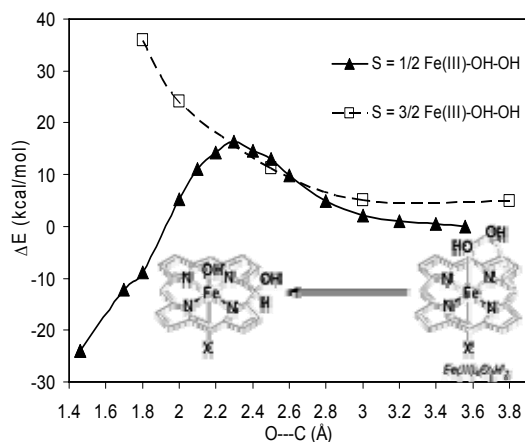


Figure 2. Potential energy surface, following meso-hydroxylation reactions in a Fe(III)-H₂O₂ as well as in a protonated Compound I ("Compound I-H); X = imidazole. Geometries were optimized with the O—C distances (shown as dotted line in the chemical structure on the far right of the diagram) constrained to values indicated in the plots, starting from the equilibrium geometry with C—O ~3.8 Å, and shortening this distance by amounts indicated in the plot. Energy differences are plotted for each model, with the energy of the S=1/2 equilibrium structure (far right side of the plot) taken as reference (zero). No O-O bond cleavage was found to occur for the equivalent S = 3/2 Fe(III)-OH-OH model under the conditions used here (instead, at the left-most point of the S=3/2 plot, O—C = 1.8 Å, the Fe-O bond was irrevocably broken).

As illustrated by Figure 2, whereas O-O bond cleavage is extremely facile in low-spin $[\text{Fe(III)-OH-OH}]^{3+}$ complexes such as those examined in the present work, it is essentially impossible in higher spin states; this is due to very long ($\sim 3 \text{ \AA}$) initial $\text{Fe-O}_2\text{H}_2$ distances which preclude efficient iron-oxygen interaction.[20] This points out to the need for the $[\text{Fe(III)-OH-OH}]^{3+}$ state to be low-spin ($S=1/2$), or perhaps to be preceded by or in equilibrium with a sigly-protonated low-spin $[\text{Fe(III)-O-OH}]^{2+}$ state, where the Fe-OOH bond would be significantly shorter.

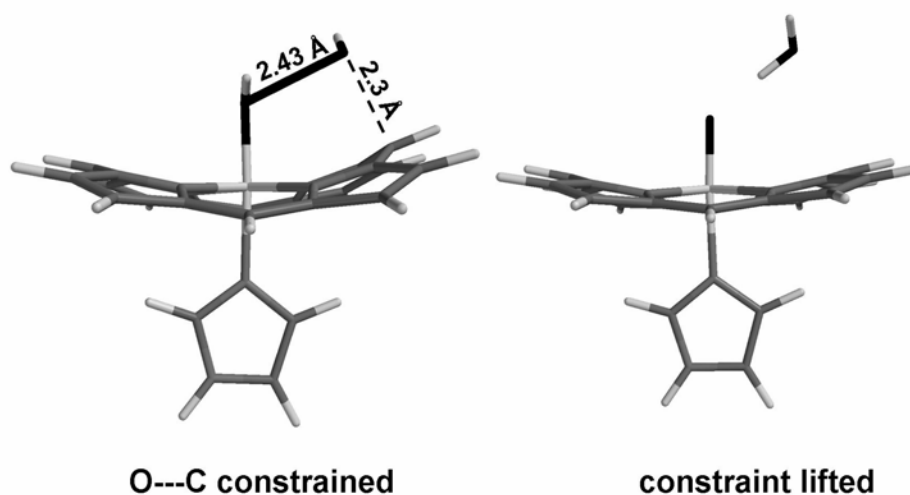


Figure 3. Optimized geometries for heme oxygenase models. Left: Fe(III)-OH-OH adduct, with the $\text{O}-\text{C}$ distance constrained to 2.3\AA , modelling a putative state on the reaction pathway leading to meso-hydroxylation. Right: same model, optimized after lifting the $\text{O}-\text{C}$ geometry constraint. Colour coding: iron and hydrogen - white, oxygen - black, carbon and nitrogen - grey.

Conclusion

O-O bond cleavage in representative examples of heme and non-heme Fe(III)-OH-OH complexes is extremely facile – perhaps even more facile than in the corresponding Fe(III)-O-OH complexes. These findings question the need to invoke the “oxy-water” state, $[\text{Fe(III)-O-OH}_2]^{3+}$, as a necessary intermediate in heterolytic O-O bond cleavage within biological systems.

Experimental

Density functional theory (DFT) methods are the main computational tools currently applied to characterization of geometries and electronic

structures of transition metal enzyme active sites and to their reaction mechanisms. For transition metal complexes, DFT usually provides very reliable geometries, but may fail in describing subtle details of spin densities.[3,6,33-36] Geometries for all models in the present work were optimized in the *Spartan* software package[37,38] without any geometry or symmetry constraints, unless otherwise specified. The UBP86 functional, which uses the gradient corrected exchange functional proposed by Becke (1988)[39] and the correlation functional by Perdew (1986),[40] and the 6-31G** basis set (in its numerical variation, DN**) were used as implemented in the *Spartan* software package. For SCF calculations the energy convergence criterion was 10^{-6} hartrees. For geometry optimization, convergence criteria were set to 4.5×10^{-4} hartrees/bohr (maximum gradient criterion) and 1.8×10^{-3} Å (maximum displacement criterion). The unrestricted formalism was used throughout, i.e., the spin-up and spin-down electrons belonging to one given molecular orbital were allowed to have different energies.

REFERENCES

1. H. B. Dunford, "Peroxidases in Chemistry and Biology" (J. Everse, K. E. Everse, and M. B. Grisham eds.), CRC Press, Boca Raton 1991, vol. II., p. 2-17,
2. A. N. P. Hiner, E. L. Raven, R. N. F. Thorneley, G. Garcia-Canovas, J. N. Rodriguez-Lopez, *J. Inorg. Biochem.*, **2002**, *91*, 27-34.
3. G. H. Loew, D. L. Harris, *Chem. Rev.*, **2000**, *100*, 407-419.
4. T. L. Poulos, *Adv. Inorg. Chem.*, **1988**, *7*, 1-36.
5. S. Shaik, S. P. de Visser, F. Ogliaro, H. Schwarz, I. Schroder, *Curr. Opin. Chem. Biol.*, **2002**, *6*, 556-567.
6. E. I. Solomon, *PNAS*, **2003**, *100*, 3589-3594.
7. B. M. Hoffman, *Acc. Chem. Res.*, **2003**, *36*, 522-529.
8. M. Sono, M. P. Roach, E. D. Coulter, J. H. Dawson, *Chem. Rev.*, **1996**, *96*, 2841-2887.
9. J. H. Dawson, R. H. Holm, R. H. Trudell, G. Barth, R. E. Linder, E. Nunnernberg, C. Djerassi, S. C. Tang, *J. Am. Chem. Soc.*, **1976**, *98*, 3707.
10. I. Schlichting, J. Berendzen, K. Chu, R. M. Sweet, D. Ringe, G. A. Petsko, S. G. Sligar, *Science*, **2000**, *287*, 1615-22.
11. E. I. Solomon, T. C. Brunold, M. I. Davis, J. N. Kemsley, S.-K. Lee, N. Lehnert, F. Neese, A. J. Skulan, Y.-S. Yang, J. Zhou, *Chem. Rev.*, **2000**, *100*, 235-350.
12. D. L. Harris, G. H. Loew, *J. Am. Chem. Soc.*, **1998**, *120*, 8941-8948.
13. D. L. Harris, *J. Inorg. Biochem.*, **2002**, *91*, 568-585.
14. V. Guallar, D. L. Harris, V. S. Batista, W. H. Miller, *J. Am. Chem. Soc.*, **2002**, *124*, 1430-1437.

15. V. Guallar, M. H. Baik, S. J. Lippard, R. A. Friesner, *Proc. Natl. Acad. Sci. USA*, **2003**, *100*, 6998-7002.
16. N. Lehnert, F. Neese, R. Y. Ho, L. Que, Jr., E. I. Solomon, *J Am Chem Soc*, **2002**, *124*, 10810-22.
17. N. Lehnert, R. Y. N. Ho, L. J. Que, E. I. Solomon, *J. Am. Chem. Soc.*, **2001**, *122*, 12802-12816.
18. N. Lehnert, R. Y. N. Ho, L. J. Que, E. I. Solomon, *J. Am. Chem. Soc.*, **2001**, *123*, 8271-8290.
19. F. Neese, M. Zaleski, K. Loeb, E. I. Solomon, *J. Am. Chem. Soc.*, **2000**, *122*, 11703-11724.
20. R. Silaghi-Dumitrescu, I. Silaghi-Dumitrescu, *Chemtracts Inorg. Chem.*, **2005**, *18*, 595-619.
21. X. Wang, S. Li, Y. Jiang, *Inorg. Chem.*, **2004**, *43*, 6479-6489.
22. R. Davydov, T. Matsui, H. Fujii, M. Ikeda-Saito, B. M. Hoffman, *J. Am. Chem. Soc.*, **2003**, *125*, 16208-16209.
23. P. K. Sharma, R. Kevorkiants, S. P. deVisser, D. Kumar, S. Shaik, *Angew. Chem. Int. Ed.*, **2004**, *43*, 1129-1132.
24. M. Wirstam, M. R. A. Blomberg, P. E. M. Siegbahn, *J. Am. Chem. Soc.*, **1999**, *121*, 10178-10185.
25. T. W. B. Ost, J. Clark, C. G. Mowat, C. S. Miles, M. D. Walkinshaw, G. A. Reid, S. K. Chapman, S. Daff, *J. Am. Chem. Soc.*, **2003**, *125*, 15010-15020.
26. P. Rydberg, E. Sigfridsson, U. Ryde, *J. Biol. Inorg. Chem.*, **2004**, *9*, 203-223.
27. E. Coulter, J. Emerson, D. M. Kurtz, Jr., D. Cabelli, *J. Am. Chem. Soc.*, **2000**, *122*, 11555-11556.
28. R. Silaghi-Dumitrescu, I. Silaghi-Dumitrescu, E. D. Coulter, D. M. Kurtz, Jr., *Inorg. Chem.*, **2003**, *42*, 446-56.
29. M. Kurtz, Jr., E. Coulter, *J. Biol. Inorg. Chem.*, **2002**, *6*, 653-658.
30. J. A. Kovacs, *Chem. Rev.*, **2004**, *104*, 825-848.
31. A. Yeh, Y. Hu, F. J. Jenney, M. Adams, D. Rees, *Biochemistry*, **2000**, *39*, 2499-2508.
32. M. D. Clay, C. A. Cospers, F. E. Jenney, M. W. Adams, M. K. Johnson, *Proc. Natl. Acad. Sci. USA*, **2003**, *100*, 3796-3801.
33. D. L. Harris, *Curr. Opin. Chem. Biol.*, **2001**, *5*, 724-735.
34. P. E. M. Siegbahn, M. R. A. Blomberg, *Annu. Rev. Phys. Chem.*, **1999**, *50*, 221-49.
35. P. E. M. Siegbahn, M. R. A. Blomberg, *Chem. Rev.*, **2000**, *100*, 421-437.
36. R. Silaghi-Dumitrescu, *unpublished results*,
37. *Spartan 5.0, Wavefunction, Inc., 18401 Von Karman Avenue Suite 370, Irvine, CA 92612 U.S.A.*,
38. *SPARTAN '02 for Windows, Wavefunction Inc., 18401 Von Karman Avenue, Suite 370 Irvine, CA 92612*,
39. A. D. Becke, *Phys. Rev.*, **1988**, 3098-3100.
40. J. P. Perdew, *Phys. Rev.*, **1986**, *B33*, 8822-8824.

A PARADIGM FOR O-O BOND CLEAVAGE IN FERRIC-HYDROPEROXO COMPLEXES

*Dedicated to Professor Ionel Haiduc,
President of The Romanian Academy at his 70th anniversary*

NEW GROUP 2 METAL SALTS OF MONODEPROTONATED (3*H*-2-THIOXO-1,3,4-THIADIAZOL-2-YL)THIOACETIC ACID. SYNTHESIS AND VIBRATIONAL CHARACTERIZATION

M.M. VENTER,^{a*} A. PASCU,^a V.N. BERCEAN,^b AND
S. CÎNTĂ PINZARU^c

ABSTRACT. Reaction of the monosodium salt of (3*H*-2-thioxo-1,3,4-thiadiazol-2-yl)thioacetic acid with group 2 metal halides produced the corresponding Mg, Ca, Sr and Ba derivatives. Preliminary vibrational studies on this new series are discussed in terms of FT-IR and FT-Raman spectroscopy. The spectral data are consistent with the deprotonation of the carboxylic unit and the thione tautomeric form of the heterocycle.

Key-words: (3*H*-2-thioxo-1,3,4-thiadiazol-2-yl)thioacetic acid, group 2 metals, FT-IR and Raman spectroscopy.

Introduction

We have recently initiated structural investigations on the new (3*H*-2-thioxo-1,3,4-thiadiazol-2-yl)thioacetic acid and a large range of d metal complexes containing the ligand in its monodeprotonated form.¹⁻³ These studies follow our on-going interest in the chemistry of mercapto-aza type heterocyclic derivatives (i.e. trithiocyanuric acid, *Bismuthiol I* and *II*), which have been proved valuable candidates for coordination and supramolecular chemistry.⁴⁻⁶ In addition, such compounds have found extensive application in analytical chemistry as well as industry.⁷⁻¹⁰

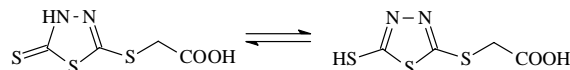
In this paper we wish to report further on the chemistry of 3*H*-2-thioxo-1,3,4-thiadiazol-2-yl)thioacetic acid, C₂HN₂S₃CH₂COOH (**1**). Compound **1**, which can theoretically exist in either thiol (N=C-SH) or thione (HN-C=S) forms (Scheme I), derives from the well known dimercapto-thiadiazol, C₂H₂N₂S₃ (also known as *Bismuthiol I*) by substitution at one of the two SH groups.¹ There are two main reasons for such a substitution. First, the insertion of a new functional group (i.e. carboxyl) might enhance the coordination behavior of the ligand. Second, the asymmetric substitution allows the

^a Faculty of Chemistry and Chemical Engineering, "Babeș-Bolyai" University, RO-400028 Cluj-Napoca, Romania. Fax: 0040-264-590818; Tel: 0040-264-593833; E-mail: monica@chem.ubbcluj.ro.

^b Faculty of Industrial Chemistry and Environment Engineering, "Politehnica" University, RO-300006 Timișoara, Romania.

^c Faculty of Physics, "Babeș-Bolyai" University, RO-400084 Cluj-Napoca, Romania.

conservation of a protonated NCS unit which proved valuable in generating interesting intermolecular interactions, such as coordination (i.e. S-monodentate and S,N-bidentate chelating), hydrogen bonding (i.e. N-H...E, E = N, O, S) and S...S interactions.⁵⁻⁶



Scheme I

Recent crystallographic investigation on the mono-sodium salt of **1**, $[\text{Na}(\text{C}_2\text{HN}_2\text{S}_3\text{CH}_2\text{COO})(\text{H}_2\text{O})_4]\cdot\text{H}_2\text{O}$ (**2**) showed that the molecular structure does not resume to a simple salt but reveals both coordination of the monodeprotonated ligand to Na^+ (i.e. $\text{C}=\text{S}\rightarrow\text{Na}$) and intermolecular hydrogen bonding and S...S interactions.³ In this respect, we have decided to extend our studies in the range of group 2 metal homologues: $[\text{M}(\text{C}_2\text{HN}_2\text{S}_3\text{CH}_2\text{COO})_2]$, M = Mg, **3**; Ca, **4**; Sr, **5**; Ba, **6**. Therefore, the aim of this work is the synthesis of the title series of new derivatives (**3** – **6**) along with their FT-IR and Raman characterization. The vibrational studies could elucidate the occurrence of the thione vs. thiol tautomeric form of the heterocyclic unit in solid state and suggest the most probable coordination sites of the ligand.

Experimental

FT-IR and FT-Raman spectra on solid samples were recorded using a Bruker FT-IR Equinox 55 Spectrometer equipped with an integrated FRA 106 S Raman module. The excitation of the Raman spectra was performed using the 1064 nm line from a Nd:YAG laser with an output power of 250 mW. An InGaAs detector operating at room temperature was used. The spectral resolution was 2 cm^{-1} .

The starting materials were purchased from commercial sources as analytical pure reagents and were used with no further purification. The (3*H*-2-thioxo-1,3,4-thiadiazol-2-yl)thioacetic acid (**1**) and its monosodium salt (**2**) were prepared following a literature protocol.^{1,2}

The group 2 metal derivatives of **1** as monodeprotonated forms **3** – **6**, $[\text{M}(\text{C}_2\text{HN}_2\text{S}_3\text{-CH}_2\text{COO})_2]$, M = Mg, **3**; Ca, **4**; Sr, **5**; Ba, **6**, were synthesised by reacting stoichiometric amounts of **2** with corresponding metal halides $\text{MgCl}_2\cdot 6\text{H}_2\text{O}$, CaCl_2 , $\text{SrCl}_2\cdot 6\text{H}_2\text{O}$ and $\text{BaCl}_2\cdot 2\text{H}_2\text{O}$, respectively, in aqueous solution, at room temperature. Preliminary microanalysis of **2** proved that the monosodium salt is tetrahydrated in solid state. However, the stoichiometry was related to anhydrous products. Therefore, the yields will be corrected as soon as microanalysis will establish the degree of hydration of **3** – **6**. In all cases, the products precipitated at once. After stirring the reaction mixtures for about 30 minutes, the crude products were filtered and recrystallized from

warm distilled water, as colorless crystalline solids. Preparation details and brief characterization of compounds **3** – **6** are given in Table 1.

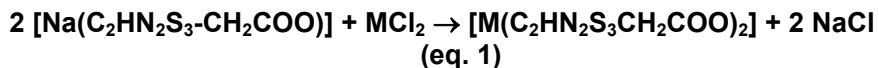
Table 1.
Preparation details and characterization of compounds **3** – **6**.

No.	Compound*	Yield* (%)	mp (°C)
3	[Mg(C ₂ HN ₂ S ₃ -CH ₂ COO) ₂]	52	224-226
4	[Ca(C ₂ HN ₂ S ₃ -CH ₂ COO) ₂]	57	185-187
5	[Sr(C ₂ HN ₂ S ₃ -CH ₂ COO) ₂]	58	226-228 (dec)
6	[Ba(C ₂ HN ₂ S ₃ -CH ₂ COO) ₂]	52	268-270 (dec)

* Due to the lack of microanalysis, the lattice water was ignored in calculations.

Results and discussion

Partial neutralisation of (3*H*-2-thioxo-1,3,4-thiadiazol-2-yl)thioacetic acid, C₂HN₂S₃-CH₂COOH (**1**) with sodium bicarbonate produced the monosodium salt, [Na(C₂HN₂S₃-CH₂COO)] (**2**).^{1,2} Compound **2** was further used in the preparation of four new alkali-earth metal homologues, [M(C₂HN₂S₃CH₂COO)₂], M = Mg, **3**; Ca, **4**; Sr, **5**; Ba, **6** (eq. 1). All the reactions worked in aqueous media, at room temperature. Compounds **3** – **4** are soluble in hot water and were isolated as crystalline solids. All metal derivatives are air and light stable in both solution and solid state.



The FT-IR and Raman spectra of **3** – **6** were recorded in the 4000 – 400 and 3500 – 200 cm⁻¹ spectral ranges, respectively. For the magnesium compound **3**, the Raman spectrum could not be recorded. The most relevant spectral data are listed in Table 2. The following discussion is based on the comparison between the current spectral data recorded for **3** – **6** and the known literature data for **1** and **2**.^{1,2}

The 4000 – 2000 cm⁻¹ spectral range is relevant for the characterization of EH groups (E = O, N, C and S) in IR and/or Raman spectra. The complex carboxylic OH band present in the IR spectrum of **1** (approx. 3100 - 2800 cm⁻¹) disappears in the IR spectra of **3** - **6**, similarly to **2**, as a result of deprotonation of the carboxylic group. The IR spectra show also broad bands at 3446 - 3334 cm⁻¹, which are assigned to the ν(H₂O) modes. The ν(NH) fundamental becomes difficult to locate due to the overlap with the broad ν(H₂O) band previously mentioned. The lack of the characteristic ν(SH) bands – usually assigned at 2600 – 2400 cm⁻¹ – in both IR and Raman spectra of **3** - **6**, confirms the occurrence of the thione tautomer in solid state. In addition, all spectra are consistent with the presence of aliphatic CH groups.

Table 2.
Selected vibrational data (cm⁻¹) for compounds **2** – **6**.

2*		3**	4		5		6		Vibrational assignment	
IR	Ra	IR	IR	Ra	IR	Ra	IR	Ra		
3487 – 3388 m,br		3406 s,br	3446 s,br		3421 – 3334 s,br		3446 s,br		v(H ₂ O)	
3106 sh	2976 w				3088 sh		3109 w,sh		v(NH)	
2939 w	2940 m	2921 w	2922 m	2927 s	2922 w	2924 m	2921 w	2922 m	v _{as} (CH)	
2893 w		2845 w	2852 m		2873 w		2852 w		v _s (CH)	
		1630 vs					1651 mw		δ(H ₂ O)	
1604 vs	1611 vw	1577 vs	1601 vs	1596 vw	1603 vs	1610 vw	1581 vs	1629 vw	v _{as} (COO)	
1518 ms	1515 vw	1527 s	1533 s	1531 vw	1541 ms	1540 vw	1539 s	1456 mw	1533 vw	v(NC)+δ(NH)
1454 m	1457 vs	1450 m	1448 m	1448 vs	1446 m	1446 vs		1454 vs		
1410 s	1406 w	1396 s	1396 s	1396 w	1383 s	1384 m	1394 s	1393 m	δ(CH ₂)	
1117 m	1110 w	1106 w	1101 mw	1104 w	1101 mw	1103 mw	1119 w	1108 w	v(NN)	
1053 s	1055 m	1051 s	1053 s	1060 m	1055 s	1060 m	1053 s	1063 m	v _{as} (S-C=S)	
717 m	723 w	717 s	717 s		717 ms		719 m	726 vw	v _{as} (CSC) _{endo}	
650 w	655 s	646 m	666 m	662 s	650 m	660 s	650 w	656 s	v _s (CSC) _{endo}	

Abbreviations: Ra – Raman, w – weak, mw – medium weak, m – medium, ms – medium strong, s – strong, vs – very strong, br – broad, sh – shoulder, v - stretching, δ - bending, endo – endocyclic.

* Literature data.²

** The Raman spectrum of **3** could not be recorded.

The 2000 – 1000 cm^{-1} spectral range is relevant for both heterocyclic and alkyl-carboxylic units of the monodeprotonated acid. The most important vibrational modes which characterize the heterocyclic unit are the $\nu(\text{C}=\text{N})$, $\nu(\text{N}-\text{N})$ and $\nu_{\text{as}}(\text{S}-\text{C}=\text{S})$ stretchings, assigned in the spectra of **3** - **6** at 1541-1527 and 1456-1446, 1119-1101 and 1063-1051 cm^{-1} , respectively. All spectral data previously mentioned are in good agreement with the corresponding fundamentals reported for compound **1** or homologue heterocyclic derivatives.^{1,11}

In addition to the lack of carboxylic $\nu(\text{OH})$ in the approx. 3100 - 2800 cm^{-1} spectral range, the current region brings new information in support of carboxyl group deprotonation. Thus, the $\nu(\text{C}=\text{O})$ mode assigned for **1** at 1693 cm^{-1} shifts to significantly lower wavenumbers in the spectra of **3** – **6** as a consequence of electron delocalization [$\nu_{\text{as}}(\text{COO})$ 1629 – 1577 cm^{-1}]. As it concerns the $\nu_{\text{s}}(\text{COO})$ fundamentals, it proved again difficult to choose between the plethora of bands located in the expected region (approx. 1450 – 1300 cm^{-1}).¹² In our previous works we have tentatively assigned this mode at 1333 – 1290 cm^{-1} , probably overlapping $\nu(\text{CN})$ modes.^{2,3} Despite the existence of homologues bands in all spectra of **3** – **6** (1309 – 1302 cm^{-1}), we shall not insist on this assignment until new spectroscopic results will support our supposition.

The 1000 – 200 cm^{-1} spectral range shows no unusual features. Many bands located in this region are assigned to group bending and other skeleton fundamentals (i.e. $\nu_{\text{as}}(\text{CSC})_{\text{endo}}$ 726 – 717 and $\nu_{\text{s}}(\text{CSC})_{\text{endo}}$ 666 – 646 cm^{-1}).

Conclusions

Both heterocyclic unit and side chain of the monodeprotonated ligand are well represented in the IR and Raman spectra. It can be concluded that the deprotonation of **1** takes place at the COOH group, while the remaining proton is located on the endocyclic nitrogen atom, giving rise to the thione tautomer. While the $\nu_{\text{as}}(\text{COO})$ mode is undoubtedly assigned in the 1603 – 1577 cm^{-1} range, its $\nu_{\text{s}}(\text{COO})$ counterpart is hard to locate.

REFERENCES

1. M. M. Venter, S. Cinta Pinzaru, I. Haiduc, V. Bercean, *Studia Univ. Babeş-Bolyai, Physica*, **2004**, XLYX(3), 285.
2. M. M. Venter, V. Chis, S. Cinta Pinzaru, V.N. Bercean, M. Ilici, I. Haiduc, *Studia Univ. Babeş-Bolyai, Chemia*, **2006**, LI(2), 65.

3. M. M. Venter, V.N. Bercean, M. Ilici, S. Cinta Pinzaru, *Rev. Roum. Chim.*, **2007**, in press.
4. I. Haiduc, M.F. Mahon, K.C. Molloy, M.M. Venter, *J. Organomet. Chem.*, **2001**, 627, 6.
5. V. Bercean, C. Crainic, I. Haiduc, M. F. Mahon, K. C. Molloy, M. M. Venter, P. J. Wilson, *J. Chem. Soc., Dalton Trans*, **2002**, 1036.
6. M. F. Mahon, K. C. Molloy, M. M. Venter, I. Haiduc, *Inorg. Chim. Acta.*, **2003**, 348, 75.
7. K. Henke, D. A. Atwood, *Inorg. Chem.*, **1998**, 37, 224.
8. V. R. Pedireddi, S. Chatterjee, A. Ranganathan, C. N. R. Rao, *J. Am. Chem. Soc.*, **1997**, 119, 10867.
9. A. Ranganathan, V. R. Pedireddi, S. Chatterjee, C. N. R. Rao, *J. Mater. Chem.*, **1999**, 9, 2407.
10. Ranganathan, V. R. Pedireddi, C. N. R. Rao, *J. Am. Chem. Soc.*, **1999**, 121, 1752.
11. H.G.M. Edwards, A.F. Johnson, E.E. Lawson, *J. Molec. Struct.*, **1995**, 351, 51.
12. K. Nakamoto, "Infrared Spectra and Raman Spectra of Inorganic and Coordination Compounds", John Wiley & Sons, New York, 1986, pp. 233.

*Dedicated to Professor Ionel Haiduc,
President of The Romanian Academy at his 70th anniversary*

CRYSTALLIZED GLASSES WITH ADDITION OF FLY ASH

**FIRUTA GOGA^a, CRINA SUCIU^a, MIRELA ANDREI^a,
MARCEL BENE^b, MARIANA MOCEAN^a**

ABSTRACT. Waste recycling represents a very significant issue for the protection of our environment. Large waste quantities (slag and ashes) are products of the coal extraction industry and its subsequent combustion in thermal power stations. The aim of this paper is to study the possibility of using fly ash from thermal power stations as a raw material in the process of obtaining crystallized glasses. Several glass samples, containing variable fly ash quantities, were elaborated and studied comparatively. The ash was used as a replacement for some initial raw materials. Optical and electronic microscopy, X-ray diffraction and thermo-differential analysis were used for the comparative study.

Introduction

One of the biggest problems for the environmental protection is the recycling of secondary and waste products. These are very well known as generators of impact and risk for the environment and public health. Among the most know are slag heaps, tars and ashes from thermal power stations. All of these are coal burning wastes and usually come in great quantities composing a large part of the environmental pollution problem.

Fly ashes from thermal power stations can be added to the process of obtaining binders, since they are silica-aluminous materials with slow hardening properties. Moreover, they are used as filling materials and to obtain some lightweight aggregates. Their usage for the production of concretes is restricted by the coal content, which should be bellow 3%, due to the fact that it reduces concretes resistance [1].

About 20-30% of the fly ash is used, the remaining quantity is deposited and thus constituting a chemical pollution source, but also an unused economic value.

Vitrification is one of the most efficient methods to reduce the wastes volume by transforming them into potential resources. Recent

^a Faculty of Chemistry and Chemical Engineering, "Babes-Bolyai" University, Arany Janos Street 11, 400028, Cluj Napoca, Romania, Tel: 40-264-593833, Fax: 40-264-593833, E-mail: fgoga@chem.ubbcluj.ro

^b Faculty of Biology and Geology, "Babes-Bolyai" University, Bilascu Street 44, 400015, Cluj-Napoca, Romania

studies [2,3,4] indicate the possibility of capitalizing fly ashes by using them as raw materials to obtain crystallized glasses.

The aim of this paper is to study the possibility of using fly ashes from the Rovinari thermal power station as raw materials to obtain crystallized glasses.

Experimental procedure

In order to choose an oxidic system to obtain these glasses, the fly ashes were firstly characterised.

The mean oxidic composition of the ash (Table 1) indicate a large quantity of silica (54.62%) and iron oxide (7.9%), but also a large quantity of coal (33.03%) which are usually lost as volatile components during further combustion.

Table 1.
The mean oxidic composition of Rovinari fly ash (wt%)

	SiO ₂	Al ₂ O ₃	Fe ₂ O ₃	Na ₂ O	K ₂ O	CaO	MgO	LOI
Fly ash	54.62	1.6	7.9	0.1	1.7	0.85	0.2	33.03

The thermal analysis of the fly ash was performed with a MOM derivatograph up to 1000°C at a heating rate of 10°C/min. The reference sample was Al₂O₃ and the samples were placed in ceramic crucibles.

The oxidation process of coal residues, during combustion, can be observed as an exothermic effect on the DTA curve, between 400-600°C (see Figure 1).

Subjected to a thermal treatment at 1300°C, with one hour plateau, the ash was transformed in an insufficiently melted material, with numerous voids due to the elimination of volatile components. The ash used in following experiments was initially calcinated in an air laboratory furnance in order to eliminate the carbon residues.

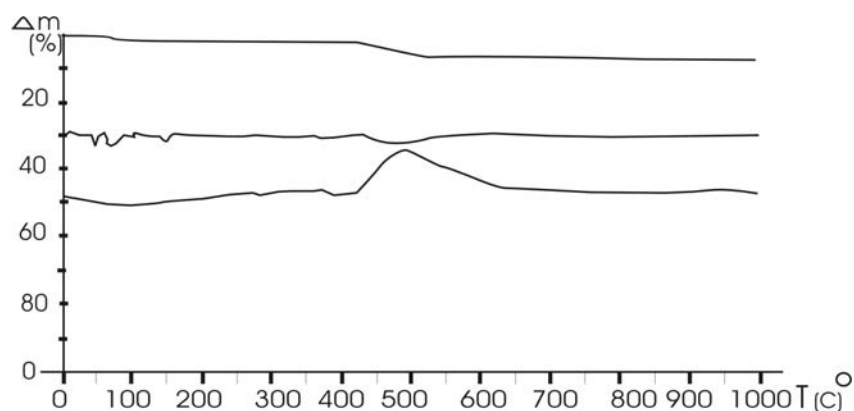


Figure 1. Differential Thermal Analysis curves of the Rovinari fly ash

CRYSTALLIZED GLASSES WITH ADDITION OF FLY ASH

The choice concerning the oxidic system for the desired crystallized glasses was taken considering the oxidic composition of the ash (high iron oxide content) and also the burning temperature of the samples, as a practical reason. Thus, the basic $\text{SiO}_2\text{-CaO-F}_2\text{O}_3$ oxidic system was chosen.

Using literature data [5], the composition of a reference sample was established as: $\text{SiO}_2 = 44.69\%$; $\text{Fe}_2\text{O}_3 = 24.35\%$; $\text{CaO} = 21.25$; $\text{Al}_2\text{O}_3 = 6.27\%$; $\text{MgO} = 3.14\%$. Quartz powder, KO1 kaolin, $\text{FeSO}_4 \cdot 7\text{H}_2\text{O}$, CaCO_3 and $\text{MgCl}_2 \cdot 6\text{H}_2\text{O}$ were used as raw materials [see Table 2].

Table 2.
The oxidic composition of the raw materials (wt%)

	SiO_2	Al_2O_3	Fe_2O_3	Na_2O	K_2O	CaO	MgO	TiO_2	LOI
Ash	54.62	1.6	7.9	0.1	1.7	0.85	0.2	-	33.03
Calcina- ted Ash	81.56	2.39	11.8	0.15	2.54	1.27	0.3	-	-
KO1 kaolin	43.55	38.58	0.8	0.2	0.2	0.3	0.19	0.19	14.79
Quartz powder	99.27	0.1	0.06	0.06	0.02	0.12	0.0	-	0.3
$\text{FeSO}_4 \cdot$ $7\text{H}_2\text{O}$	-	-	28.72	-	-	-	-	-	71.27
CaCO_3	-	-	-	-	-	56	-	-	44
$\text{MgCl}_2 \cdot$ $6\text{H}_2\text{O}$	-	-	-	-	-	-	19.8	-	80.17

Partial replacement of $\text{FeSO}_4 \cdot 7\text{H}_2\text{O}$ with ash was sought. From the total quantity of 23.45% Fe_2O_3 , different ratios of 5%, 10%, 15% and 20%, respectively, came from fly ashes. Nucleation agents, i.e. TiO_2 and Cr_2O_3 , were used for samples R1 and R7. The former constituted the reference sample and the latter contained the largest amount of fly ash. Both nucleation agents were added in excess of 4%. The recipes of the studied glasses are given in Table 3.

The melting treatment was achieved in a laboratory electrical furnace at a maximum temperature of 1300°C , with one hour plateau. Next, the melts were leaked out on a plane surface.

The reference sample R1 was subjected to thermal analysis in order to establish the crystallization thermal treatment. The thermal analysis of the glass was performed in the same way as for the fly ash. An exothermic effect was observed in the temperature range $800\text{-}900^\circ\text{C}$ (see Figure 2).

The crystallization thermal treatment was carried out in two ways:

1. - the samples, obtained after a quick cooling of the melts, were heated up to 850°C and were kept at this temperature for periods between 1 and 5 hours for each sample;

2. - after the initial thermal treatment, the obtained melts were slowly cooled down to 850°C and kept at this temperature for 10 hours.

Table 3.
Recipes of the studied glasses (wt%)

	Ash	Calci-nated Ash	SiO ₂	KO1 kaolin	FeSO ₄ * 7H ₂ O	MgCl ₂ * 6H ₂ O	CaCO ₃	Nucle-ators	
R1	-	-	19.74	8.4	43.84	8.09	19.93	TiO ₂	Cr ₂ O ₃
R ₁ N ₁			19.74					4	
R ₁ N ₂									4
R2	39.9	-	-	6.9	33.56	3.24	19.36		
R3	-	35.33	-	6.6	32.09	7.45	18.53		
R4	-	5.43	15.69	8.2	42.41	8.13	20.1		
R5	-	11.1	11.55	7.97	40.91	8.19	20.31		
R6	-	16.84	7.28	7.79	39.29	8.27	20.53		
R7	-	22.89	2.82	7.58	37.58	8.35	20.76		
R ₇ N ₁	-	22.89	2.82	7.58	37.58	8.35	20.76	4	
R ₇ N ₂	-	22.89	2.82	7.58	37.58	8.35	20.76		4

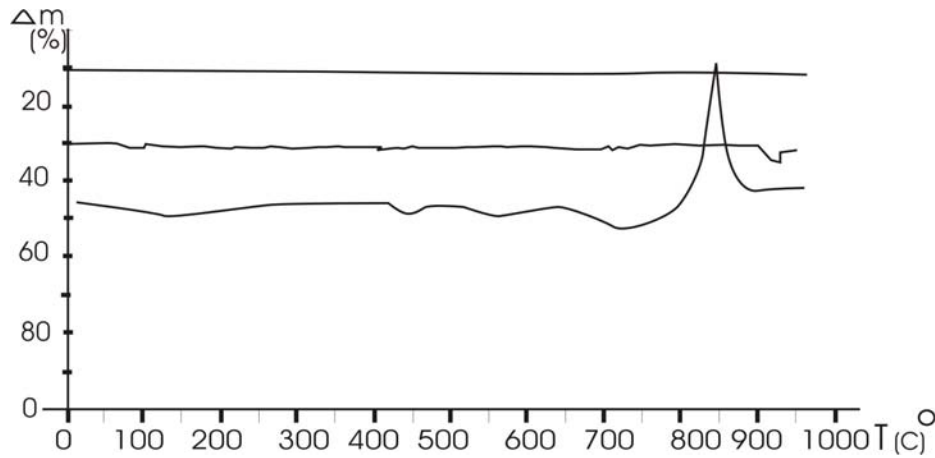


Figure 2. Differential Thermal Analysis curves for the R1 sample

The obtained glasses were studied through:

- Optical microscopy using an optical microscope with polarized light;
- Scanning electron microscopy using a JEOL-100S microscope;
- X-ray diffraction using a DRON3 diffractometer with CuK α radiation.

Results and discussions

Figure 3 contains optical microscopy images for the samples which underwent the first crystallization thermal treatment.

Figures 4 and 5 contain results of the same investigation method for the second thermal treatment samples.

Analysing the microscopy data, the following can be stated:

- the samples which were thermally treated for short periods presented an isotropy similar to glasses, with imperceptible crystallization phenomena;
- the R1 reference sample, treated at 850°C through heating, did not present a perceptible crystalline structure, not even after a 5 hour thermal treatment (see Figure 3 – a, b, c);
- for the samples R7 with high ash content, small and unevenly distributed crystals were observed (see Figure 3 – f, g, h);
- the difference between the samples R1 and R7 shows the nucleation function of the fly ash, which might be explained by the different way of introducing Fe₂O₃ (as FeSO₄ or as Fe₂O₃ from the ash);
- the slowed cooling treatment applied to melts favoured the appearance of phase separations and crystals even for the sample which did not contain any ash.

Generally, there are two types of crystals in the samples. A third one can also be observed in the contact area between the melt and the crucible (see Figure 4a). The samples containing nucleators presented a higher tendency to crystallize. TiO₂ favoured the growth of black dendritic crystals dispersed in a glassy matrix of a lighter colour in both R1N1 (see Figure 4c) and R7N1 (see Figure 5b).

Macroscopically, the samples containing Cr₂O₃ present a surface with voids which can be explained to a possible reaction between itself and a mixture component that leads to gaseous products. The pores can be observed in the microscopic section (see Figure 4d and Figure 5c). The crystals which are developed in the vitreous matrix, in the presence of Cr₂O₃, are different from the TiO₂ ones and presented anisotropy.

The difference between the two nucleators was highlighted through SEM (see Figure 6). Figures 6a and 6b present the samples R1 and R7 and figures 6c and 6d present the samples R7N1 and R7N2 without nucleators which underwent the second crystallisation thermal treatment.

Also, the vitreous phase separation, which is more pronounced in sample R7N2, can be observed through SEM (see Figure 6d).

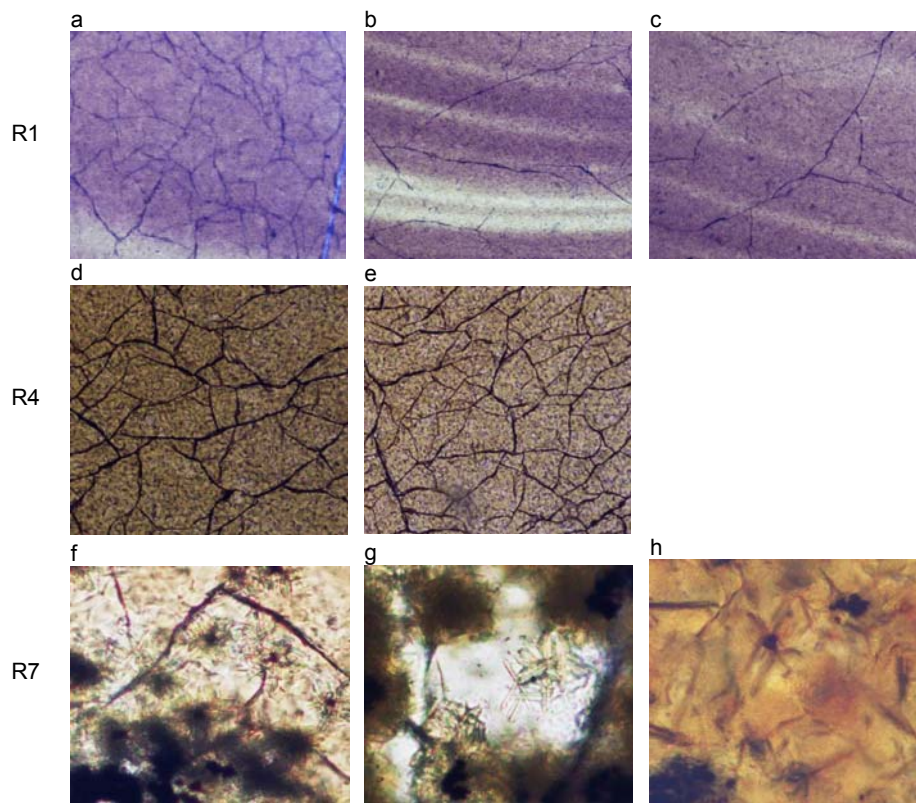


Figure 3. Optical microscopy images of the samples obtained after the first crystallization thermal treatment (x90)

- R1 – a – R1 sample thermal treated at 850°C – 1h plateau
- b – R1 sample thermal treated at 850°C – 3h plateau
- c – R1 sample thermal treated at 850°C – 5h plateau
- R4 – d – R4 sample thermal treated at 850°C – 1h plateau
- e – R4 sample thermal treated at 850°C – 3h plateau
- R7 – f – R7 sample thermal treated at 850°C – 1h plateau
- g – R7 sample thermal treated at 850°C – 3h plateau
- h – R7 sample thermal treated at 850°C – 5h plateau

CRYSTALLIZED GLASSES WITH ADDITION OF FLY ASH

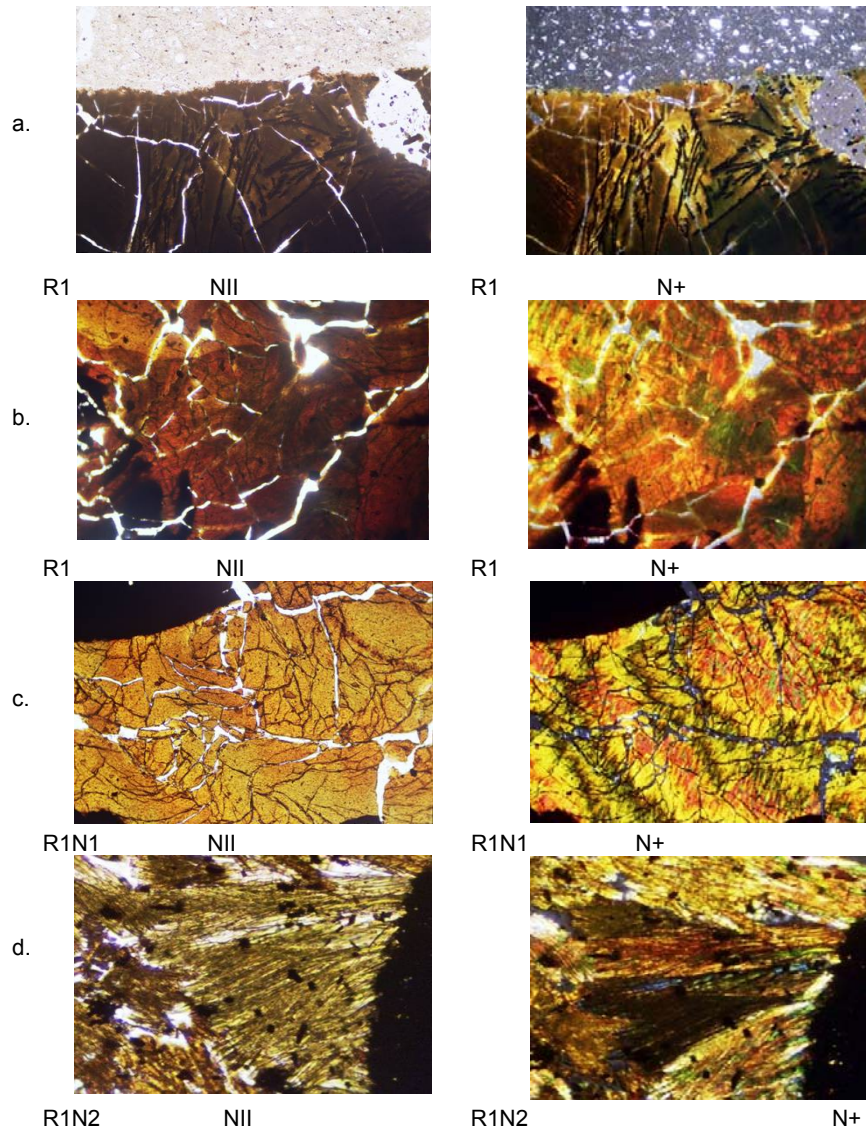


Figure 4. Optical microscopy images of the R1 sample obtained after the second crystallization thermal treatment (x90)

a, b – the R1 sample thermal treated at 850°C – 10h plateau
 c – the R1 sample with TiO₂ nucleator thermal treated at 850°C – 10h plateau
 d – the R1 sample with Cr₂O₃ nucleator thermal treated at 850°C – 10h plateau
 NII – parallel nicols; N+ - crossed nicols

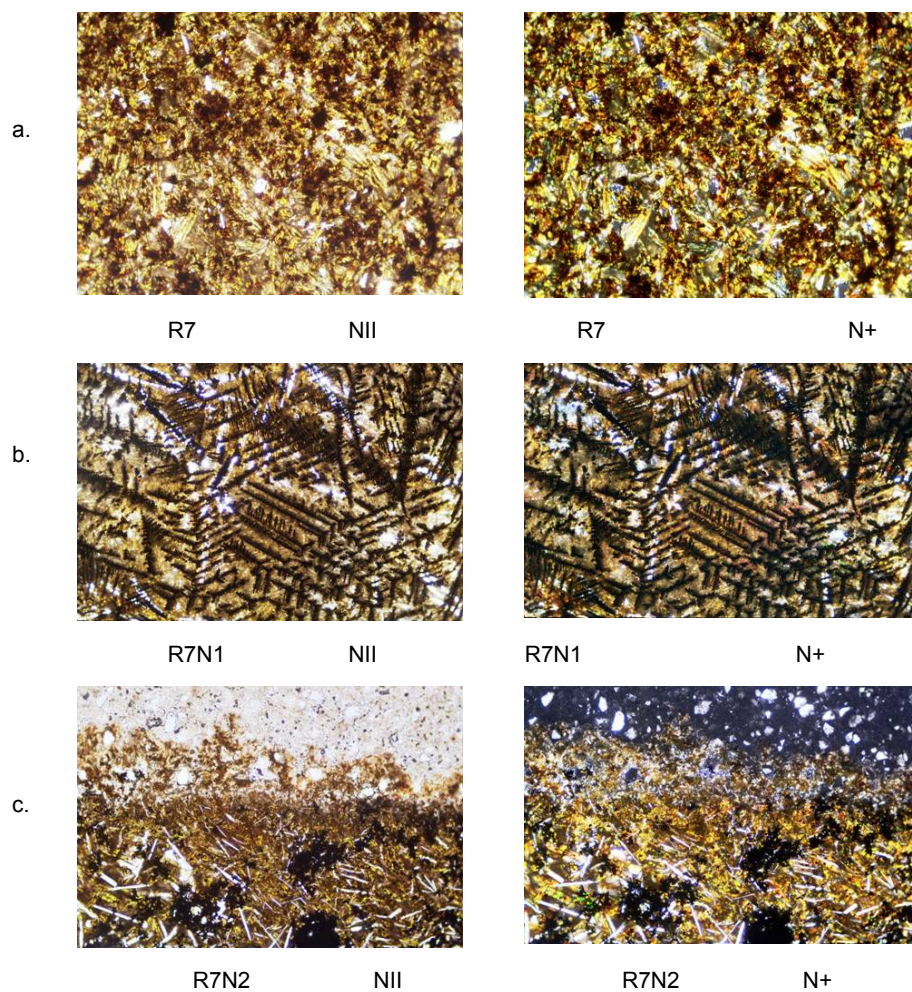


Figure 5. Optical microscopy images of the R7 sample obtained after the second crystallization thermal treatment (x90)

- a – the R7 sample thermal treated at 850°C – 10h plateau
 - b – the R7 sample with TiO_2 nucleator thermal treated at 850°C – 10h plateau
 - c – the R7 sample with Cr_2O_3 nucleator thermal treated at 850°C – 10h plateau
- NII – parallel nicols; N+ - crossed nicols

CRYSTALLIZED GLASSES WITH ADDITION OF FLY ASH

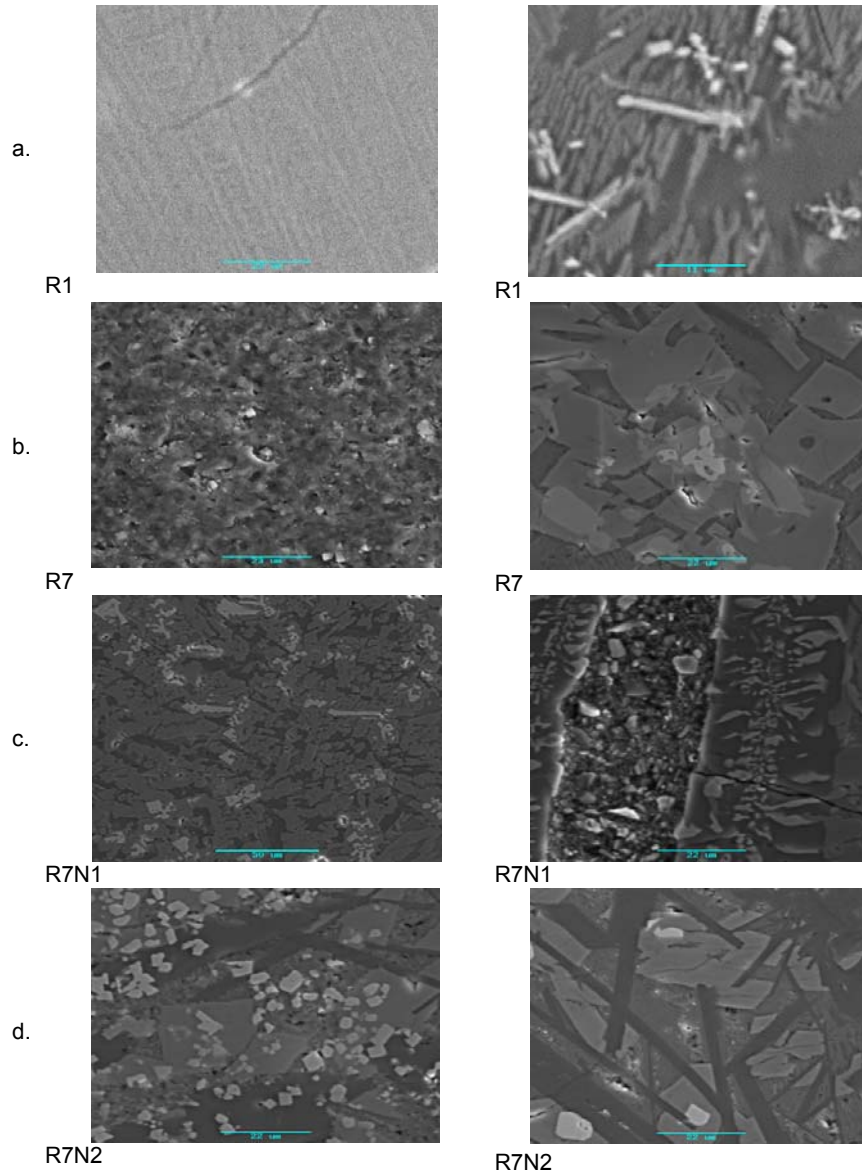


Figure 6. SEM images of the samples obtained through the second thermal treated
a – the R1 sample thermal treated at 850°C – 10h plateau
b – the R7 sample thermal treated at 850°C – 10h plateau
c – the R7 sample with TiO₂ nucleator thermal treated at 850°C – 10h plateau
d – the R7 sample with Cr₂O₃ nucleator thermal treated at 850°C – 10h plateau

In order to identify the crystalline phases the R1N1 and R2N2 samples were analysed by X-ray diffraction (see Figure 7). Due to reduced crystal dimensions, the specific peaks can be noticed as very weak.

The crystalline phases, developed inside the vitreous matrix for both cases, are:

- in the TiO_2 samples: hematite and hedenbergite $\text{Ca}(\text{FeMg})(\text{SiO}_3)_2$;
- in the Cr_2O_3 samples: ferrous fassaite $\text{Ca}(\text{Mg Fe Al})(\text{Si Al})_2\text{O}_6$, magnesiochromite with iron substitution $(\text{Mg Fe})(\text{Cr Al})_2\text{O}_4$, Cr_2O_3 , as well as hedenbergite.

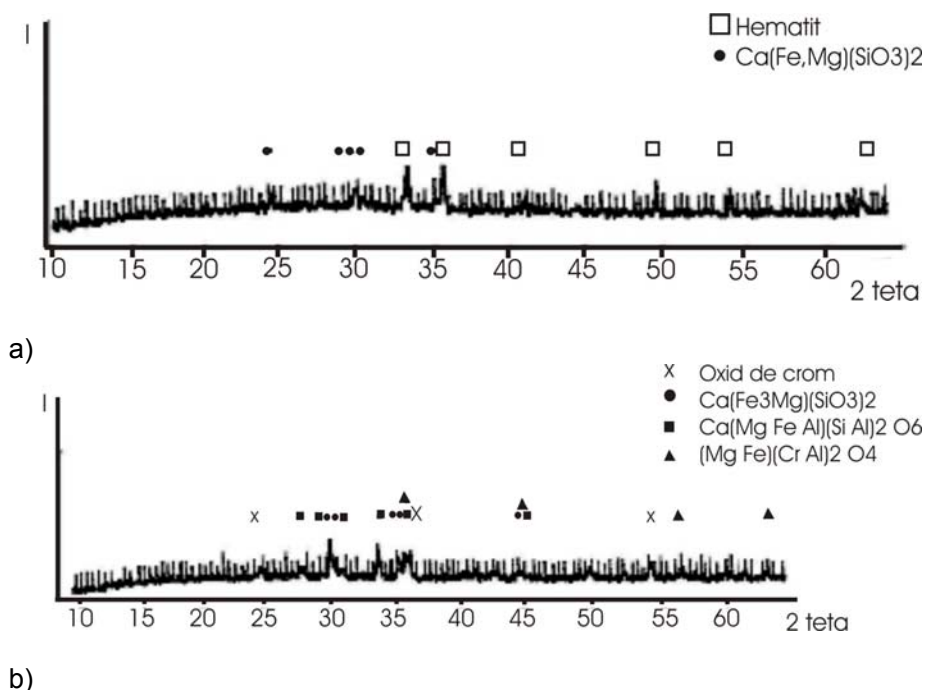


Figure 7. X-ray diffraction pattern for the samples R1N1 (a) și R1N2 (b)

Conclusions

The present study emphasized the following conclusions:

- the Rovinari fly ash can be used to obtain crystallized glasses in the basic oxidic system $\text{SiO}_2\text{-CaO-Fe}_2\text{O}_3$;
 - the crystallization tendency is more pronounced for samples with a higher ash content; moreover, the crystallization can occur without nucleation agents;
 - the crystallization thermal treatment was applied in two ways: through heating with a plateau at 850°C and through slowed cooling of the
- 70

melt and a plateau at the same temperature; the second was proven to be the most efficient;

- the crystallization phenomena are favoured when using TiO_2 and Cr_2O_3 as nucleation agents, thus producing two types of different crystals;

- immiscibility phenomena of the vitreous phases were observed through SEM analysis, especially for the Cr_2O_3 samples.

REFERENCES

1. M.Benea, *Mineralogie ambientală*, Ed. Casa Cărții de Știință, Cluj- Napoca, **2003**.
2. Jae-Myung Kim, Hyung-Sun Kim, *Journal of the European Ceramic Society*, **2004**, 24, 2373-2382.
3. T.W.Cheng, Z.S. Chen, *Ceramics International*, **2004**, 30, 343-349.
4. M.Rezvani, B.Eftekhari-Zekta, M.Solati-Hasjin, V.K.Margussian, *Ceramics International*, **2005**, 31, 75-80.
5. V. Duca, *Petrurgia – Sinteza materialelor vitrocristaline piroxenice*, Ed. Etnograf, Cluj-Napoca, **2003**.

FIRUTA GOGA, CRINA SUCIU, MIRELA ANDREI, MARCEL BENEA, MARIANA MOCEAN

*Dedicated to Professor Ionel Haiduc,
President of The Romanian Academy at his 70th anniversary*

NEW METAL COORDINATION COMPOUNDS OF SODIUM {2-[(2,6-DICHLOROPHENYL)AMINO]PHENYL}ACETATE

L.M. GHIZDAVU^a AND L.GHIZDAVU^b

ABSTRACT. The reaction of $\text{MgCl}_2 \cdot 6\text{H}_2\text{O}$, $\text{CaCl}_2 \cdot 6\text{H}_2\text{O}$, $\text{SnCl}_2 \cdot 2\text{H}_2\text{O}$, $\text{VOSO}_4 \cdot 3\text{H}_2\text{O}$ and PtCl_2 with deprotonated diclofenac, sodium {2-[(2,6 dichlorophenyl)amino] phenyl} (L) were studied in aqueous solutions. Coordination compounds of the formulae $[\text{Mg}(\text{L})_2(\text{H}_2\text{O})_4] \cdot 6\text{H}_2\text{O}$, $[\text{Ca}(\text{L})_2(\text{H}_2\text{O})_4] \cdot \text{H}_2\text{O}$, $[\text{Sn}(\text{L})_2(\text{H}_2\text{O})_2]$, $[\text{VO}(\text{L})_2(\text{H}_2\text{O})_2]$ and $[\text{Pt}(\text{L})_2(\text{H}_2\text{O})_2]$ were synthesized and characterized by elemental analyses, spectral (UV-VIS, IR) and thermal analysis. In all studied compounds, {2-[(2,6-dichlorophenyl)amino]-phenyl}acetate act as a monodentate ligand with coordinate involving the carboxylate oxygen atom. The studied compounds heated in air, lose crystallization water molecules below 423K where as that water eliminated above 423 K is considered as coordination water.

Keywords: coordination compound, sodium {2-[(2,6 dichlorophenyl)amino] phenyl} acetate, sodium diclofenac, TG, IR, UV-VIS spectroscopy.

Introduction

The interaction of metal ions with diclofenac, sodium {2-[(2,6-dichlorophenyl) amino]phenyl}acetate administered for therapeutic reasons is a subject of considerable interest [1-3]. It is known that a number of metal(II) coordination compounds of diclofenac – a potent non-steroidal antiinflammatory drug, have been shown to be more effective anti-inflammatory agents than their parent. The anti-inflammatory effect of $[\text{MnL}_2(\text{H}_2\text{O})_2]$; $[\text{CoL}_2(\text{H}_2\text{O})_2] \cdot 0,5\text{H}_2\text{O}$; $[\text{CoL}_2(\text{H}_2\text{O})]$, $[\text{NiL}_2(\text{H}_2\text{O})_2] \cdot 2\text{H}_2\text{O}$ and $[\text{PdL}_2(\text{H}_2\text{O})_2]$ is 35-50% while for the diclofenac is 17% [2].

In order to obtain further information on understanding drug-metal interactions, the magnesium(II), calcium(II), tin(II), vanadyl(II) and platinum(II), coordination compounds with deprotonated diclofenac ligand were prepared and investigated by thermal analysis and IR respectively UV-VIS spectroscopy.

Results and discussion

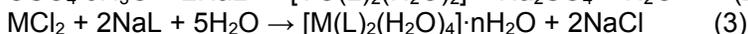
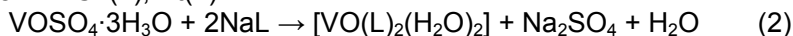
The coordination compounds: $[\text{Mg}(\text{L})_2(\text{H}_2\text{O})_4] \cdot 6\text{H}_2\text{O}$ (**1**), $[\text{Ca}(\text{L})_2(\text{H}_2\text{O})_4] \cdot \text{H}_2\text{O}$ (**2**), $[\text{Sn}(\text{L})_2(\text{H}_2\text{O})_2]$ (**3**), $[\text{VO}(\text{L})_2(\text{H}_2\text{O})_2]$ (**4**), $[\text{Pt}(\text{L})_2(\text{H}_2\text{O})_2]$ (**5**), were formed according to equations (1-3):

^a "Babeș-Bolyai" University, Chemistry Department, 11 Arany Janos, 400028 Cluj-Napoca, România

^b Université Libre de Bruxelles, Belgique



where M = Sn(II), Pt(II)



where M = Mg(II), Ca(II) and n = 6, 1

The compounds are white (1-3), blue-white(4) and yellow-brown (5), microcrystalline, powdery solids that appear to be air and moisture-stable. They are soluble in CH₃OH, C₂H₅OH and C₆H₆ and are insoluble in water. The structure of coordination compounds (1-5) is supported by thermal analysis, UV-VIS and IR spectroscopic data.

Table 1.
Analytical data of compounds.

	GM	Yield	Elemental analysis, [%]				
			found, (calcd.)				
		[%]	C	H	N	Cl	M
[Na(H ₂ O) ₄] ⁺ L ⁻	390,07		43,15 (43,06)	4,64 (4,61)	3,55 (3,59)	17,40 (18,17)	5,57 (5,89)
[Mg(L) ₂ (H ₂ O) ₄].6H ₂ O 1	794,49	62,5	42,30 (42,27)	5,08 (5,03)	3,47 (3,52)	17,31 (17,83)	3,14 (3,06)
[Ca(L) ₂ (H ₂ O) ₄].H ₂ O 2	720,10	64,08	46,62 (46,70)	3,49 (3,47)	3,84 (3,89)	19,52 (19,71)	5,51 (5,57)
[Sn(L) ₂ (H ₂ O) ₂] 3	744,45	84,6	45,16 (45,09)	3,30 (3,22)	3,70 (3,76)	18,90 (19,03)	15,83 (15,92)
[VO(L) ₂ (H ₂ O) ₂] 4	693,00	82,8	48,58 (48,49)	3,52 (3,46)	4,01 (4,04)	20,29 (20,46)	7,29 (7,35)
[Pt(L) ₂ (H ₂ O) ₂] 5	821,14	86,7	40,98 (40,89)	2,98 (2,29)	3,34 (3,41)	17,11 (17,26)	23,64 (23,74)

where L = (C₁₄H₁₂O₂NCl₂)⁻.

Thermal behavior

The thermal behavior of the ligand and of the synthesized coordination compounds (1-5) is presented in Table 2. Thermal stability domains, decomposition phenomena (followed as endo and exo effects in the DTA curves and as mass losses, calculated from the TG and DGT cuves) and their assignment are presented.

Table2.
Thermal data of the synthesized coordination compounds

Compound	Temp. Range, K	DTA peak, K		TG data, %		Assignment
		Endo	Exo	Calc.	Exp	
NaL·4H ₂ O	293 – 473	403	-	18,45	8,21	4H ₂ O
	473 – 1273	555	-	-	-	Melting
		-	558	11,28	11,15	CO ₂
		-	673	55,22	55,46	Pyrolysis of org.rest
		1048	-	14,98	14,71	NaCl residue
1	293 – 473	368	-	13,59	3,35	6H ₂ O
	473 – 1273	443	-	9,06	3,99	4H ₂ O
		-	543	5,54	5,68	CO ₂
		-	678	66,71	6,80	Pyrolysis of org.rest
	973	-	5,10	5,18	MgO residue	
2	293 – 473	372	-	2,50	2,53	1 H ₂ O
	473 – 1273	457	-	9,99	0,18	4 H ₂ O
		-	533	6,11	5,02	CO ₂
		-	683	75,82	5,98	Pyrolysis of org.rest
	848	-	7,79	7,71	CaO residue	
3	293 – 473	443	-	4,83	4,60	2H ₂ O
	473 – 1273	-	548	5,90	5,83	CO ₂
		-	693	73,34	1,74	Pyrolysis of org.rest
		720	-	18,08	7,83	SnO residue
4	293 – 473	457	-	5,19	5,40	2 H ₂ O
	473 – 1273	-	541	6,35	5,14	CO ₂
		-	685	75,39	5,40	Pyrolysis of org.rest
		958	953	13,12	3,06	V ₂ O ₅ residue
5	293 – 473	435	-	4,49	4,11	2 H ₂ O
	473 – 1273	-	542	5,35	5,40	CO ₂
		-	673	66,52	66,752	Pyrolysis of org.rest
		833	-	23,64	3,74	Pt residue

Between 293-473 K an endo peak at 423 K in the TDA curve of [Na(H₂O)₄]⁺L⁻ indicated the loss of four water molecules. X-ray scattering studies [16] show that in various crystalline salts, Na⁺ forms tetrahedral [Na(H₂O)₄]⁺ ions, where four tetrahedrally arranged H₂O molecules are directly coordinated. These results are in agreement with structure and thermal behaviour of sodium diclofenac salts studied [17-20]. The anhydrous sodium diclofenac, NaL is stable up to 555 K where an endo peak marks its melting. The decomposing starts with the shoulder at 558 K which was assigned to the loss of decarboxylate group. In the temperature range 473-1273 K an exothermic peak situated at 673 K marks the pyrolysis of the organic residue and at 1048 K the formation of NaCl residue is observed. The coordination compounds synthesized, (**1-5**), are stable in air and can be stored without change. When heated in air, the coordination compounds decompose in various ways (Table 2). According to Nikolaev et al [10,21-23,] water released

below 423 K can be considered as crystallization water, whereas that eliminated above 423 K, as chemically bounded to the central ion through weak coordination bonds.

The decomposition of the coordination compounds occurs in the 435-457K temperature range, when the coordination water separate from each molecule. In the case of $[\text{Mg}(\text{L})_2(\text{H}_2\text{O})_4] \cdot 6\text{H}_2\text{O}$ (**1**) and $[\text{Ca}(\text{L})_2(\text{H}_2\text{O})_4] \cdot \text{H}_2\text{O}$ (**2**) compounds a stepped dehydration reaction is observed. The two endo peaks at 368K (**1**), 372K (**2**) (first step) can be assigned to six molecules and one molecule of hydrating water, respectively. Another two peaks at 443K (**1**) and 457K (**2**) (second step) can be assigned to four molecules of coordination water in both cases (**1** and **2**). The derivatograms recorded on $[\text{Sn}(\text{L})_2(\text{H}_2\text{O})_2]$ (**3**), $[\text{VO}(\text{L})_2(\text{H}_2\text{O})_2]$ (**4**) and $[\text{Pt}(\text{L})_2(\text{H}_2\text{O})_2]$ (**5**) compounds present one in every case, peak at 443K, 457K and 435K, respectively which were assigned to the loss of the coordination water. For the studied compounds, the thermal decomposition of the ligand starts in the 540-550 K region indicating the destabilization of the ligand due to the weakening of the carboxylic group bond, as a consequence of M-O bond formation.

An exothermic peak situated in the 675-695 K region marks the pyrolysis of the organic rest. In the 720-1273K temperature range, the formation of intermediates is observed, followed by the thermal decomposition to oxides: MO, M(II)=Mg, Ca, Sn (**1-3**), V_2O_5 (**4**), and to metal (Pt) (**5**).

The thermal analysis results of the investigated compounds confirm the atom ratio M:L:O = 1:2:2 when M(II)= Sn, VO, Pt and atom ratio M:L:O = 1:2:4 when M(II)=Mg, Ca.

IR –spectras

The modes of coordinated ligands in the complexes have been investigated by means of infrared absorbtion spectra. The most important infrared frequencies attributed to the vibrations of the complexes (**1–5**) are reported in Table 3.

The absorption bands $\nu(\text{OH})$ and $\nu(\text{OHO})$ which occur in the range $3570\text{-}3560\text{ cm}^{-1}$ confirm the presence of crystallization water. The absorbtion bands $\nu\text{M-O}_{\text{H}_2\text{O}}$ which occur in the range $425 - 410\text{ cm}^{-1}$ confirm the presence of coordinated water in the complexes [10]. The presence of crystallization and coordination water in the synthesized compounds is supported by the thermal decomposition data.

As the carboxylic hydrogen is more acidic than the amino hydrogen, the deprotonation occurs in the carboxylate group. The characteristic bands for the secondary amino groups and for the coordinated carboxylate group are discussed [11–13].

Table 3.
Frequencies of characteristic absorption bands in IR spectra of sodium {2-[(2,6-dichlorophenyl)amino]phenyl}acetate tetrahydrate and its coordination compounds, (cm^{-1})

Compound	ν OH; ν OHO	$\nu_{\text{as}} \text{COO}^-$	$\nu_{\text{s}} \text{COO}^-$	ΔCOO^-	$\nu \text{M} - \text{O}_{\text{H}_2\text{O}}$	$\nu \text{M} - \text{O}_{\text{COO}^-}$
NaL·4H ₂ O	3560 br	1572 s	1402 s	170	410 w	-
1	3570 br	1655 s	1410 s	245	420 mw	402 m
2	3565 br	1662 s	1420 s	242	415 mw	405 m
3	-	1660 s	1420 s	240	425 mw	402 m
4	-	1665 s	1366 s	299	425 mw	405 m
5	-	1630 s	1325 s	305	420 mw	403 m

* s = strong, m = medium, w = weak, br = broad

The strong band at 3388 cm^{-1} , which appears in diclofenac, is assigned to the stretching motion and the broad band at 3260 cm^{-1} is taken to represent the $\nu(\text{NH}\dots\text{O})$ mode, due to intramolecular hydrogen bonding [3]. The absence of large systematic shifts of the $\nu(\text{NH})$ and $\delta(\text{NH})$ bands in the spectra of the coordination compounds (**1-5**) compared with those of the ligand indicated that there is not interaction between the NH group and the metal ions.

It is known that carboxylate ions can coordinate to metal ions in a number of ways such as monodentate, bidentate (chelating) or bridging and there is an evidence of that fact in the IR spectrum. The analysis of COO^- group bands frequencies allowed the determination of parameter $\Delta \nu \text{COO}^- = \nu \text{COO}^- (\text{as}) - \nu \text{COO}^- (\text{s})$. For the complexes (**1-5**), the difference $\Delta \nu > 170 \text{ cm}^{-1}$ ($240\text{-}305 \text{ cm}^{-1}$) higher than that of the free ion (sodium diclofenac salt), is in a good agreement with the literature data for unidentately bonded acetates structures [23]. The absorption bands $\nu(\text{M}-\text{O})$ in the range $402\text{-}405 \text{ cm}^{-1}$ confirm the coordination of diclofenac to metallic ions through the oxygen atom of the carboxylate group.

UV-VIS spectra

The UV spectrum of the organic ligand, diclofenac anion, L^- , contain two absorption bands at about 214 nm and 270 nm which are assigned due to the allowed intraligand $\pi - \pi^*$ transition and to the $n \rightarrow \pi^*$ transition, respectively [23, 24].

Each of the coordination compounds (**1-5**) in an aqueous solutions displayed in the UV spectrum two absorption bands in the 214-300 nm region. The bathochromic shift of about 25 nm for the compounds (**1-3**) was assigned to the additional conjugation with the two adjacent benzene rings. The coordination compounds (**4**) and (**5**) in an aqueous solutions displayed in the UV-VIS spectrum two other absorption bands in the 480-600 nm region

(Table 4). The absorption band near 600 nm may be assigned to the $d \rightarrow d$ transition due to the axial coordination of oxygen atoms from ligand to the metallic ion: VO(II), and Pt(II).

Table 4.
Electronic spectral data (nm) of the ligand and their coordination compounds in aqueous solution

Compound	λ (nm) (ϵ)			
Na ⁺ L ⁻ ·4H ₂ O	214 (6000)	270 (8000)		
1	239 (6200)	295 (8100)		
2	240 (6400)	298 (8050)		
3	242 (6350)	297 (8080)		
4	240 (6475)	295 (8180)	500	595 (608)
5	238 (6400)	298(8160)	480	602 (750)

Experimental part

Preparation of compounds

The coordination compounds were prepared by mixing hot aqueous solution of the ligand diclofenac (sodium diclofenac salt tetrahydrate) (pH~5,5-6,5) and aqueous solution of metal salt (3:1 ligand to metal molar ratio). The reaction mixture was stirred for 5h at 323K. The resulting powders were filtered, washed with hot water to remove Na⁺ and Cl⁻ ions, data dried at 303K to a constant mass. The yields and the elemental analyses are presented in Table 1.

Measurements

The carbon, hydrogen and nitrogen content in the coordination compounds were determined by elemental analyses using a Perkin Elmer CAN 2000 analyzer. The chlorine content was measured by the Schöninger method. The Mg(II), Ca(II), Sn(II), VO(II), and Pt(II), contents was determined by AAS method using an Atomic Absorbance Spectrometer AAS-3 Carl Zeiss, Jena. The experimental results are in accordance with the calculated data (Table 1). Thermal analysis were performed with an OD-103 MOM Derivatograph using a sample weight of 100±1-2 mg, at a heating rate of 10 K min⁻¹, with Al₂O₃ as reference material in static air atmosphere.

IR spectra were recorded over the range of 4000-400 cm⁻¹ using a FT-IR JASCO 600 spectrophotometer, in KBr pellets. UV-VIS spectra were recorded with an UV-VIS Specord spectrophotometer.

Conclusions

All the coordination compounds (**1-5**) are stable in air and soluble in methanol, ethanol and benzene. Heating the compounds first results in a release of crystallization water molecules in complexes (**1**) and (**2**). The

decomposition of the compounds (1-5) occurs with the loss of the coordination water and is continued with thermal decomposition of the ligand (L). The results reveal that metallic oxides are left as residue (excepting compound 5). Infrared data are in accordance with the literature data for unidentately bonded acetate structures (1-5) [20, 21]. Diclofenac is coordinated to metal(II) through the oxygen atom of its carboxylate group. The preliminary study has shown that the complexes do have a biological activity.

REFERENCES

1. D.P.Kessisoglou, G.E.Manoussakis, A.G.Hatjidimitrion, M.G.Kanatzidis, *Inorg. Chem.*, **1987**, 26, 1395.
2. I.Konstantidinou, D.Kovala-Demertzi, M.A.Demertzi, *J.Inorg. Biochem.*, **1998**, 70, 63.
3. D.Kovala-Demertzi, S.K.Hadjikakon, M.A.Demertzi, *J.Inorg. Biochem.*, **1998**, 64, 223.
4. A.B.P.Lever, *Inorganic Electronic Spectroscopy*, Second edition, Elsevier publishing Company, Amsterdam, **1984**
5. C.N.Rao, *Ultraviolet and Visible Spectroscopy*, Butterworths, London, **1961**
6. J.Kracmar, J.Kracmarova, *Pharmazie*, **1966**, 15 (68), 121.
7. J.Kracmar, J.Kracmarova, *Pharmazie*, **1966**, 16 (21), 460.
8. J.Kracmar, A.Sotolongo, J.Kracmarova, J.Petranova, *Pharmazie*, **1976**, 31 (9), 614.
9. G.Deveto, G.Ponticelli, C.Preti, *J.Inorg.Nucl.Chem.*, **1975**, 37, 1635.
10. S.C.Mojumdar, M.Melnik, E.Jona, *J.Therm. Anal.Cal.*, **2000**, 61, 915
11. G.Maistralis, N.Katsaros, S.P.Perlepes, D.Kovala-Demertzi, *J.Inorg. Biochem.*, **1992**, 45
12. G.B.Deacon, R.J.Phillips, *Coord. Chem. Rev.*, **1980**, 33, 227.
13. K.Nakamoto, "Infrared Spectra of Inorganic and Coordination Compounds", 2nd edn Wiley Interscience, New York, **1970**.
14. P.Moser, A.Sallmann and I.Weisenberg, *J.Med.Chem.*, **1990**, 33, 2358
15. D.Stoilova, G.Nikolov, K.Balarev, *Izv.Akad.Nauk SSSR, Ser.Khim.*, **1976**, 9, 371
16. F.A.Cotton, G.Wilkinson, "Advanced Inorganic Chemistry", Fifth Ed., John Wiley & Sons, New York, **1988**
17. G.Reck, G.Faust, G.Dietz, *Die Pharmazie*, **1988**, 43 (11), 771.
18. P.W.Borthwich, *Acta Cryst.*, **1980**, B36, 628.
19. R.Mattes, G.Uckelmann, *Acta Cryst.*, **1981**, B37, 207
20. V.Barrans, M.Alleaume, G.Jeminet, *Acta Cryst.*, **1892**, 338, 1144.
21. A.V.Nikolaev, V.A.Lodviengo, L.J.Myachina, "Thermal Analysis", vol.2, Academic Press, New York, **1969**
22. B.Singh, B.A.Agarwala, P.L.Mourya, A.K.Dey, *J.Indian Chem.Soc.*, **1992**, 59, 1130.
23. R.C.Mehotra, R.Bohra, "Metal Complexes", Academic Press, Oxford, **1998**
24. W.Brzyska, W.Ozga, *J.Therm.Anal.Cal.*, **2002**, 70, 467.

L.M. GHIZDAVU AND L.GHIZDAVU

*Dedicated to Professor Ionel Haiduc,
President of The Romanian Academy at his 70th anniversary*

**NEW COPPER(I) AND COPPER(II)
TETRAORGANODICHALCOGENOIMIDODIPHOSPHINATES.
CRYSTAL AND MOLECULAR STRUCTURE OF THE FIRST
MONOTHIOIMIDODIPHOSPHINATO COPPER(I) COMPLEX,
 $\text{Cu}_4[(\text{OPMe}_2)(\text{SPPH}_2)\text{N}]_4 \cdot 6\text{CH}_2\text{Cl}_2$**

**ADINA ROTAR¹, OVIDIU MOLDOVAN,¹ SORIN I. FARCAS,² RICHARD
A. VARGA,¹ CRISTIAN SILVESTRU¹ AND ANCA SILVESTRU^{1,*}**

ABSTRACT. New copper complexes containing dichalcogenoimidodiphosphinato ligands, *i.e.* $\text{Cu}_4[(\text{OPMe}_2)(\text{SPPH}_2)\text{N}]_4$ (1), $(\text{Ph}_3\text{P})_2\text{Cu}[(\text{SPMe}_2)(\text{SPPH}_2)\text{N}]$ (2) and $\text{Cu}[(\text{SPMe}_2)(\text{SPPH}_2)\text{N}]_2$ (3), were prepared and characterized. The molecular structure of the complex $1 \cdot 6\text{CH}_2\text{Cl}_2$ was established by single-crystal X-ray diffraction. The crystal contains discrete tetranuclear units with a distorted Cu_4 tetrahedron [$\text{Cu} \cdots \text{Cu}$ 2.702(3) and 3.060(2) Å] and bimetallic triconnective monothio ligands [$\text{Cu}-\text{S}$ 2.258(3), 2.267(4) Å; $\text{Cu}-\text{O}$ 1.969(9) Å]. All four copper centers are tricoordinated (CuOS_2 core), in an almost planar, trigonal arrangement.

Key-words: copper, imidodiphosphinato ligands, solution NMR studies, RES, X-ray diffraction

Introduction

During last decade copper complexes containing dichalcogenoimidodiphosphinato ligands raised considerable interest as structural model compounds for the active-sites in copper-containing enzymes and proteins [1-3], compounds with nonlinear optical properties [4] or precursors for solid state materials [5]. In most cases reported so far phosphorus ligands containing the same chalcogen in the molecular unit were used. When protic solvent conditions were used the reduction of copper(II) salts of dithio ligands resulting in the isolation of copper(I) complexes was observed. Ionic Cu(I) compounds containing tetranuclear cations, *i.e.* $[\text{Cu}_4\{(\text{SPPH}_2)_2\text{N}\}_3][\text{X}]$ ($\text{X} = [\text{CuCl}_2]^-$ [6], $[\text{BF}_4]^-$ [7], $[\text{I}_3]^-$ [8]), $[\text{Cu}_4\{(\text{SePPH}_2)_2\text{N}\}_3][\text{BF}_4]^-$ [7], or a cluster anion in $[\text{Et}_4\text{N}]_4[\text{Mo}_4\text{Cu}_8\text{O}_4\text{S}_{12}\{(\text{SPPH}_2)_2\text{N}\}_4]$ [4], as well as neutral trinuclear complexes, *i.e.* $[\text{Cu}\{(\text{EPPH}_2)_2\text{N}\}_3]$ ($\text{E} = \text{S}$ [9], Se [5]),

¹ Faculty of Chemistry & Chemical Engineering, "Babes-Bolyai" University, RO-400028 Cluj-Napoca, Romania. Fax: 0040-264-590818; Tel: 0040-264-593833; E-mail: ancas@chem.ubbcluj.ro

² National Institute for R&D of Isotopic and Molecular Technology, PO Box 700, RO-400293, Cluj-Napoca, Romania

$[\text{Cu}\{(\text{SPPr}^i)_2(\text{SPPH}_2\text{N})\}_3]$, $[\text{Cu}\{(\text{SPPr}^i)_2(\text{SP}(\text{OPh})_2\text{N})\}_3]$ [9], $[\text{Cu}\{(\text{SP}(\text{OC}_6\text{H}_4\text{Bu}^t-2)_2)_2\text{N}\}_3]$ [10], were structurally characterized by single-crystal X-ray diffraction. Mononuclear Cu(I) complexes can be obtained in the presence of triphenylphosphine, e.g. $(\text{Ph}_3\text{P})\text{Cu}[(\text{EPPH}_2)_2\text{N}]$ (E = S [11], Se [12]) and $(\text{Ph}_3\text{P})_2\text{Cu}[(\text{OPPh}_2)_2\text{N}]$ [13]. Recently, ionic Cu(I) complexes containing protonated imidodiphosphinato ligands, i.e. $[\text{Cu}\{(\text{SPPH}_2)_2\text{NH}\}_2][\text{I}_3]$ [8] and $[\text{Cu}\{(\text{OPPh}_2)_2\text{NH}\}_3][\text{PF}_6]$ [14], were also reported. Copper(II) complexes were found to be generally stabilized by the use of oxo ligands, i.e. monomeric $\text{Cu}\{[\text{OP}(\text{OPh})_2]_2\text{N}\}_2$ [15], $\text{Cu}[(\text{OPPh}_2)_2\text{N}]_2$ [13], and dimeric $[\text{Cu}\{(\text{OPPh}_2)_2\text{N}\}(\text{O}_2\text{PPh}_2)]_2$ [16]. So far, the molecular structure of only one copper(II) complex containing mixed dichalcogenoimidodiphosphinato ligands, $\text{Cu}[(\text{OPPh}_2)(\text{SPPH}_2)\text{N}]_2$ [13], was established by X-ray diffraction.

We report here on the synthesis and characterization of the first tetranuclear Cu(I) monothioimidodiphosphinate, $\text{Cu}_4[(\text{OPMe}_2)(\text{SPPH}_2)\text{N}]_4$, as well as the dithioimidodiphosphinato derivatives $(\text{Ph}_3\text{P})_2\text{Cu}[(\text{SPMe}_2)(\text{SPPH}_2)\text{N}]$ and $\text{Cu}[(\text{SPMe}_2)(\text{SPPH}_2)\text{N}]_2$.

Experimental

The organophosphorus starting materials were prepared according to literature methods: $\text{Na}[(\text{OPMe}_2)(\text{SPPH}_2)\text{N}]$ [17], $\text{K}[(\text{SPMe}_2)(\text{SPPH}_2)\text{N}]$ [18]. Room-temperature ^1H and ^{31}P NMR spectra were recorded in dried CDCl_3 on a BRUKER AVANCE 300 instrument operating at 300.11 and 121.48 MHz, respectively. The chemical shifts are reported in ppm relative to the residual peak of the deuterated solvent (ref. CHCl_3 : ^1H 7.26 ppm) and H_3PO_4 85%, respectively. ESR measurements were performed on powder compound at room temperature (r.t.) on a Radiopan SE/X-2543 9 GHz ESR spectrometer, using a 100 kHz field modulation.

Preparation of $\text{Cu}_4[(\text{OPMe}_2)(\text{SPPH}_2)\text{N}]_4$ (1)

A mixture of $\text{CuCl}_2 \cdot 2\text{H}_2\text{O}$ (0.170 g, 1 mmol) and $\text{Na}[(\text{OPMe}_2)(\text{SPPH}_2)\text{N}]$ (0.663 g, 2 mmol) in CH_2Cl_2 (30 ml) was stirred for 6 h at room temperature. After removing NaCl, the solvent was evaporated to dryness. The remaining colorless solid was recrystallized from a mixture of $\text{CH}_2\text{Cl}_2/n$ -hexane to afford the title compound. Yield: 0.27 g (74%, with respect to copper), m.p. 127-129°C. ^1H NMR: δ 0.91t (6H, CH_3 , $^2\text{J}_{\text{PH}}$ 13.8 Hz), 7.35m (6H, C_6H_5 - meta+para), 7.93ddd (4H, C_6H_5 - ortho, $^3\text{J}_{\text{PH}}$ 13.8, $^3\text{J}_{\text{HH}}$ 6.0, $^4\text{J}_{\text{HH}}$ 2.2 Hz). ^{31}P NMR: δ 42.7s (Ph_2PS), 47.7s (Me_2PO).

Preparation of $(\text{Ph}_3\text{P})_2\text{Cu}[(\text{SPMe}_2)(\text{SPPH}_2)\text{N}]$ (2)

A mixture of $(\text{Ph}_3\text{P})_2\text{CuNO}_3$ (0.356 g, 0.55 mmol) and $\text{K}[(\text{SPMe}_2)(\text{SPPH}_2)\text{N}]$ (0.199 g, 0.55 mmol) in CH_2Cl_2 (30 ml) was stirred for 6 h at room temperature. The insoluble KNO_3 was filtered off and the solvent was

evaporated to dryness under vacuum. The remaining colorless solid was recrystallized from a mixture of CH_2Cl_2 /n-hexane to afford the title compound. Yield: 0.4 g (80%), m.p. 132°C. ^1H NMR: δ 1.84d (6H, CH_3 , $^2J_{\text{PH}}$ 13.1 Hz), 7.34m [30H, $\text{P}(\text{C}_6\text{H}_5)_3$], 7.47m (4H, C_6H_5 – *meta*), 7.71m (2H, C_6H_5 – *para*), 7.89ddd (4H, C_6H_5 – *ortho*, $^3J_{\text{PH}}$ 13.3, $^3J_{\text{HH}}$ 7.7, $^4J_{\text{HH}}$ 1.7 Hz). ^{31}P NMR: δ -3.2s [$\text{P}(\text{C}_6\text{H}_5)_3$], 32.4d (Ph_2PS , $^1J_{\text{PC}}$ 109.0, $^2J_{\text{PP}}$ 11.8 Hz), 38.3s (Me_2PS , $^1J_{\text{PC}}$ 75.7, $^2J_{\text{PP}}$ 11.8 Hz).

Preparation of $\text{Cu}[(\text{SPMe}_2)(\text{SPPH}_2)\text{N}]_2$ (**3**)

A mixture of $\text{CuCl}_2 \cdot 2\text{H}_2\text{O}$ (0.143 g, 0.84 mmol) and $\text{K}[(\text{SPMe}_2)(\text{SPPH}_2)\text{N}]$ (0.614 g, 1.69 mmol) in CH_2Cl_2 (30 ml) was stirred for 6 h at room temperature. The resulted KCl was filtered off and the solvent was evaporated to dryness under vacuum. The remaining yellow-brown solid was recrystallized from a mixture of CH_2Cl_2 /n-hexane to afford the title compound. Yield: 0.26 g (43%), m.p. 285°C. ^{31}P NMR: δ 21.2s, 38.0s (broad signals). ESR (X band): g_{\parallel} 2.78 \pm 0.01, g_{\perp} 2.77 \pm 0.01.

X-ray Crystallographic Study

Data were collected with a SMART APEX diffractometer (*National Center for X-Ray Diffractometry*, “Babes-Boyal” University, Cluj-Napoca, Romania) at 297 K, using a graphite monochromator to produce a wavelength ($\text{Mo-K}\alpha$) of 0.71073 Å. The crystal structure measurement and refinement data for compound $1 \cdot 6\text{CH}_2\text{Cl}_2$ are given in Table 1. Absorption corrections were applied using the multi-scan (Bruker SAINT) method [19]. The structure was solved by direct methods (full-matrix least-squares on F^2). All non hydrogen atoms were refined with anisotropic thermal parameters. For structure solving and refinement a software package SHELX-97 was used [20]. The drawings were created using the Diamond program by Crystal Impact GbR [21].

Table 1.
Crystallographic data for compound $1 \cdot 6\text{CH}_2\text{Cl}_2$

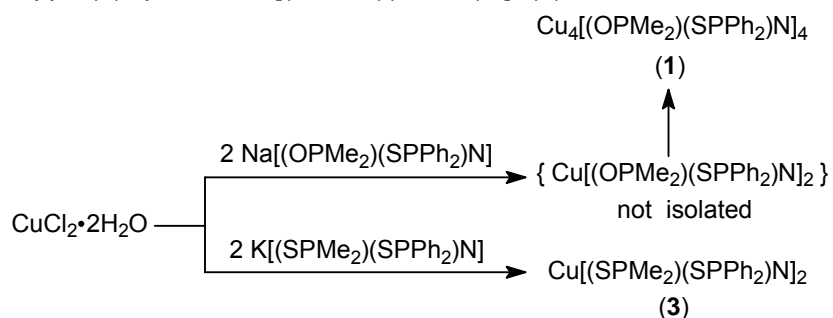
Empirical formula	$\text{C}_{62}\text{H}_{76}\text{Cl}_{12}\text{Cu}_4\text{N}_4\text{O}_4\text{P}_8\text{S}_4$		
Formula mass	1996.91	$F(000)$	2024
Crystal system	Tetragonal	Crystal size [mm]	0.48x0.34x0.30
Space group	$P4(2)/n$	$\mu(\text{Mo-K}\alpha)$ [mm^{-1}]	1.633
a [Å]	14.742(6)	θ range [°]	1.72-26.36
b [Å]	14.742(6)	No. of reflections collected	22761
c [Å]	19.858(16)	No. of independent reflections	4408
			($R_{\text{int}} = 0.0928$)
α [°]	90	No. of parameters	224
β [°]	90	R_1 [$I > 2\sigma(I)$]	0.1644
γ [°]	90	wR_2	0.3123
V [Å ³]	4316(4)	GOF on F^2	1.381
Z	2	Largest difference electron density [$\text{e}/\text{Å}^3$]	1.838/-0.810
$D_{\text{calcd.}}$ [g/cm^3]	1.537		

CCDC-642236 (1·6CH₂Cl₂) contains the supplementary crystallographic data for this paper. These data can be obtained free of charge at www.ccdc.cam.ac.uk/conts/retrieving.html [or from the Cambridge Crystallographic Data Centre, 12, Union Road, Cambridge CB2 1EZ, UK; fax: (internat.) +44-1223/336-033; E-mail: deposit@ccdc.cam.ac.uk].

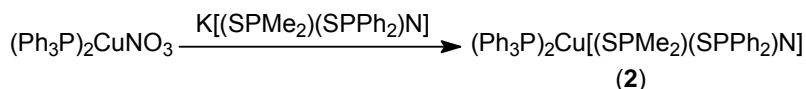
Results and discussion

Synthesis and spectroscopic characterization

The reaction of CuCl₂·2H₂O with Na[(OPMe₂)(SPPH₂)N] affords the isolation of the tetranuclear Cu₄[(OPMe₂)(SPPH₂)N]₄ (**1**), formed by reduction of the intermediate copper(II) species, Cu[(OPMe₂)(SPPH₂)N]₂, which could not be isolated under the conditions used. By contrast, the reaction of CuCl₂·2H₂O with K[(SPMe₂)(SPPH₂)N] resulted in the isolation of the copper(II) species, Cu[(SPMe₂)(SPPH₂)N]₂ (**3**):



The metathesis reaction between (Ph₃P)₂CuNO₃ and K[(SPMe₂)(SPPH₂)N] resulted in the expected mononuclear copper(I) complex, (Ph₃P)₂Cu[(SPMe₂)(SPPH₂)N] (**2**):



The copper(I) complexes were isolated in good yield as colorless solids, while the copper(II) complex was obtained as a yellow-brown solid. They are air-stable compounds, soluble in common organic solvents.

All compounds were investigated by NMR spectroscopy (¹H, ³¹P) in CDCl₃ solutions. For copper(I) species the solution NMR spectra of the isolated products are consistent with the formation of the complexes **1** and **2**. The ¹H NMR spectra, recorded in CDCl₃, showed the resonances for the organic groups attached to phosphorus atoms, with the expected splitting due to phosphorus-proton. The ³¹P NMR spectra exhibit two resonances, consistent with non equivalent phosphorus atoms in a

dichalcogenoimidodiphosphinato unit. The signals were assigned by comparison with the spectra of the free acids or the alkali salts used as starting materials. For compound **2** the ^{31}P signals are surrounded by satellites and the magnitude of the phosphorus-carbon couplings is consistent with the assignments for the corresponding resonances. In addition, for compound **2** a resonance at δ -3.2 ppm was also observed, which is indicative for the presence of the Ph_3P ligands coordinated to the metal centre.

The ^{31}P NMR spectrum of compound **3** exhibits two very broad resonances, a behavior which is indicative for a copper(II) species. Evidences for its paramagnetic nature were provided by the ESR spectrum which shows two lines located at about 2392 and 2399 Gs, respectively. The half width of the lines is very close to the values of 2.23 and 2.67 Gs. We consider these lines to appear due to the Cu^{2+} ions in an axial symmetry. The g -factors are 2.78 and 2.77, respectively, and they represent the middle of the parallel and perpendicular spectra. However, it was not possible to observe the hyperfine structure due probably to (i) the very high concentration of the paramagnetic ions, (ii) the covalent nature of the compound, and/or (iii) the exchange interactions between the paramagnetic ions.

On the basis of the spectroscopic data monomeric structures with tetrahedral CuP_2S_2 and CuS_4 cores are proposed for compounds **2** and **3**, respectively. Similar structures were established for $(\text{Ph}_3\text{P})_2\text{Cu}[(\text{OPPh}_2)_2\text{N}]$ and $\text{Cu}[(\text{OPPh}_2)_2\text{N}]_2$ [13].

Single-crystal X-ray diffraction studies

Single-crystals of $1 \cdot 6\text{CH}_2\text{Cl}_2$, suitable for X-ray diffraction studies, were obtained by slow diffusion from a mixture of CH_2Cl_2 and hexane (1/4, v/v). The crystal consists of discrete tetranuclear $\text{Cu}_4[(\text{OPMe}_2)(\text{SPPPh}_2)\text{N}]_4$ units separated by normal van der Waals distances. The ORTEP diagram of the molecular structure of **1** (solvent molecules were omitted for clarity), with the atom numbering scheme, is shown in Figure 1. Selected interatomic distances and angles are listed in Table 2.

The tetranuclear unit contains a central Cu_4 core of distorted tetrahedral geometry. Alternatively, the Cu_4 core can be described as a folded square system [dihedral angle $\text{Cu}(1)\text{Cu}(1a)\text{Cu}(1c) / \text{Cu}(1)\text{Cu}(1b)\text{Cu}(1c)$ 86.8°] and strong transannular copper-copper interactions [$\text{Cu}(1)\text{-Cu}(1c)$ 3.060(2) Å]. The $\text{Cu}\cdots\text{Cu}$ distances [$\text{Cu}(1)\text{-Cu}(1a)$ 2.702(3) Å] in the folded square system are significantly shorter than those observed in the $[\text{Cu}_4\{(\text{SPPPh}_2)_2\text{N}\}_3]^+$ cations [range 2.763(3)-2.815(3) Å [6], 2.773(2)-2.844(2) Å [7], 2.758(1)-2.837(1) Å [8]), but in the range [2.658(5)-2.757(5) Å] found for the related dithiocarbamate $\text{Cu}_4(\text{S}_2\text{CNet}_2)_4$ [22]. The transannular $\text{Cu}\cdots\text{Cu}$ distances in **1** compare well with the longest metal-metal distances [3.092(2) Å] found in the tetranuclear $\text{Cu}_4[\text{SC}(\text{NH}_2)_2]_6(\text{NO}_3)_4 \cdot 4\text{H}_2\text{O}$ [23].

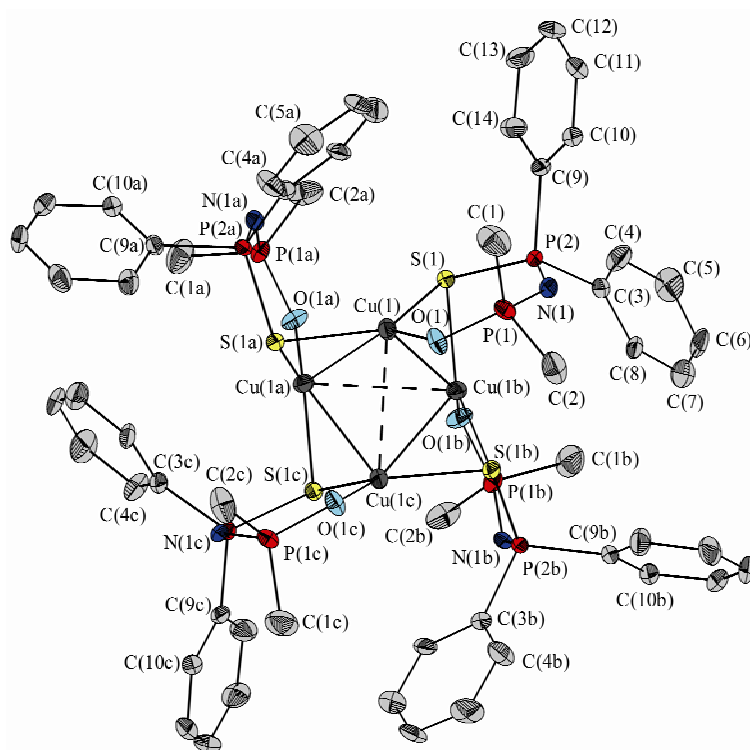


Figure 1. ORTEP representation at 20% probability and atom numbering scheme for $\text{Cu}_4[(\text{OPMe}_2)(\text{SPPH}_2)\text{N}]_4 \cdot 6\text{CH}_2\text{Cl}_2$ (**1**) (for clarity, solvent molecules and hydrogen atoms are not shown).

The central Cu_4 core is surrounded by four monothioimidodiphosphinato ligands, each exhibiting a *bimetallic triconnective* coordination pattern. The oxygen atom of a ligand unit is bound to one copper atom [Cu(1)-O(1) 1.969(9) Å], while the sulfur atom is bridging two metal centers in a symmetrical fashion [Cu(1)-S(1) 2.267(4) Å, Cu(1b)-S(1) 2.258(3) Å]. The lengths of the Cu-O and Cu-S bonds in **1** compare well with those observed in the tetrahedral isomer of $\text{Cu}[(\text{OPPh}_2)(\text{SPPH}_2)\text{N}]_2$ [Cu-O 1.940(2) / 1.934(2) Å; Cu-S 2.284(1) / 2.293(1) Å], but are considerably shorter than those observed in the copper(I) species $(\text{Ph}_3\text{P})_2\text{Cu}[(\text{OPPh}_2)_2\text{N}]$ [Cu-O 2.122(2) / 2.165(2) Å] and $(\text{Ph}_3\text{P})_2\text{Cu}(\text{S}_2\text{PMe}_2)$ [Cu-S 2.434(1) / 2.480(1) Å] [13].

As result of the coordination pattern of the monothioimidodiphosphinato ligands, the copper atoms achieve a distorted trigonal environment, with the S-Cu-S angle more opened on the expense of the O-Cu-S angles (Table 1). The

metal atom is 0.186 Å out of the plane defined by the oxygen and the two sulfur atoms, being displaced towards the centre of the Cu₄ core.

Table 2.
Interatomic bond distances (Å) and angles (°) for compound 1·6CH₂Cl₂.^a

Cu(1)-Cu(1a)	2.702(3)	Cu(1)-Cu(1b)	2.702(3)
Cu(1a)-Cu(1c)	2.702(3)	Cu(1b)-Cu(1c)	2.702(3)
Cu(1)-Cu(1c)	3.060(2)	Cu(1a)-Cu(1b)	3.060(2)
Cu(1)-O(1)	1.969(9)		
Cu(1)-S(1)	2.267(4)	Cu(1b)-S(1)	2.258(3)
Cu(1)-S(1a)	2.258(3)		
P(1)-O(1)	1.518(9)	P(2)-S(1)	2.052(4)
P(1)-N(1)	1.611(11)	P(2)-N(1)	1.537(12)
P(1)-C(1)	1.756(17)	P(2)-C(3)	1.806(12)
P(1)-C(2)	1.779(16)	P(2)-C(9)	1.828(12)
O(1)···S(1) ^b	3.569(9)		
Cu(1a)-Cu(1)-Cu(1b)	68.97(7)	Cu(1b)-Cu(1)-Cu(1c)	55.51(5)
Cu(1a)-Cu(1)-Cu(1c)	55.51(5)		
O(1)-Cu(1)-S(1)	114.6(3)	S(1)-Cu(1)-S(1a)	128.90(9)
O(1)-Cu(1)-S(1a)	114.3(3)		
O(1)-Cu(1)-Cu(1a)	147.3(3)	S(1)-Cu(1)-Cu(1a)	90.06(12)
O(1)-Cu(1)-Cu(1b)	107.9(3)	S(1)-Cu(1)-Cu(1b)	53.18(10)
O(1)-Cu(1)-Cu(1c)	95.0(3)	S(1)-Cu(1)-Cu(1c)	107.92(9)
S(1a)-Cu(1)-Cu(1a)	53.47(9)	S(1a)-Cu(1)-Cu(1b)	121.45(10)
S(1a)-Cu(1)-Cu(1c)	81.63(9)		
Cu(1)-S(1)-Cu(1b)	73.35(11)		
Cu(1)-O(1)-P(1)	124.1(5)	Cu(1)-S(1)-P(2)	101.28(16)
		Cu(1b)-S(1)-P(2)	100.42(14)
O(1)-P(1)-N(1)	116.6(5)	S(1)-P(2)-N(1)	120.1(4)
P(1)-N(1)-P(2)	136.4(7)		

^a Symmetry equivalent positions (*y*, 1.5-*x*, 0.5-*z*), (1.5-*y*, *x*, 0.5-*z*) and (1.5-*x*, 1.5-*y*, *z*) are denoted by "a", "b" and "c"; ^b Non-bonding distances.

Although the phosphorus-nitrogen bonds within the OPNPS skeleton are apparently not equivalent, suggesting a single P_O-N [1.611(11) Å] and a double P_S=N [1.537(12) Å], the difference is not significant in view of the ±3σ parameter (esd). The lengths of the phosphorus-oxygen [1.518(9) Å] and phosphorus-sulfur [2.052(4) Å] bonds are typical for single

bonds [c.f. $\text{Ph}_2\text{P}(=\text{O})\text{OH}$ [24]: P–O 1.526(6), P=O 1.486(6) Å; $\text{Me}_3\text{Sb}(\text{O}-\text{PPh}_2=\text{N}-\text{PPh}_2=\text{S})_2$ [25]: P–O 1.544(6) / 1.556(5) Å, P=S 1.962(3) / 1.972(3) Å, P_O=N 1.571(7) / 1.564(6) Å, P_S-N 1.601(7) / 1.618(6) Å; Me–S–PPh₂=N–PPh₂=S [25]: P–S 2.071(1), P=S 1.954(1), P–N 1.610(2), P=N 1.562(2) Å].

The six-membered CuOSP₂N ring is not planar, but folded along the axis joining the phosphorus atoms, with a dihedral angle of 26.7° between the best plane through Cu(1), O(1), S(1), P(1) and P(2) atoms [deviations: Cu(1) -0.001, O(1) -0.126, S(1) 0.013, P(1) 0.016, and P(2) -0.012 Å] and the P(1)N(1)P(2) plane.

Acknowledgements

This work was supported by MEdCT (grant CERES 4-62/2004) and the National University Research Council of Romania (CNCSIS grant, A-1456/2007). We thank the *National Center for X-Ray Diffraction* ("Babes-Bolyai" University, Cluj-Napoca) for support of the single-crystal X-ray diffraction studies.

REFERENCES

1. R. L. Lieberman, A. C. Rosenzweig, in: A. B. P. Lever (Ed.), *Comprehensive Coordination Chemistry II*, Vol. 8, Elsevier Pergamon, Amsterdam, Oxford, **2004**, pp. 195–211.
2. K. R. Brown, G. L. Keller, I. J. Pickering, H. H. Harris, G. N. George, D. R. Winge, *Biochemistry*, **2002**, *41*, 6469.
3. I.J. Pickering, G. N. George, C. T. Dameron, B. Kurz, D. R. Winge, I. G. Dance, *J. Am. Chem. Soc.*, **1993**, *115*, 9498.
4. Y.-Y. Niu, Y.-L. Song, H.-G. Zheng, D.-L. Long, H.-K. Fun, X.-Q. Xin, *New J. Chem.*, **2001**, *25*, 945.
5. M. Afzaal, D. J. Crouch, P. O'Brien, J. Raftery, P. J. Skabara, A. J. P. White, D. J. Williams, *J. Mater. Chem.*, **2004**, *14*, 233.
6. C. P. Huber, M. L. Post, O. Siiman, *Acta Crystallogr., Sect. B*, **1978**, *34*, 2629.
7. H. Liu, N. A. G. Bandeira, M. J. Calhorda, M. G. B. Drew, V. Felix, J. Novosad, F. F. de Biani, P. Zanello, *J. Organomet. Chem.*, **2004**, *689*, 2808.
8. M. C. Aragoni, M. Arca, M. B. Carrea, F. Demartin, F. A. Devillanova, A. Garau, M. B. Hurthouse, S. L. Huth, F. Isaia, V. Lippolis, H. R. Ogilvie, G. Verani, *Eur. J. Inorg. Chem.*, **2006**, 200.
9. D. J. Birdsall, A. M. Z. Slawin, J. D. Woollins, *Inorg. Chem.*, **1999**, *38*, 4152.
10. P. Moore, W. Errington, S. P. Sangha, *Helv. Chim. Acta*, **2005**, *88*, 782.
11. I. Haiduc, R. Cea-Olivares, R. A. Toscano, C. Silvestru, *Polyhedron*, **1995**, *14*, 1067.
12. J. Novosad, M. Necas, J. Marek, P. Veltsistas, C. Papadimitriou, I. Haiduc, M. Watanabe, J. D. Woollins, *Inorg. Chim. Acta*, **1999**, *290*, 256.

NEW COPPER(I) AND COPPER(II) TETRAORGANODICHALCOGENOIMIDODIPHOSPHINATES

13. A. Silvestru, A. Rotar, J. E. Drake, M. B. Hursthouse, M. E. Light, S. I. Farcas, R. Rosler, C. Silvestru, *Can. J. Chem.*, **2001**, *79*, 983.
14. H. Liu, M. J. Calhorda, M. G. B. Drew, V. Felix, J. Novosad, L. F. Veiros, F. F. de Biani, P. Zanello, *J. Chem. Soc., Dalton Trans.*, **2002**, 4365.
15. H. Richter, E. Fluck, H. Riffel, H. Hess, *Z. Anorg. Allg. Chem.*, **1983**, *496*, 109.
16. X. Wang, S.-C. Xiang, T.-L. Sheng, R.-B. Fu, Y.-M. Li, X.-T. Wu, *Jiegou Huaxue (Chinese J. Struct. Chem.)*, **2006**, *25*, 459.
17. R. Rösler, M. Stanciu, J. Yang, J. E. Drake, C. Silvestru, I. Haiduc, *Phosphorus, Sulfur & Silicon*, **1998**, *132*, 231.
18. R. Rösler, C. Silvestru, G. Espinosa-Perez, I. Haiduc, R. Cea-Olivares, *Inorg. Chim. Acta*, **1996**, *241*, 47.
19. G. M. Sheldrick, *SADABS, Program for area detector adsorption correction*, Institute for Inorganic Chemistry, University of Göttingen, Germany, **1996**.
20. Sheldrick GM, *SHELXTL-97*, University of Göttingen, Germany, **1997**.
21. DIAMOND – Visual Crystal Structure Information System, CRYSTAL IMPACT: Postfach 1251, D-53002 Bonn, Germany, **2001**.
22. R. Hesse, *Ark. Kemi*, **1963**, *20*, 481.
23. E. H. Griffith, G. W. Hunt, E. L. Amma, *J. Chem. Soc., Chem. Commun.*, **1976**, 432.
24. D. Fenske, R. Mattes, J. Löns, K.-F. Tebbe, *Chem. Ber.*, **1973**, *106*, 1139.
25. I. Ghesner, A. Soran, C. Silvestru, J. E. Drake, *Polyhedron*, **2003**, *22*, 3395.

ADINA ROTAR, OVIDIU MOLDOVAN ET AL.

*Dedicated to Professor Ionel Haiduc,
President of The Romanian Academy at his 70th anniversary*

STUDIES ON SOME OZONE DECOMPOSITION CATALYSTS BASED ON NICKEL OXIDE

**CRINA DAN¹, ELISABETH-JEANNE POPOVICI²,
FLORICA IMRE^{1,2}, EMIL INDREA³, PETRE MĂRGINEAN³
AND IOAN SILAGHI-DUMITRESCU¹**

ABSTRACT. In order to obtain some efficient ozone decomposition catalysts, nickel oxide powders or alumina-supported nickel oxide samples were prepared and characterised. The catalytic activity of NiO-based catalysts for O₃ decomposition, in correlation with their crystalline structure and surface characteristics is investigated.

Key words: catalysts; ozone decomposition; nickel oxide; alumina;

1. Introduction

Ozone is a toxic substance commonly found or generated in human environments (aircraft cabins, offices with photocopiers, laser printers). Moreover, ozone is used in many industrial applications as oxidising agent for example for bleaching, sterilization and wastewaters treatment. For this reason, catalytic ozone decomposition is of practical significance. It proceeds in the presence of precious metals or/and other transition metal oxides deposited onto alumina, and/or titania and/or silica support [1-6]. The catalysts composition and preparation technique as well as the carrier characteristics affect their physico-chemical properties and catalytic activity in the process of destruction of ozone in industrial waste gases [7,8].

In order to prepare some efficient ozone decomposition catalysts for environment protection, a complex study has been initiated in our group. In this respect, the preparation and characterisation of some alumina supported manganese, nickel, silver and/or copper based catalysts and their catalytic behaviour in ozone decomposition process was investigated. Our previous works showed that manganese oxide supported on gamma alumina is efficient for ozone destruction [9,10]. The present paper refers to the preparation and characterisation of some nickel based catalysts. The goal of the study is to establish the correlation between the catalytic activity and crystalline structure and surface area of catalysts.

¹ Faculty of Chemistry and Chemical Engineering "Babes-Bolyai" University, 400028, Cluj-Napoca,

² "Raluca Ripan" Institute for Research in Chemistry, Fântânele 30, 400294 Cluj-Napoca,

³ "National Institute for R & D for Isotopic and Molecular Technology, 400293 Cluj-Napoca, Romania

2. Experimental part

Nickel oxide-based catalysts were obtained by thermal dissociation of nickel nitrate. Sample **K70**, the un-supported NiO catalyst, was prepared from $\text{Ni}(\text{NO}_3)_2 \cdot 6\text{H}_2\text{O}$ (Merck) crystals calcined for 2 hrs at 500°C. Sample **K66**, the supported NiO/ Al_2O_3 catalyst, was prepared by impregnation method. The pre-heated support was immersed into 1.0 M solution of nickel nitrate (10 g Al_2O_3 extrudates in 25 ml nickel nitrate solution). After 24 hrs, the impregnated support was filtered, dried and calcined for 2hrs at 500°C.

All thus prepared materials have been investigated by X-ray diffraction (DRON 3M Diffractometer; CuK_α radiation), FT-IR spectroscopy (JASCO-610 Spectrophotometer; KBr disks) and Brunauer- Emmett –Teller (BET) analysis (krypton adsorption isotherms). The catalytic activity was measured for ozone decomposition process, by using a testing installation containing a thermostated Al- reactor ($\varnothing=4$ mm). Ozone was prepared from oxygen, with a generator manufactured by S.C.RAAL S.A. Bistrița (Romania). The gas flow was 15 l/h and the measuring temperature was 25°C. Ozone concentration before and after passing through the catalyst layer (~0.06 g material) was determined with an OZOMAT analyser (ANSEROS)

3. Results and discussion

Alumina supported nickel-based catalyst was prepared by impregnation method and was compared with the corresponding un-supported sample, in order to correlate the catalytic performances with the physical-chemical characteristics. The catalytic active substance, resulting from the thermal dissociation of the adsorbed nickel nitrate, was formed on and inside the alumina grains. The influence of the substrate surface on the crystalline organisation, structural purity and catalytic activity of catalysts was illustrated by usual investigations.

The crystalline structure of samples was evaluated on the basis of XRD patterns (Figure 1). The support, sample **S1**, shows the typical cubic crystalline structure of gamma-alumina (in agreement with PDF file 100425, from Powder Data File database). The characteristic lines (311), (400) and (440) appear at $2\theta = 37.20$; 45.60 and 67.03 respectively. The unsupported catalyst, sample **K70**, is a black powder of NiO with cubic crystalline structure (cf. PDF 780423). The characteristic lines (-111), (111) and (-202) appear at $2\theta = 35.43$, 38.62 and 48.81 respectively. XRD pattern of the supported catalyst, sample **K66**, is dominated by the diffraction lines of the gamma-alumina support. Additional lines of NiAl_2O_4 spinel (cf. PDF 780552) superimposed over the support bands are put in evidence. The characteristic lines (220), (311) and (400) of the cubic NiAl_2O_4 can be noticed at $2\theta = 31.57$, 36.39 and 44.80.

The infrared absorption spectra of precursor, support and catalysts are used to illustrate “the structural” purity of materials (Figure 2). FT-IR spectrum of γ - Al_2O_3 contains some specific absorption bands in the small wavenumber domain [$\nu(\text{Al-O}) \sim 598 \text{ cm}^{-1}$]. The bands assigned to NO_3 group and HO and HOH bonds of the entrained water can be noticed in precursor spectrum, sample **K70p**. During the precursor calcination stage, the specific $\nu_{\text{asym}}(\text{NO}_3) \sim 1385 \text{ cm}^{-1}$ and $\pi(\text{NO}_3) \sim 824 \text{ cm}^{-1}$ bands disappear, irrespective of the presence or absence of the support.

The surface area S_σ of materials was of $269 \text{ m}^2/\text{g}$ for **S1**, $269 \text{ m}^2/\text{g}$ for sample **K66** and $15.6 \text{ m}^2/\text{g}$ for sample **K70**. The surface area of supported catalyst is determined by the γ - Al_2O_3 characteristics. The deposition of the catalytic active substance does not change the support porosity and surface area, which determines the specific properties of the catalyst. The supported NiO catalyst possesses a surface area of about 17 times larger than that of the un-supported material.

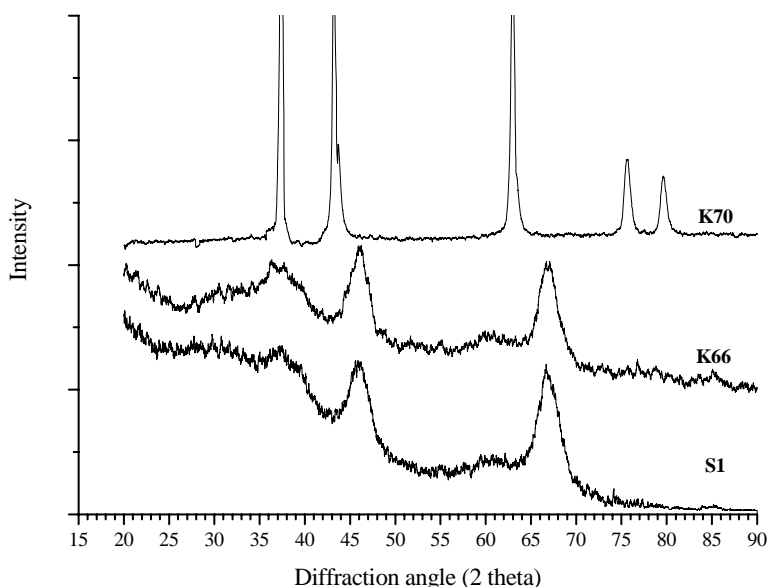


Figure 1. XRD patterns of Al_2O_3 -support (**S1**), NiO (**K70**) and NiO/ Al_2O_3 (**K66**)

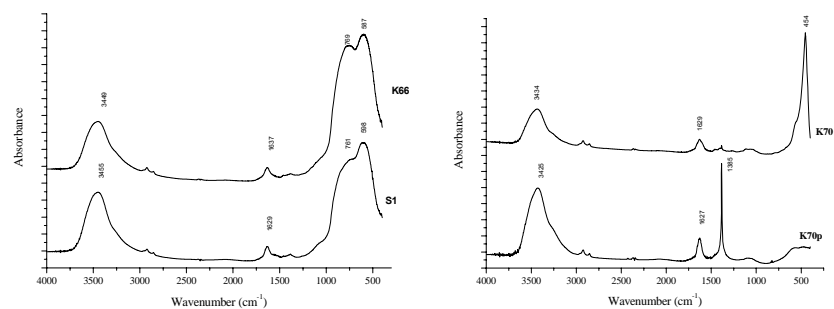


Figure 2. FT-IR spectra of Al₂O₃-support (**S1**), NiO/Al₂O₃ (**K66**), NiO (**K70**) and Ni(NO₃)₂·6H₂O precursor (**K70p**)

The catalytic activity of samples was evaluated for ozone decomposition $O_3 \xrightarrow{k_1} 3/2 O_2$, on the basis of the conversion yield (η) expressed by $\eta = 100(C_0 - C)/C_0$, where C_0 and C is the O_3 -concentration before and after passing through the catalyst layer, for a certain material amount.

The ozone conversion yield determined in identical experimental conditions (catalysts amount, space velocity, reagent concentration) is a direct measure of the catalytic efficiency of catalysts used for ozone decomposition. The time dependence of the conversion yield of investigated materials is presented in Figure 3.

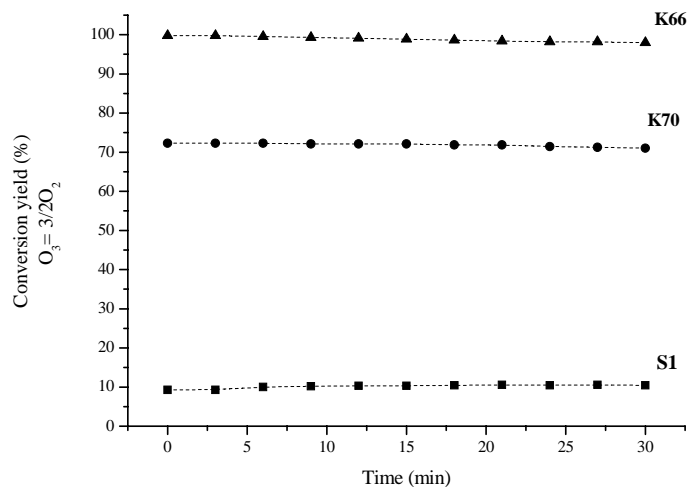


Figure 3. Catalytic efficiency of Al₂O₃-support (**S1**), NiO (**K70**) and NiO/Al₂O₃ (**K66**)

The sample **K66** (NiO/Al₂O₃) with very large surface area produces the decomposition of over 99% ozone in the first 6 testing minutes. The efficiency decreases to 97 %, in 30 minutes. The catalytic efficiency of un-supported **K70** catalyst is only 71% and decrease very little during the testing period. As expected, the alumina support itself, sample **S1**, induces a small ozone decomposition effect, probable due to the porosity/surface effect.

The catalytic efficiency of NiO-based catalysts is much higher than that of the corresponding MnO₂-based catalysts [10]. The catalytic efficiency is ~70% for MnO₂/Al₂O₃ while for NiO/ Al₂O₃ it is 99%. One of the major differences between the two kinds of catalysts is the presence of NiAl₂O₄ spinel generated by the interaction of nickel compound with the support. One can suppose that the high catalytic efficiency is associated with the presence of some active centres that involve the highly dispersed spinel material over the alumina surface.

4. Conclusions

Several nickel - based catalysts were prepared and characterised. The catalytic activity for ozone decomposition process in correlation with some peculiar physical-chemical characteristics was investigated. The major role of alumina support on the increase of catalyst – gas contact surface was put in evidence.

Acknowledgement

The financial support of the Romanian Ministry of Education and Research [MATNANTECH Project 225(405)] is gratefully appreciated.

REFERENCES

1. F. Arena, T. Torre, C. Raimondo, A.Parmalina, *Phys.Chem.Chem. Phys.*, **2001**, 3, 1911-1917.
2. R. Radhakrishnan, S. T. Oyama, *J. Catal.*, **2001**, 199, 282-290.
3. Wei Li, G.V.Gibbs, S.T.Oyama *J. Am. Chem. Soc.*, **1998**, 35, 9041-9046.
4. H. Einaga, M. Harada, *J. Catal.*, **2004**, 227, 304-312.
5. C. Subrahmanyam, D. A. Bulushev, L. Kiwi-Minsker, *Applied Catal. B; Environ.*, **2005**, 61, 98-106.
6. H. Falke, G. Strauss US 503467, 23 July, **1991**.
7. P.H. Bolt, F.H.P.M. Habraken, J.W. Geus, *J Solid State Chem.*, **1998**, 135, 59-69.
8. B.Dhandapani, S.T.Oyama, *Applied Catal. B. Environm.*, **1997**, 11, 129-166.
9. A.-M. Valean, E.-J. Popovici, C. Dan, V.Pop, P. Margineanu, *Stud.Univ.Babes Bolyai, Physica*, **2005**, L(3), 467-470.
10. C. Dan, E.-J. Popovici, A.-M. Valeanu, E.I Indrea, P. Margineanu, *Stud. Univ. Babes Bolyai, Physica*, **2005**, L(3), 463-467.

CRINA DAN, ELISABETH-JEANNE POPOVICI ET AL.

*Dedicated to Professor Ionel Haiduc,
President of The Romanian Academy at his 70th anniversary*

LYSINE MEDIATED ASSEMBLY OF GOLD NANOPARTICLES

OSSI HOROVITZ¹, AURORA MOCANU¹, GHEORGHE TOMOAI², LIVIU BOBOS¹, DIANA DUBERT¹, IULIA DAIAN¹, TRAIANOS YUSANIS³ AND MARIA TOMOAI-COTISEL¹

ABSTRACT. This paper reports the data of an investigation of the gold nanoparticles assembly mediated by organic molecules, such as lysine. Gold nanoparticles were synthesized in citrate aqueous solution and characterized by UV-Vis spectroscopy and a strong absorption band at 528 nm is found for surface plasmon resonance. Transmission electron microscopy (TEM) images indicate a mean gold nanoparticle size of about 14 nm. The aqueous colloidal gold solution is stable in time, indicating a good electrostatic stabilization of gold nanoparticles through the adsorbed monolayer of citrate anions on nanoparticle surface. The interaction between the citrate capped gold nanoparticles in aqueous solution and lysine was investigated monitoring their UV-Vis spectra. At a certain lysine/gold ratio a new, large absorption band appears between 600 and 700 nm, which increases in time, while the color of the colloidal gold solution changes from red to blue. The 528 nm band decreases, as a consequence of the assembly formation of gold nanoparticles mediated by lysine. The nanostructure of the lysine mediated assembly of gold particles is analyzed by TEM and atomic force microscopy (AFM). The TEM and AFM images evidence the assembly of gold nanoparticles, where particles are not in direct physical contact. This effect could be explained primarily through the zwitterion-type electrostatic interactions between the charged amine and acid groups of the lysine molecules adsorbed and bound to different gold nanoparticles. These findings provide new insights into the precise control of interfacial interactions between organic molecules anchored on gold nanoparticles.

Keywords: *gold nanoparticles, lysine, self-assembly, UV-Vis spectra, TEM, AFM.*

Introduction

One of the problems which has attracted the attention of both science and industry is the integration of nanoparticles and organic molecules, in order to develop new materials for electronics and optics and new applications in biomedical and bioanalytical areas, such as controlled drug delivery, medical diagnosis devices and biosensors [1-6].

Amino acids are a promising class of organic compounds to be used in biofunctionalization of gold nanoparticles, as protective layers and for their

¹ Babes-Bolyai University of Cluj-Napoca, Faculty for Chemistry and Chemical Engineering, 400028 Cluj-Napoca, Romania,

² Iuliu Hatieganu University of Medicine and Pharmacy, Department of Orthopedic Surgery, 400015 Cluj-Napoca, Romania,

³ Aristotle University of Thessaloniki, 54006 Thessaloniki, Greece

assembly. Functional groups such as -SH and -NH₂ present a high affinity for gold, and since amino acids contain some of these groups, they are expected to stabilise gold nanoparticles. Their capacity of generating structural diversity was recognised [7], and gold surfaces capped with amino acids are considered to represent the simplest mimics for protein surfaces [8]. However, there are relatively few reports in the literature on surface modifications of gold nanoparticles with amino acid molecules [9–14], but no systematic study of amino acid interactions with gold nanoparticles is available.

Amino acids can be used in the assembly formation of inorganic nanoparticles. If such molecules are adsorbed and bonded to the nanoparticle surface, amino acids belonging to two different nanoparticles can be connected through a condensation reaction with peptide bonding formation, thus leading to a peptide-linked assembly of nanoparticles. The properties of such assemblies could be designed rationally by choosing the initial amino acid.

Alternatively, amino acids can be adsorbed on the metallic particle surface already during the formation of nanoparticles, using the amino acid itself as reduction agent [14–18], or latter, by ligand exchange reactions or binding on the former adsorbed stabilising molecules. In this way protecting homogeneous or heterogeneous, mixed monolayers of metallic nanoparticles can be obtained.

In our previous work, we synthesized gold nanoparticles in aqueous solutions of citrate and used them to be functionalized with biomolecules, such as protein extracted from aleurone cells of barley [19]. How citrate anions, capping agents of gold nanoparticles, are involved in the interaction between gold nanoparticles and amino acids and how colloidal solution pH influences the nanoparticle assembly are questions to be answered.

The aim of this investigation is to gain insights into the assembly formation of gold nanoparticles and interparticle interactions in the presence of lysine, which could have potential application for the analytical detection of amino acids found in various media. The investigation of the effect of lysine concentrations on the surface plasmon resonance (SPR) band evolution of gold nanoparticles is examined to describe the lysine effect on electrostatic interactions and on interparticle binding properties. The results provide important information on the affinity of gold nanoparticles to lysine molecules and its optical applications.

Lysine (three-letter code: Lys or one-letter code: K) is an amino acid with a ϵ -amine group on the side chain (Fig.1). It is a basic, positively charged, polar amino acid, with hydrophilic properties [20]. Its pK_a values are: 2.20 (for the carboxylic group), 9.20 (for the α -amine group) 10.1 (for the ϵ -amine group); and the isoelectric pH is about 9.65. Therefore, lysine is a monocationic molecule in a large interval of pH from about 4 to almost 8.

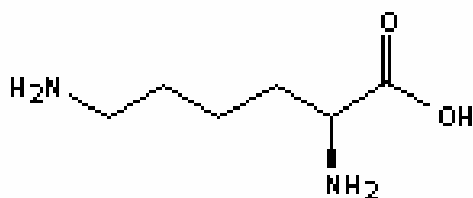


Fig.1. Lysine formula

The understanding of the gold interparticle binding properties, in the presence of lysine, where both hydrogen bonding and electrostatic interactions could be operative in the assembly process of gold nanoparticles, is an important focus in this investigation.

Experimental part

An aqueous colloidal gold solution was prepared by HAuCl_4 reduction with sodium citrate, in variants of the Turkevich method, as adapted from [19, 21]. Deionized water with resistivity of $18 \text{ M}\Omega\cdot\text{cm}$ was used in all experiments and it was obtained from an Elgastat water purification system. A 200 mL 0.005% (w/w) $\text{HAuCl}_4\cdot 3\text{H}_2\text{O}$ solution stirred vigorously was refluxed. To the boiling solution 15.3 mg trisodium citrate ($\text{Na}_3\text{C}_6\text{H}_5\text{O}_7\cdot 2\text{H}_2\text{O}$), solved in a minimum amount of water, was added. After color change, the heat was turned off and the solution was allowed to cool overnight to room temperature. The gold content in the final colloidal solution (c_{Au}) is 25 mg/L. The resulting solution of colloidal gold nanoparticles was stored in a brown bottle and kept at 4°C .

Solid L-lysine was purchased from Sigma and used without further purification. Lysine was dissolved in deionized water.

The UV/Vis absorption spectrum of all solutions was studied using a Jasco UV/Vis V-530 spectrophotometer with 10 mm path length quartz cuvettes in the 190 – 900 nm wavelengths range.

The molar concentrations (c_K) of lysine solutions used in the experiments were the following: 0.01, 0.10 and 0.54.

The investigated mixtures were obtained from the gold colloidal solution (c_{Au}) and the lysine solutions (concentration c_K), by successive removal of small amounts of the previous mixture and the adding of equal amounts of amino acid solution. The gold and lysine contents in the resulting mixtures and their ratios, used in most of the determinations, are given in Table 1.

The gold nanoparticles suspension in the absence and in the presence of lysine was air-dried on the specimen grid and observed with a transmission electron microscope (TEM: JEOL – JEM 1010). TEM

specimens consist of carbon or collodion coated copper grids. TEM images have been recorded with a JEOL standard software.

Table 1.
Gold / lysine ratios in the investigated mixtures. The concentration of the colloidal gold solution is c_{Au} ; the concentration of the lysine solution is c_K .

Gold content reported to c_{Au}	Lysine content reported to c_K	Content Au/K ratio reported to (c_{Au}/c_K)
0.833	0.167	5 / 1
0.695	0.306	2.2 / 1
0.579	0.421	1.4 / 1
0.483	0.518	1 / 1.1
0.402	0.598	1 / 1.5
0.335	0.665	1 / 2
0.322	0.679	1 / 2.1
0.214	0.786	1 / 3.7

Atomic force microscopy (AFM) investigations were executed on the gold nanostructured films without and with lysine using a commercial AFM JEOL 4210 equipment with a 10 x 10 (x-y) μm scanner operating in tapping (noted *ac*) mode on thin ordered gold adsorbed films on glass plates, that are optically polished and silanized with 3-aminopropyl-trietoxysilane or are prior treated to be positively charged. Standard cantilevers, non-contact conical shaped of silicon nitride coated with aluminum, were used. The tip was on a cantilever with a resonant frequency in the range of 200 - 300 kHz and with a spring constant of 17.5 N/m. AFM observations were repeated on different areas from 30 x 30 μm^2 to 250 x 250 nm^2 of the same gold film. The images were obtained from at least ten macroscopically separated areas on each sample.

All images were processed using the standard procedures for AFM. The sizes of nanoparticles were measured directly from AFM 2D-topographic images and their 3D-views. The thickness (vertical distance) variations were estimated from vertical linear cross sections and height distributions on AFM images [22-26]. AFM images consist of multiple scans displaced laterally from each other in y direction with 512 x 512 pixels. Low pass filtering was performed to remove the statistical noise without to loose the features of the sample. All AFM experiments were carried out under ambient laboratory conditions (about 20 °C) as previously reported [23, 25].

Results and discussion

Characterization of the colloidal gold solution.

The size of the colloid gold particles has been measured by TEM imaging. Two representative TEM images of these gold particles are shown in Fig.2. The particles show mostly spherical or elliptical (ovaliform) shape,

just a few triangles, pentagons or hexagons are observed. From the sizes of a great number of particles, measured on the TEM images, an average size (diameter) of about 14.2 nm with a standard deviation of 2.6 nm were calculated as well as the extreme values of the sizes, from 8.5 to 24 nm.

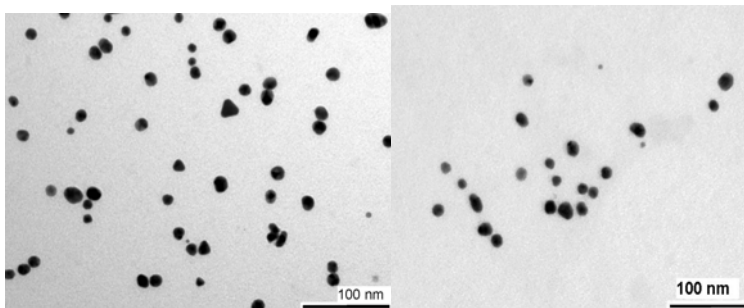


Fig.2. TEM images of gold nanoparticles

From these, the approximate average mass of a nanoparticle (considered spherical) is estimated as $2.9 \cdot 10^{-17}$ g, the number of gold atoms in a particle $8.8 \cdot 10^4$ and the number of particles per cm^3 of solution: $8.6 \cdot 10^{11}$.

The visible absorption spectra of the aqueous colloidal gold solution presents a well-defined absorption maxima at the wavelength $\lambda_{\text{max}} = 528 - 529$ nm (Fig. 3). This value is characteristic for plasmon absorbance for nanometric gold particles. The wavelength was not significantly modified during a year after preparation.

Thus, the colloidal gold solution proved to be very stable in time, without observable modifications in the UV-Vis spectrum for a year after preparation. This indicates electrostatic stabilization via citrate anions adsorbed on the surface of gold nanoparticles and the gold nanoparticles are negatively charged.

Interactions of the colloidal gold with lysine.

The UV-Vis spectrum of lysine solutions presents no absorption bands in the range of wavelengths investigated here.

The adding of a diluted 0.01 M lysine solution (Fig. 3a) produces no or little modification in the UV-Vis spectrum of the colloidal gold solution. Besides the lowering of the absorbance due to the dilution of the gold solution, the absorption maxima are lightly shifted towards longer wavelength. This shift is due to the changes in the dielectric constant in the adsorption layer anchored on the gold nanoparticles surface. This effect, probably, is due to an increase

of the average refractive index of the environment surrounding the gold nanoparticles and to the size increase of particles by the adsorbed layer.

For a more concentrated lysine 0.1 M solution (Fig. 3b) the shift towards higher wavelengths is much more important. For higher quantities of lysine added to the colloidal gold solution the SPR band becomes substantially larger, suggesting an increasing assembly formation of gold nanoparticles.

Thus, these data (Fig. 3b) show the appearance of the broad peak at longer wavelengths in the UV-Vis spectrum. This fact results from the coupling of surface plasmon resonance of two adjacent nanoparticles. This finding is an indication of the anisotropic optical properties of the gold nanoparticles self-assembled or aggregated in agreement with other published data on related systems [27].

With a very concentrated (0.54 M) lysine solution, the band for the assembly formation of gold nanoparticles mediated by lysine appears at once (maximum at about 634 nm, Fig. 3c), while the 529 nm band for individual gold particles decreases and appears only as a shoulder in the spectrum. The maximum of the broad absorption band continues its shift towards higher wavelengths in time (Fig. 3c).

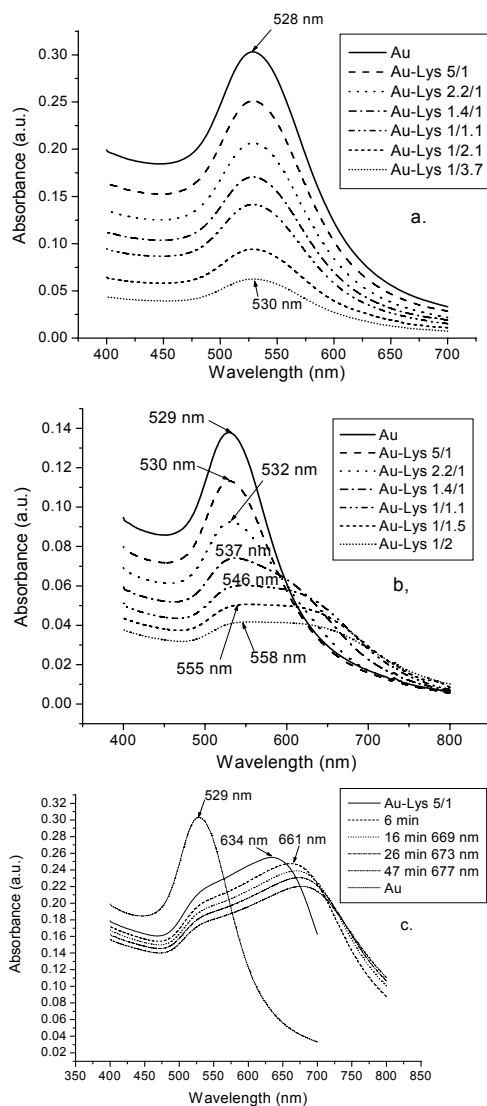


Fig. 3. Optical spectrum of colloidal gold solution with added 0.01 M (a) and 0.1 M (b) lysine solution at different ratios, and with 0.54 M lysine solution in time (c).

LYSINE MEDIATED ASSEMBLY OF GOLD NANOPARTICLES

The color of the solution is changed from reddish to blue. This kind of color change is considered as an effect of the self-assembly or aggregation phenomenon [28, 29]. When the interparticle distance in the assemblies or aggregates decreases to less than about the average nanoparticle diameter, the electric dipole–dipole interaction and the coupling between the plasmons of neighboring particles result in the bathochromic shift of the absorption band.

Lysine adsorption on gold nanoparticles has been investigated [30], using 13 nm diameter gold particles and a $7 \cdot 10^{-4}$ M L-lysine solution at pH about 10.7. The UV-Vis spectrum showed a SPR peak at 520 nm, similar to that found for citrate coated nanoparticles. This result is similar to our results, using the most diluted lysine solution. By adding a condensing agent, the authors [30] observed that gold particles were aggregated by the formation of peptide bonds between two lysine molecules adsorbed on different gold nanoparticles. In the UV-Vis spectrum the SPR band of gold nanoparticles was shifted to 527 nm and a new broad peak appeared at 633 nm. For this situation, the spectrum is similar to that obtained by us at high concentrations of the lysine solution, pleading for assembly formation of gold nanoparticles mediated by lysine.

TEM images for gold nanoparticles with a 0.1 M lysine solution (Fig. 4) show both linearly ordered nanoparticles and more complex arrangements. Finally, these arrangements generate an almost ordered assembly of gold nanoparticles, mediated by lysine molecules, as also evidenced by AFM observations.

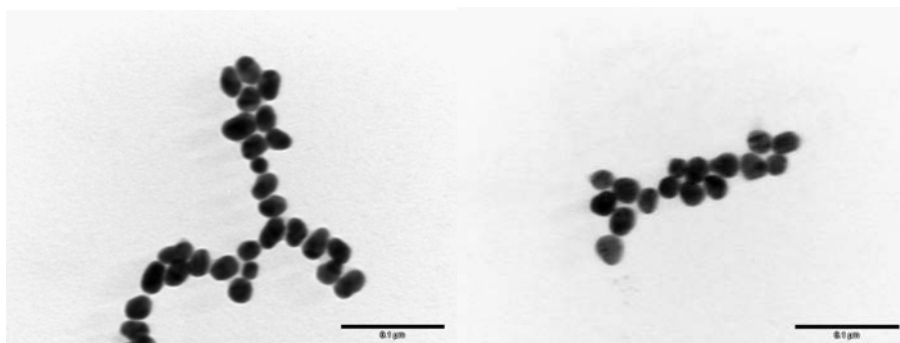


Fig.4. TEM images of gold nanoparticles capped with lysine (0.1 M), for the volume ratio 1:1 of aqueous solutions, at 30 sec after the mixing process.

The atomic force microscope allows simultaneous acquisition of multiple images, such as topography and phase images, under tapping mode operation. The assembly of gold nanoparticles, mediated by lysine,

was deposited on planar hydrophobic glass or on positively charged glass surfaces. Then, the assembly was observed by AFM under tapping mode and the structural features are visualized in Fig. 5. The two-dimensional topographic image (Fig. 5a) shows the morphology of an almost ordered

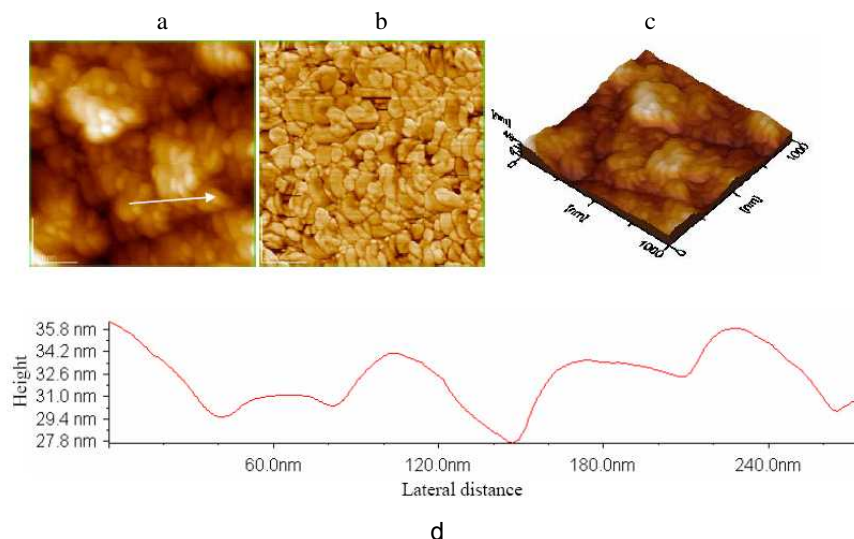


Fig. 5. 2D-topographic (a) and phase (b) AFM images of the assembly of gold nanoparticles, mediated by lysine, deposited on glass after one hour deposition time; scanned area 1000 x 1000 nm²; 3D-view (c) of the topography (a); (d) cross section profile along the arrow in panel a; RMS of image panel (a) is 2.6 nm.

structure within domains, with small defects at domain boundaries. For this assembly of gold nanoparticles mediated by lysine, immobilized on planar glass surface, individual gold nanoparticles are visible from 2D-topography (Fig. 5a) and 3D-view (Fig. 5c). The image phase (Fig. 5b) show also that the assembly of gold nanoparticles mediated by lysine is almost compact.

The AFM images were acquired with high resolution as in the case of imaging assemblies of lipid molecules [22-26], assemblies of protein molecules [31, 32] or assemblies of gold nanoparticles mediated by different organic molecules [19], despite the structural complexity of molecules or of gold nanoparticles arrangements.

The AFM images evidence both the selectivity of lysine adsorption and its orientation on gold surface and the self-assembly process of gold nanoparticles within a compact network, as observed by UV-Vis spectroscopy (Fig. 3). Also, the gold nanoparticles appear almost ordered both in AFM images and in cross section profile (Fig. 5d) in substantial agreement with TEM images.

For lysine the binding with the gold nanoparticles surface may be achieved through the ϵ -amine group. The binding could occur through the electrostatic interaction of the lysine protonated ϵ -amine group ($-\text{NH}_3^+$) with the negatively charged citrate anions adsorbed on gold surface. On the other hand, a direct bonding of the amine group to the gold surface can not be excluded (Fig. 6).

All the charged amino acids present such strong interactions with gold surface, so are the amino acids that are usually *positively charged* (i.e. protonated), such as lysine (K), arginine (R) and histidine (H). A possible amino acid binding to gold nanoparticles and the formation of particle aggregates are schematized for lysine in Fig.6.

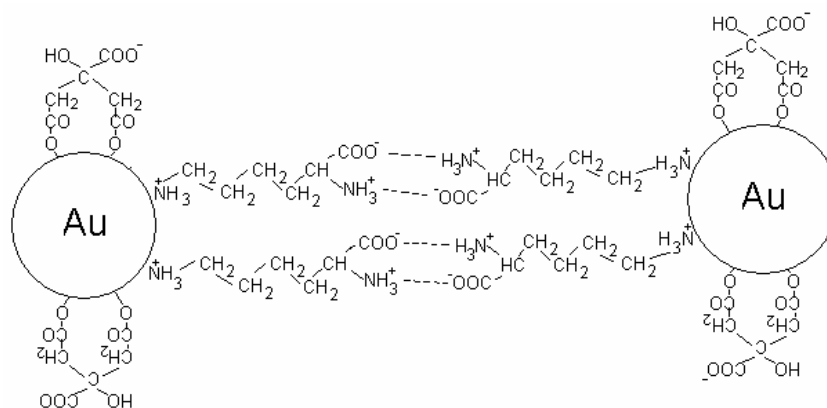


Fig. 6. Schema of lysine binding to citrate capped gold nanoparticles and bonds formation between gold nanoparticles.

Conclusions

Our investigations indicate that the assembly of gold nanoparticles can be induced by lysine, an amino acid possessing an additional functional group, i.e. ϵ -amine, besides the alpha-amine group. The correlation between physical and chemical properties of amino acids, such as hydrophobicity and acidity or basicity in various protolytic equilibria, and their molecular structure is in substantial agreement with their assembly effect on the gold nanoparticles. This effect could be explained primarily through the zwitterion-type electrostatic interactions between the charged amine and acid groups of lysine adsorbed and bound to different gold nanoparticles.

The affinity of gold nanoparticles towards lysine can lead to the development of new detection methods for analytical purposes, medical diagnostics and biosensors and to potential controlled drug delivery applications. On the other hand, the use of amino acids both in the

functionalization of gold nanoparticles and in the cross-linking of amino acid capped gold nanoparticles leading to stable self-assemblies are promising ways to the synthesis of nanostructured biomaterials. The stabilization of gold nanoparticles through amino acids is also important for the understanding of complex phenomena involved in the formation of new biomaterials by binding of proteins with gold nanoparticles with important implications in nanoscience and nanotechnology.

In future studies, the nanoengineering approach will be extended to explore the possible improvement in nanofabrication methods to reach amino acids and protein immobilization at molecular precision to control both the lateral and perpendicular orientations of functionalized gold nanoparticles. Definitely, the high-resolution engineering and imaging studies reveal the nanoscale and molecular level details for supramolecular chemistry and self-assembly processes, e.g., the influence of size, orientation and the local orders, with applications in bioscience [32]. Thus, the assemblies can be designed to contain the desired charged or chemical functionalities that will affect the intermolecular interactions such as van der Waals forces, hydrogen bonding, polar attractions and hydrophobic interactions.

Acknowledgement

This research was financially supported by the Romanian Ministry of Education and Research (Scientific research project no.5/2005, within the Excellency Research Program).

REFERENCES

1. M. Zheng, X. Huang, "Biofunctionalization of Gold Nanoparticles". In "Biofunctionalization of Nanomaterials", Editor: C.S.S.R. Kumar, Wiley-VCH Verlag GmbH & Co KGaA, Weinheim, **2005**, pp. 99-124.
2. D. Fitzmaurice, S. Connolly, *Adv. Mater.*, **1999**, *11*, 1202-1205.
3. S. Mann, W. Shenton, M. Li, S. Connolly, D. Fitzmaurice, *Adv. Mater.*, **2000**, *12*, 147-150.
4. M. C. Daniel, D. Astruc, *Chem. Rev.*, **2004**, *104*, 293-346.
5. N. L. Rosi, C. A. Mirkin, *Chem. Rev.*, **2005**, *105*, 1547-1562.
6. J. C. Love, L. A. Estroff, J. K. Knebel, R. G. Nuzzo, G. M. Whitesides, *Chem. Rev.*, **2005**, *105*, 1103-1170.
7. G. M. Coppola, H. F. Schuster, "Asymmetric Synthesis. Construction of Chiral Molecules Using Amino Acids", Wiley, New York, 1987.
8. C. C. You, M. De, G. Han, V. M. Rotello, *J. Am. Chem. Soc.*, **2005**, *127*, 12873-12881.

9. R. Levy, R. C. Doty, "Stabilization and Functionalization of Metallic Nanoparticles: the Peptide Route". In "Biofunctionalization of Nanomaterials", Editor: C.S.S.R. Kumar, Wiley-VCH Verlag GmbH & Co KGaA, Weinheim, **2005**, pp. 235-269.
10. J. Zsang, Q. Chi, J.U. Nielsen, E.P. Friis, J.E.T. Andersen, J. Ulstrup, *Langmuir*, **2000**, *16*, 7229-7237.
11. S. Mandal, S. Phadtare, M. Sastry, *Curr. Appl. Phys.*, **2005**, *4*, 118-127.
12. P. R. Selvakannan, S. Mandal, S. Phadtare, R. Pasricha, M. Sastry, *Langmuir*, **2003**, *19*, 3545-3549.
13. H. Joshi, P. S. Shirude, V. Bansal, K. N. Ganesh, M. Sastry, *J. Phys. Chem. B*, **2004**, *108*, 11535-11540.
14. Y. Shao, Y. Jin, S. Dong, *Chem. Commun.*, **2004**, 1104-1105.
15. S. Mandal, P. Selvakannan, S. Phadtare, R. Pasricha, M. Sastry, *Proc. Indian Acad. Sci. (Chem. Sci.)*, **2002**, *114*, 513-520.
16. P. Selvakannan, S. Mandal, S. Phadtare, A. Gole, R. Pasricha, S. D. Adyanthaya, M. Sastry, *J. Colloid Interface Sci.*, **2004**, *269*, 97-102.
17. S. Aryal, B.K. Remant, B. Narayan, C.K. Kim, H.Y. Kim, *J. Colloid Interface Sci.*, **2006**, *299*, 191-197.
18. S.K. Bhargava, J.M. Booth, S. Agrawal, P. Coloe, G. Kar, *Langmuir*, **2005**, *32*, 5949-5956.
19. O. Horovitz, A. Mocanu, Gh. Tomoaia, L. Olenic, Gh. Mihăilescu, O. Borosțean, A. Popoviciu, C. Crăciun, T. Yupsanis, M. Tomoaia-Cotișel, "Synthesis, Characterization and Properties of Gold Nanoparticles in Colloidal Aqueous Solutions in the Absence and in the Presence of Globular Proteins. Auto-Assembled Gold Nanostructures in Thin Films". In "Convergence of Micro-Nano-Biotechnologies", Series "Micro and Nanoengineering", **Volume 9**, Editors: M. Zaharescu, E. Burzo, L. Dumitru, I. Kleps and D. Dascalu, Romanian Academy Press, Bucharest, **2006**, pp. 132-146.
20. M.J. Betts, R.B. Russell, "Amino Acid Properties and Consequences of Substitutions". In "Bioinformatics for Geneticists", Editors: M.R. Barnes and I.C. Gray, Wiley, **2003**.
21. S. Chah, M.R. Hammond, R.N. Zare, *Chemistry & Biology*, **2005**, *12*, 323-328.
22. M. Tomoaia-Cotișel, Gh. Tomoaia, A. Mocanu, D.-V. Pop, N. Apetroaei, G. Popa, *Studia, Univ. Babeș-Bolyai, Chem.*, **2004**, *49*(2), 167-181.
23. M. Tomoaia-Cotișel, Gh. Tomoaia, V.-D. Pop, A. Mocanu, O. Cozar, N. Apetroaei, Gh. Popa, *Studia, Univ. Babeș-Bolyai, Phys.*, **2004**, *49*(3), 141-152.
24. M. Tomoaia-Cotișel, Gh. Tomoaia, V.-D. Pop, A. Mocanu, N. Apetroaei, Gh. Popa, *Rev. Roum. Chim.*, **2005**, *50*(5), 381-390.
25. M. Tomoaia-Cotișel, Gh. Tomoaia, V.-D. Pop, A. Mocanu, O. Cozar, N. Apetroaei, Gh. Popa, *Rev. Roum. Chim.*, **2005**, *50*(6), 471-478.
26. M. Tomoaia-Cotișel, V.-D. Pop, Gh. Tomoaia, A. Mocanu, Cs. Racz, C. R. Ispas, O. Pascu, O. C. Borosțean, *Studia, Univ. Babeș-Bolyai, Chem.*, **2005**, *50*(1), 23-37.
27. N.R. Jana, L. Gearheart, S.O. Obare, C.J. Murphy, *Langmuir*, **2002**, *18*, 922-927.
28. K.S. Mayya, V. Patil, M. Sastry, *Langmuir*, **1997**, *13*, 3944-3947.
29. U. Kreibitz, L. Genzel, *Surface Sci.*, **1985**, *156*, 678-700.

30. L. Xu, Y. Guo, R. Xie, J. Zhuang, W. Yang, *Nanotechnology*, **2002**, *13*, 725-728.
31. M. Tomoaia-Cotisel, "The Nanostructure Formation of the Globular Seed Storage Protein on Different Solid Surfaces Studied by Atomic Force Microscopy", In "Convergence of Micro-Nano-Biotechnologies", Series "Micro and Nanoengineering", **Volume 9**, Editors: M. Zaharescu, E. Burzo, L. Dumitru, I. Kleps and D. Dascalu, Romanian Academy Press, **2006**, Bucharest, pp. 147 - 161.
32. G. Y. Liu, N. A. Amro, PNAS, **2002**, *99*, 5165-5170.

*Dedicated to Professor Ionel Haiduc,
President of The Romanian Academy at his 70th anniversary*

CARBON PASTE ELECTRODES INCORPORATING SYNTHETIC ZEOLITES AND METHYLENE BLUE FOR AMPEROMETRIC DETECTION OF ASCORBIC ACID

CODRUTA VARODI, DELIA GLIGOR AND LIANA M. MURESAN*

ABSTRACT. Two new electrodes were obtained by incorporating two synthetic zeolites modified with Methylene Blue (MB) in carbon paste. The electrochemical behavior of the modified electrodes (MB-13X-CPEs and MB-4A-CPEs) was investigated using cyclic voltammetry and the independence of formal standard potential vs. the pH of the surrounding solution was put on evidence. The modified electrodes were successfully tested for electrocatalytic oxidation of ascorbic acid (AA) in phosphate buffer (pH 7.0), at an applied potential with more than 500 mV lower than that used on unmodified carbon paste electrodes. The amperometric sensors for ascorbic acid were characterized by a linear concentration range of 10^{-5} M - 10^{-3} M AA for MB-13X-CPEs and 10^{-5} M - 10^{-4} M AA for MB-4A-CPEs. The theoretical detection limits, calculated from the slope of the regression equation and standard deviation of the calibration curve, were 4.7×10^{-5} M for MB-13X-CPEs and 1.7×10^{-5} M for MB-4A-CPEs.

Keywords: ascorbic acid, electrocatalytic oxidation; Methylene Blue; modified carbon paste electrode.

Introduction

L-Ascorbic acid (AA), also known as Vitamin C, is an organic compound playing a key role in living bodies, being essential for the formation of bone and connective tissue, helping the absorption of iron and helping burns and wounds heal. Like vitamin E, vitamin C is an antioxidant, protecting cells against damage by free radicals, which are reactive by-products of normal cell activity. This is the reason why L-Ascorbic acid is widely used as a dietary supplement and is also added to manufacture foods as an antioxidant for preservation [1]. Consequently, measuring ascorbic acid content is very important for assessing food product quality.

Satisfactory techniques for the determination of ascorbic acid must ideally be specific, reproducible, rapid, simple and sensitive and that is why electrochemical methods have been proposed for its determination.

* "Babes-Bolyai" University, Department of Physical Chemistry, 400028 Cluj-Napoca
Corresponding author: limur@chem.ubbcluj.ro

However, electrode fabrication for routine quantitative determination presents difficulties such as low selectivity or difficult preparation [2, 3].

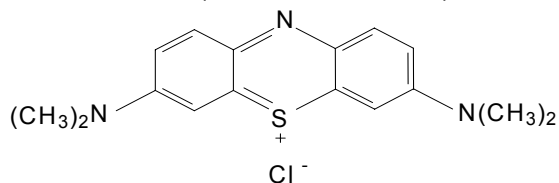
Among the new electrode materials used for ascorbic acid detection, those based on modified zeolites seem to be very attractive, since zeolites offer a number of chemical, physical and structural characteristics of high interest in the design of electroanalytical systems: shape, size and charge selectivities, physical and chemical stabilities, high ion-exchange capacity and hydrophilic character [4-7]. Moreover, zeolites present the ability to immobilize efficiently different redox mediators with electrocatalytic properties towards ascorbic acid oxidation [4, 8]. On the other hand, the well-known advantages of carbon paste (low background current, wide potential window, versatility etc.) can be exploited to obtain efficient entrapping matrices for modified zeolites.

In this context, using a highly efficient technique for zeolite immobilization in a carbon paste matrix [9], two new sensors incorporating synthetic mesoporous zeolites (4A and 13X, Aldrich) modified with Methylene Blue were designed and tested for ascorbic acid amperometric detection. Methylene Blue is a water-soluble cationic dye molecule, with a formal standard potential (E^0) of -110 mV vs. SCE [8], suitable to catalyze AA oxidation and to prevent fouling of the electrode surface by oxidation products [10].

Experimental part

Chemicals

Methylene Blue (MB) (see Scheme 1), graphite powder and paraffin oil were purchased from Fluka (Buchs, Switzerland).



Scheme 1. Structure of Methylene Blue (MB).

The 13X type zeolite, $1\text{Na}_2\text{O}:1\text{Al}_2\text{O}_3:2.8\pm 0.2 \text{SiO}_2 \times \text{H}_2\text{O}$ (particle size, 3-5 μ ; pore diameter, 10 Å; specific surface area 548.69 m²/g; bulk density 480.55 kg/m³; Si/Al ratio 1.5) and the 4A type zeolite, $1\text{Na}_2\text{O}:1\text{Al}_2\text{O}_3:2.0\pm 0.1 \text{SiO}_2 \times \text{H}_2\text{O}$ (particle size, 2-3 μ ; pore diameter, 4 Å; bulk density 480.55 kg/m³; Si/Al ratio 1) were purchased from Aldrich (Germany).

Ascorbic acid (AA) was purchased from Sigma (SUA), K₂HPO₄·2H₂O and KH₂PO₄·H₂O were purchased from Merck (Darmstadt, Germany). All other reagents were of analytical grade and used as received.

The supporting electrolyte was a 0.1 M phosphate buffer solution. The pH was adjusted in the interval 1-9 using appropriate H₃PO₄ or NaOH solutions.

Electrode preparation

50 ml of a 0.001 % (w/v) MB solution in water were shaken (3 days) with 50 mg 13X type and 4A type zeolite. The modified zeolite was filtered, washed and dried. 25 mg of the modified zeolite were mixed with 25 mg graphite powder and 10 μ l paraffin oil in order to obtain the modified carbon paste electrodes (MB-13X-CPEs and MB-4A-CPEs).

The preparation of MB-13X-CPEs and MB-4A-CPEs was reproducible when the experimental conditions and variables were maintained constant during the preparation period. The current response of the electrodes did not change significantly by storing them in air for several months.

Electrochemical measurements

Electrochemical experiments were carried out using a typical three-electrode electrochemical cell. The modified carbon paste electrode was used as working electrode, a platinum ring as counter electrode and an Ag|AgCl/KCl_{sat} as reference electrode.

Cyclic voltammetry experiments were performed on a PC-controlled electrochemical analyzer (Autolab-PGSTAT 10, EcoChemie, Utrecht, The Netherlands).

Batch amperometric measurements at different AA concentrations were carried out at an applied potential with 120 mV more positive than formal standard potential ($E^{0'}$) of the mediator, under magnetic stirring, using 0.1 M phosphate buffer solution (pH 7) as supporting electrolyte. The current-time data were collected using the above-mentioned electrochemical analyzer.

For each electrode, the surface coverage (Γ , mol cm⁻²) was estimated from the under peak areas, recorded during the cyclic voltammetry (CV) measurements at low potential scan rate ($v \leq 10$ mV s⁻¹) [11] and considering the number of transferred electrons equal to 2 [12, 13].

The experimental results are the average of at least 3 identically prepared electrodes, if not otherwise mentioned.

Results and discussions

Electrochemical characteristics of MB-Z-CPEs

The carbon pastes incorporating unmodified zeolites (4A-CPEs and 13X-CPEs) do not exhibit any redox activity in the potential range from -800 at +410 mV vs. Ag|AgCl/KCl_{sat} (results not shown). When MB is immobilized onto the synthetic zeolites, a well-defined peak pair was observed on the cyclic voltammograms, with the formal standard potentials ($E^{0'}$) at -175 mV and -195 mV vs. Ag|AgCl/KCl_{sat} for MB-13X-CPEs and MB-4A-CPEs, respectively (Figure 1). The peak pair was attributed to the oxidation / reduction of MB. The small positive shift of $E^{0'}$ for MB-Z-CPEs in comparison with the value observed for MB in solution (-230 mV vs. SCE)

[14] gives evidence that the reduced form of the dye interacts much more strongly with the matrix than the oxidized form does [15]. It should be mentioned that a small additional wave around 400 mV vs. Ag|AgCl/KCl_{sat} also appears, reflecting the existence of a second form of MB bound to the synthetic zeolites [10]. This wave is more visible when zeolite 4A is used.

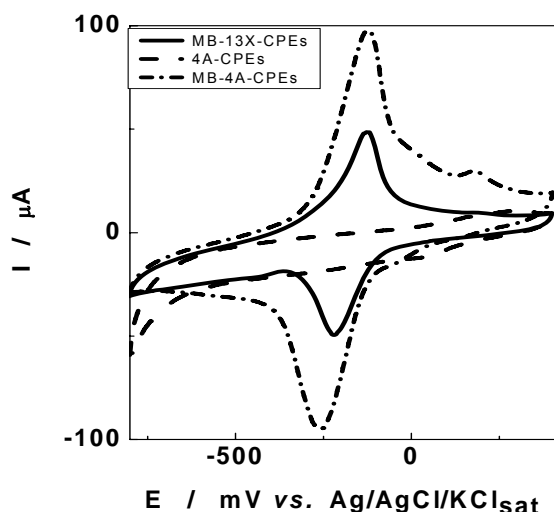


Figure 1. Cyclic voltammograms for 4A-CPEs, MB-13X-CPEs and MB-4A-CPEs. Experimental conditions: starting potential, -800 mV vs. Ag|AgCl/KCl_{sat}; potential scan rate, 10 mV s⁻¹; supporting electrolyte, 0.1 M phosphate buffer, pH 7.0.

The peak separations for the main peak, ΔE_p , were found to be 90 and 136 mV for MB-13X-CPEs and MB-4A-CPEs, respectively, and increases with the scan rate (results not shown) indicating a quasi-reversible redox process for both modified electrodes. This is an indication that the kinetic of electron transfer on the electrode surface is not very fast, as consequence of the nature of the matrix, whose resistance is considerable [8].

Since it is well known that the redox potential of MB in solution phase is strongly dependent on the pH, the study of pH influence on the electrochemical behavior of MB-Z-CPEs is of great interest [8]. Figure 2 presents the dependence of formal standard potential on the pH of the supporting electrolyte. Surprisingly, the slopes of these dependencies are very small (only 5 mV/ Δ pH and 2 mV/ Δ pH for MB-13X-CPEs and MB-4A-CPEs, respectively). These results may suggest that the amino groups of

MB at positions 3 and 7 as well as the heterocyclic nitrogen are very strongly involved in the binding to zeolite and as a result, the pH of the solution does not affect E^0 . The cause for the independence of E^0 towards pH variation could be the adsorption of MB into the channels of the synthetic zeolites in a confined position and the acidity of the environment surrounding the dye, which does not change with the solution pH.

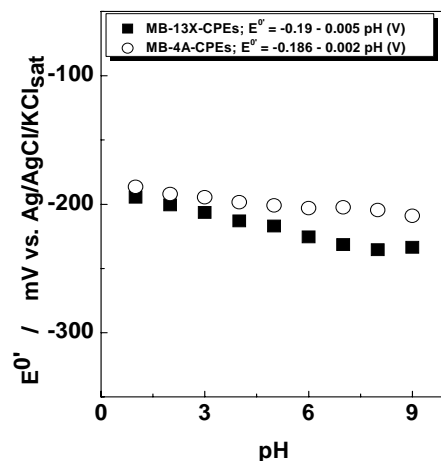


Figure 2. Variation of E^0 with pH for MB-13X-CPEs and MB-4A-CPEs. Experimental conditions: starting potential, -800 mV vs. Ag|AgCl/KCl_{sat}; potential scan rate, 50 mV s⁻¹; supporting electrolyte, 0.1 M phosphate buffer.

Electrocatalytic oxidation of ascorbic acid

The cyclic voltammograms recorded in 0.1 M phosphate buffer pH 7 at MB-13X-CPEs and MB-4A-CPEs in the presence of different concentrations of AA are depicted in Figure 3. As it can be observed, when AA is present, the anodic peak current of the main voltammetric wave practically does not change, while for the smallest, but more positive wave (at around 250 mV vs. Ag|AgCl/KCl_{sat}.) the current strongly increases, reflecting the influence of the thermodynamic driving force on the efficiency of the electrocatalytic reaction [10]. Moreover, a new peak appears at about 0 mV vs. Ag|AgCl/KCl_{sat}, which could be ascribed to the AA electro-oxidation on the zeolite modified electrodes. This is supported by the fact that the peak is also present, even if much less developed, on 4A-CPEs and 13X-CPEs (see inset in Figure 3). The anodic peak current increases significantly and the oxidation potential is much lower than that recorded on unmodified carbon paste (+490 mV vs. SCE [10]).

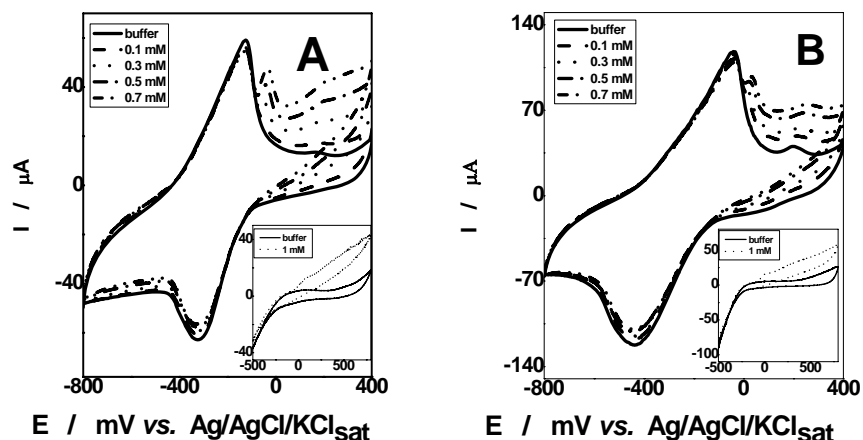
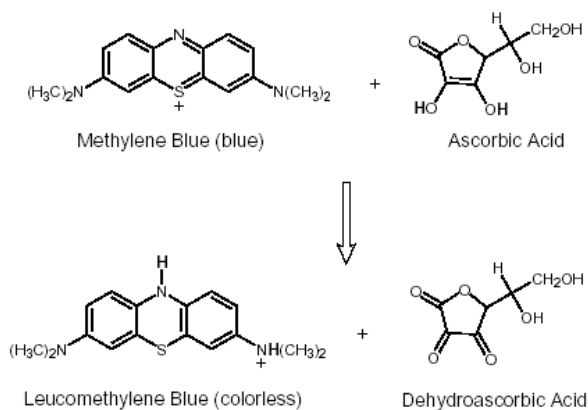


Figure 3. Cyclic voltammograms obtained at MB-13X-CPEs and 13X-CPEs (inset) (A) and MB-4A-CPEs and 4A-CPEs (inset) (B), in the absence and in the presence of different concentrations of AA. Experimental conditions: potential scan rate, 10 mV s^{-1} ; starting potential, $-800 \text{ mV vs. Ag/AgCl/KCl}_{\text{sat}}$; supporting electrolyte, 0.1 M phosphate buffer, $\text{pH } 7.0$.

The reaction at the electrode-solution interface and into the electrode can be written as follows [16]:



Scheme 2. Methylene blue reduction by ascorbic acid.

Figures 4A and 4B present the calibration curves for AA. The inset of these figures display current-time recordings obtained at MB-13X-CPEs and MB-4A-CPEs for successive injections of 0.1 mM AA when the applied potential was -50 mV vs. Ag|AgCl/KCl_{sat}. The curve was fitted by the equations: for MB-13X-CPEs, $I = 3.1 \times 10^{-4} (\pm 0.2 \times 10^{-4})[AA] / [AA] + 3.8 \times 10^{-2} (\pm 0.003)$, with a correlation coefficient R^2 of 0.999 for $n = 28$, and for MB-4A-CPEs, $I = 1.4 \times 10^{-4} (\pm 1.42 \times 10^{-6})[AA] / [AA] + 9.17 \times 10^{-3} (\pm 1.6 \times 10^{-4})$, with a correlation coefficient R^2 of 0.999 for $n = 59$, where I is the current in A and $[AA]$ is the ascorbic acid concentration in mol l⁻¹. The reproducibility of the electrocatalytic effect of MB-Z-CPEs was confirmed by repetitive amperometric measurements (~ 3 measurements).

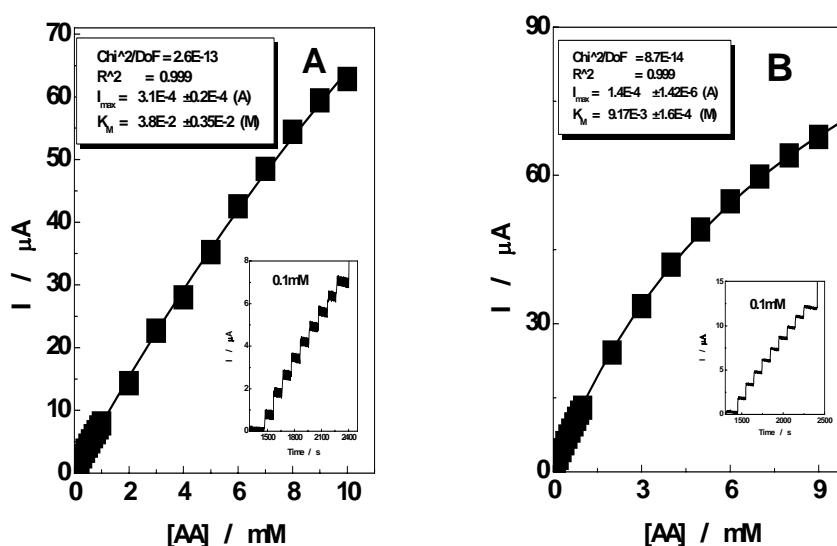


Figure 4. Calibration curves at MB-13X-CPEs (A) and MB-4A-CPE (B) and amperometric response to successive increments of 0.1 mM AA (inset). Experimental conditions: applied potential, -50 mV vs. Ag|AgCl/KCl_{sat}; rotation speed, 500 rpm; supporting electrolyte, 0.1 M phosphate buffer, pH 7.0.

Both modified electrodes exhibit a short current time response (5s) and can act as AA sensors. As can be observed, the relationship between the steady-state current and the concentration of AA was linear in the range from 10^{-5} M to 10^{-3} M AA for MB-13X-CPEs and 10^{-5} M to 10^{-4} M AA for MB-

4A-CPEs. The theoretical detection limits, calculated from the slope of the regression equation and standard deviation of the calibration curves were 4.7×10^{-5} M for MB-13X-CPEs and 1.7×10^{-5} M for MB-4A-CPEs (Table 1).

Table 1.
Analytical parameters corresponding to amperometric sensors for AA.

Electrode	Detection limit (M)	Sensitivity (A / M)	Linear concentration range (M)	R/N	Log I vs. Log c	
					slope	R/N
MB-13X-CPEs	4.7×10^{-5}	8×10^{-3}	$10^{-5} - 10^{-3}$	0.999/20	0.90	0.999/28
MB-4A-CPEs	1.7×10^{-5}	11×10^{-3}	$10^{-5} - 10^{-4}$	0.987/ 11	0.88	0.997/28

As can be seen, the slope of Log I vs. Log c dependence is close to 1, proving the existence of kinetic control.

The analytical parameters of the MB-zeolite modified carbon paste electrodes are in accordance with those obtained for other electrodes used as amperometric sensors for AA reported in the literature (Table 2).

Table 2.
Analytical parameters for different modified electrodes reported as amperometric sensors for AA.

E_{app} (mV vs. Ag AgCl/KCl _{sat})	Electrode	pH / solution	Detection limit (M)	Linear range (M)	Ref.
+ 550	Fe ³⁺ /Y/ZCME	6.8 /PhB	1.5×10^{-6}	1.58×10^{-6} - 2.15×10^{-2}	[17]
+ 200	Mordenite-MB-CP/ GC	6.2 /PhB.	1.2×10^{-5}	2×10^{-5} - 8×10^{-4}	[8]
+ 100	ZrP-MB-CP	7 /PhB	10^{-6}	10^{-6} - 4×10^{-5}	[10]
- 40	GC	10 /AB+ MB (2.5×10^{-5} M)	1.1×10^{-6}	1.2×10^{-6} - 1.12×10^{-3}	[18]

PhB = phosphate buffer; AB = ammonia buffer; GC = glassy carbon; ZrP = zirconium phosphate.

Conclusions

Two new electrodes based on synthetic mesoporous zeolites modified with MB incorporated in carbon paste were obtained and characterized. These

modified electrodes presented good electrocatalytic effect towards ascorbic acid oxidation in neutral aqueous solution, at an overpotential with more than 500 mV lower than that observed on unmodified electrodes. The MB-Z-CPEs offer the advantages of easy fabrication and cleaning, fast response time, high sensitivity, a low background current and detection limit, which are suitable for routine determinations.

REFERENCES

1. J. C. Bauernfeind, D. M. Pinkert, "Ascorbic Acid as an Added Nutrient to Beverage", Hoffmann-La Roche, Basel, **1970**, 24–28.
2. G. M. Greenway, P. Ongowo, *Analyst*, **1990**, *115*, 1297–1301.
3. G. C. B. Fernandes, L. T. Kubota, G. de Oliveira Neto, *Analytica Chimica Acta*, **1999**, *385*, 3–12.
4. A. Walcarius, *Analytica Chimica Acta*, **1999**, *384*, 1-8.
5. D. R. Rolison, R. J. Nowak, T. A. Welsh, C. G. Murray, *Talanta*, **1991**, *38*, 27-35.
6. J. Lipkowski, P. Ross, "The Electrochemistry of Novel Materials", VCH Publishers Inc., New York, **1994**.
7. A. Walcarius, *Electroanalysis*, **1996**, *8*, 971-986.
8. M. Arvand, Sh. Sohrabnezhad, M. F. Mousavi, *Analytica Chimica Acta*, **2003**, *491*, 193-201.
9. J. P. Pereira-Ramos, R. Messina, J. Perichon, *Journal of Electroanalytical Chemistry and Interfacial Electrochemistry*, **1983**, *146*, 157-169.
10. Y. Dilgin, Z. Dursun, G. Nisli, L. Gorton, *Analytica Chimica Acta*, **2005**, *542*, 162-168.
11. H. Huck, *Physical Chemistry Chemical Physics*, **1999**, *1*, 855-859.
12. B. Liu, Z. Liu, D. Chen, J. Kong, J. Deng, *Fresenius Journal of Analytical Chemistry*, **2000**, *367*, 539-544.
13. C. Lei, Z. Zhang, H. Liu, J. Kong, J. Deng, *Analytica Chimica Acta*, **1996**, *332*, 73-81.
14. L. T. Kubota, L. Gorton, *Electroanalysis*, **1999**, *11*, 719-728.
15. C. A. Pessoa, Y. Gushikem, L. T. Kubota, L. Gorton, *Electroanalysis*, **1997**, *9*, 800-803.
16. S. Mowry, P. J. Ogren, *Journal of Chemical Education*, **1999**, *76*, 970-973.
17. Y. Jiang, M. Zou, K. Yuan, H. Xu, *Electroanalysis*, **1999**, *11*, 254-259.
18. A. A. Ensafi, *Analytical Letters*, **2003**, *36*, 591-604.

CODRUTA VARODI, DELIA GLIGOR AND LIANA M. MURESAN

*Dedicated to Professor Ionel Haiduc,
President of The Romanian Academy at his 70th anniversary*

METALLOGRAMS OF SIALOCONCREMENTS WITH METABOLIC AND NUTRITIONAL ASPECTS NOTE I. ALKALINE AND ALKALINE-EARTH METALS

**ZENO GÂRBAN¹, GABRIELA GÂRBAN², ILIE VASILUȚĂ³, LUDOVIC
SAYTI⁴, MIHAELA PUP⁵, GEORGE-DANIEL GHIBU⁵**

ABSTRACT. Investigations concerning the biogenesis of various concretions are of interest for biochemistry and pathobiochemistry (by the induced homeostatic disturbances); pathophysiology (by their composition and mechanism of formation, i.e. precipitative and / or co-precipitative processes) and morphopathology (due to their localization).

From an anatomic point of view, lithiasis presents numerous localizations, the most important ones being the urolithiasis, cholelithiasis and the sialolithiasis.

Our investigations were performed on a number of 23 salivary calculi (extracted surgically) and the metallogram of the alkaline and alkaline-earth metals was obtained. For this purpose by atomic absorption spectroscopy (AAS) the concentrations of some alkaline (Na, K), alkaline-earth metals (Ca, Mg) were determined. The obtained results revealed that the highest quantities of metals have been in the case of alkaline-earth metals (in the relation Ca>Mg) and alkaline metals (in the relation Na>K) – values expressed in mg/g calculus.

Keywords: salivary calculi, alkaline and alkaline-earth metals

Introduction

Saliva is a complex fluid produced by a number of specialized glands which discharge into the oral cavity of the glands of mammalian vertebrates. Most of the saliva is produced by the major salivary glands (parotid,

¹ Department of Biochemistry and Molecular Biology, Faculty of Food Products Technology, University of Agricultural Science and Veterinary Medicine of Banat Timișoara, Calea Aradului Nr. 119, RO-300.657, Timișoara, Roumania. E-mail: zgarban@yahoo.com

² Institute of Public Health Timișoara, Blvd. Dr. V.Babeș Nr. 16, RO-300 226 Timișoara, Roumania

³ University Clinic of Maxilo-Facial Surgery, Faculty of Dentistry, University of Medicine and Pharmacy Timișoara, Blvd. Tache Ionescu Nr. 5 , RO-300 062 Timișoara, Roumania

⁴ Institute of Chemistry of the Roumanian Academy, Timișoara, Blvd.M .Viteazul Nr. 24, RO-300 223, Timișoara, Roumania

⁵ Faculty of Chemistry and Environmental Engineering, University Politehnica Timișoara, Pta Victoriei, Nr.2 RO-300 006 Timișoara, Roumania

submandibular, and sublingual), but a small contribution is made by the numerous small labial, buccal, and palatal glands which line the [1- 4].

Saliva is a viscous, colorless and opalescent fluid having a pH value around 6.2 which, in the presence of air, may become more acid [5]. Under microscope, the saliva shows nucleated squamous cells from the oral lining, disintegrating leucocytes and gland cells, as well as a large variety of microorganisms. Saliva is the watery fluid containing 98% water and many important substances, including electrolytes (cationic such as Na, K, Ca, Mg, Cu and anionic: P, Cl, I, F) , mucus, antibacterial compounds and various enzymes [6]. In the presence of carbon dioxide or by bacterial action salivary constituents can precipitate and their deposition takes place on the teeth as tartar or as calculi in the salivary ducts [7]. At the level of salivary glands, especially of salivary ducts, crystals with the specificity of lithiasis and sometimes even concrements can be produced. These are known as salivary lithiasis (sialolithiasis). Biogenesis of salivary calculus similar to renal and biliary calculi [8, 9] starts from the heterogeneous nucleation principles. In nucleation an important role is played by the organic compounds which, generally, define the type of sialolithiasis, and the inorganic compounds which are especially metallic ions. In the first phase crystallization nuclei are formed which often are called “primers” or “starters” of the lithogenic process [10]. Literature data in the domain discuss about microliths [11, 12]. Microliths are visible only at the microscope and are considered to simply be evolutive/intermediary forms between starters and calculus.

Materials and methods

Analytical investigations were made on surgically obtained salivary calculi. The sialoconcrements were mainly extracted from the level of submandibular glands and their ducts. Salivary calculi were collected from the Clinic of maxilo-facial surgery in a period of 10 years. Sizes of concrements were 3-11 mm. After the obtainment, calculi were washed repeatedly with distilled water, desiccated and thereafter powdered.

The purpose of the investigations was to measure the concentrations of the main alkaline (Na, K), alkaline-earth (Ca, Mg) metals. In our investigations we have determined biometals from the group of alkaline metals Na, K, alkaline-earth metals Ca, Mg and trace elements Zn, Cu, Mn. Also we have determined some elements with toxic potential Pb, Cd, Al, Cr [13]. In the present “report” are presented the results referring only to the alkaline and alkaline-earth metals.

Analytical determinations were made by atomic absorption spectroscopy (AAS) method. It was used successively a Pye-Unicam - Series 1900 apparatus and an Analyst-100 apparatus produced by Perkin Elmer.

Obtained data were statistically evaluated, determining the mean value (X) and the standard deviation (SD).

Results and discussions

Saliva, like other body fluids, is a dilute aqueous fluid containing both electrolytes and protein with an osmolality less than or equal to that of plasma [14]. Also present in saliva is a certain amount of cell debris arising from the epithelial cells of the mouth together with food residues [15]. The osmolality is principally determined by the type of gland and by secretory activity, whose degree is affected by many factors including sex, age, nutritional or emotional state, season of the year [16, 17], darkness and a variety of diseases and many pharmacological agents.

The total volume of saliva produced each day in adults is 500 to 1500 ml [18]. Mixed saliva consists mainly of the secretions of submandibular (65%), parotid (23%), and sublingual (4%) glands, the remaining 8% being provided by the minor numerous glands [15]. These proportions are a function of the type, intensity and duration of stimulation. The important stimulus for secretion is the presentation and ingestion of food; the quantity and quality of the secretion vary with the nature of nutrition.

Systematic studies on the composition of sialolithiasis with specific analytical investigations for that period were related in 1938 by Lock and Murray [19].

Between the organic components that are found more frequently in sialolithiasis one can mention the presence of phosphates, carbonates, cholesterol, urates. In order to evidence these substances various chemical and physico-chemical methods are used. For practical considerations, the infrared spectroscopy was more often utilized.

In general, saliva contains the usual electrolytes of the body fluids, the principal ions being sodium, potassium, chloride and bicarbonate. The acinar cells forming the secretory endpiece of the salivary gland actively pump sodium ions from the blood into the lumen of the endpiece. The resulting osmotic pressure difference between the blood and the fluid in the endpiece causes water to flow from the blood, through the tight junctions between the acinar cells, and into the lumen of the endpiece. Thus, the primary secretion (as it leaves the endpiece) is thought to be almost isotonic with plasma [20].

The initial fluid moves down the ductal system of the salivary gland and, an energy-dependent transport process reabsorbs sodium and chloride. Potassium, bicarbonate and lithium ions are actively secreted into saliva. However, the ductal membranes are relatively impervious to water, so the resulting saliva becomes increasingly hypotonic as it moves down the ductal system [21]. Data referring to the composition of saliva are compiled from literature after Altman and Dittmer [22, 23] – see Table 1.

Table 1.
Chemical composition of saliva - inorganic substances

Component		UM	Saliva (sample)	Average	Range
Cations	Ca total	mg / dL	Mixed	5.80	5.2 – 9.7
			Submaxillary	8.80	4.4 – 13.1
			Parotid	3.50	2.1 – 6.7
	Co	µg / dL	Mixed	2.44	0 – 12.53
	Cu	µg / dL	Mixed	31.70	5.0 – 76.0
	Mg	mg / dL	Mixed	0.50	0.15 – 0.93
Anions	K	mg / dL	Mixed	80.3	56 - 148
	Na	mg / dL	Mixed	23.2	8 – 56
	Cl	mEq / L	Mixed	15.5	8.4 – 17.7
	F	mEq / L	Mixed		0 – 0.005
	I	µg / dL	Parotid	6.46	
			Submaxillary	3.65	
	P total	mg / dL	Mixed	20.40	
	P anorg	mg / dL	Mixed	14.90	7.4 – 21.1
P org	mg / dL	Mixed	5.50		
Bicarbonate	mEq / L	Mixed	6.44	3.48 – 10.70	

Salivary glands lithiasis (sialolithiasis) is the most common disease of the major salivary glands after mumps and accounts for approximately 30% of all salivary disorders and about 0.01-1.0% of the population is held to be affected, with a higher incidence in males aged between 30 and 60 years.

Metallograms of sialoconcrements may offer important data for the biochemistry, physiology and physiopathology of lithogenic processes and can be used as a clinical guideline in dentistry [7, 24].

In the present study the concentrations of alkaline (Na, K), alkaline-earth (Ca, Mg) were determined. The obtained results are given in table 2.

Table 2.
Concentration of the main alkaline and alkaline-earth metals

Speci- fication	UM	Nr. of calculi	Concentration X + SD	Range of concentration
Na	mg/g	23	4 843.21 ± 1 071.16	3 170 – 8 750
K		23	518.74 ± 88.31	320 – 710
Ca		23	227 293.00 ± 50 193.12	154 250 – 221 400
Mg		23	1 185.93 ± 329.84	920 – 2 150

Metabolism of calcium and magnesium is conditioned by the quantity of micronutrients (minerals and vitamins – especially vitamins D) in the consumed food and influenced by thyro-parathyroid hormones. In this

context we mention that parathyroid hormone increases blood calcium level while calcitonine (thyrocalcitonine) lowers blood-calcium level

The most common localization is the submandibular gland where 92% of calculi are found, the duct being more frequently affected than the parenchyma. The parotid gland is affected in 6% of cases. The sublingual gland is affected in 2% of cases and other minor salivary glands in another 2%.

Sialoliths are concrements detectable only microscopically in the ductal system of the salivary glands. They contain calcium and phosphorus with formation of hydroxylapatite crystals as well as organic secretory material in granulated form and necrotic cellular residues.

The chemical composition of the sialoliths varies from one gland to another. Calculi generally consist of a mixture of different calcium phosphates (mainly hydroxy-apatite and carbonate-apatite) together with an organic matrix [25-28]. Submandibular gland stones tend to have higher concentrations of calcium, which explains why 85% of submandibular stones are visible on x-ray, whereas only 15% of parotid duct stones are visible.

Despite the relative frequency of sialolithiasis, current research has not led to definitive conclusions about the exact cause of sialolith formation. Several theories have been proposed to explain the development of sialoliths.

One early theory suggested that sialoliths resulted from disturbances in the secretion and precipitation of the components of the saliva as a result of inflammatory processes within the salivary gland [2, 12]. A later theory proposed that specific changes in the structure of the organic molecules in saliva allowed the formation of a supportive frame for calcium crystals [12, 29]. By contrast, Rauch [12, 30], was of the view that the primary precipitation was of minerals, upon which the organic substances later accumulated. Another theory explains the formation of sialoliths as a metabolic disturbance, caused by the alkalinity of bicarbonate and the precipitation of calcium phosphates [12,31].

Due to the fact that sialoliths appear mainly in a single gland, especially the submandibular gland, the local factors (morpho-anatomic such as: salivary duct stenosis, salivary duct diverticuli, etc.) for development of sialoliths are etiologically significant.

Disturbed salivary secretion and a change in the composition of saliva (high supersaturation, crystallization inhibitor deficit, etc.), which is called dyschylia, can lead to an increase in salivary viscosity and to a mucous obstruction in the terminal ducts of the salivary gland [11, 12, 32].

Studies on animal models showed that microliths are generated due to autophagocytosis of organelles that are rich in calcium. The accumulation of organic substances, especially of glycoproteins with higher calcium affinity, and mineralization of the organic matrix in the ductal system, is the most important phase of lithogenesis [12]. Mineralization is supported by accumulation of

calcium and an increase in pH, which then decreases the solubility of the calcium phosphates in saliva

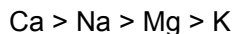
Usually treatment of salivary lithiasis means surgical intervention and, in the last decade, lithotripsy procedures based on treatment with ultrasounds.

Nowadays, the first choice treatment of salivary gland stones is shock wave lithotripsy, because it is considered a non-invasive and successful treatment with low risk [33].

Sialolithogenesis is related to the biochemical homeostasis variations which must be correlated with the nutrients intake and also with metabolic disturbances generated by the presence of infections, the appearance of antibodies and salivary ducts anatomic anomalies. These kinds of situations facilitate the stagnation of secretions and, in time, the initiation of heterogeneous nucleation process.

Conclusions

1. Metallograms of sialoconcrements evidenced the decrease of concentration in the successive series for alkaline and alkaline-earth metal bioelements:



2. Data referring to metal composition of sialoconcrements are of importance for physiopathology and is a veritable guideline for the dentistry clinic for the prophylaxy and metaphylaxy of sialolithiasis. We note that our results differ slightly from other analyses published in the field (e.g., Ref. [34], reporting a somewhat larger concentration for Ca), which opens up a discussion on the origin and nature of such differences (with instrumental methods as well as patient-related factors bound to be investigated). Such aspects constitute the focus of further research from our part.

REFERENCES

1. W. R. Amberson, R. Höber, *J Cell. Comp. Physiol.*, **1932**, 2, 201.
2. A.C. Furstenberg, *JAMA*, **1948**, 136, 1-4.
3. J. G. Van Dam, A.C. Van Loenen, *Pharmaceutisch Weekblad*, **1978**, 113, 65.
4. R.F. Vining, R.A. McGinley, "Transport of steroids from blood to saliva", pp. 56-63, in *Immunoassays of steroids in saliva* (Eds. G. F. Read, D. Riad-Fahmy, R. F. Walker, K. Griffiths), Cardiff, Alpha Omega Publ. Ltd, **1982**.
5. W.F. Ganong, "Review of Medical Physiology", 17th edition, Lange Medical Book, Norwalk, CT., **1995**
6. Z. Garban, Gabriela Garban, "Nutriția umană, Vol. I, Probleme fundamentale", ediția 2-a, Editura Orizonturi Universitare, Timișoara, **2003**.

7. I.Vasiluță, Z. Garban, Mihaela Pup, Gr. Sigartău, „Investigations concerning the metallic composition of the surgically removed sialoconcrements”, pp.309-312, in *Metal Elements in Environment, medicine and Biology* (Eds. Z. Garban, P. Drăgan), Tome IV, Publishing House Eurobit, Timișoara, **2000**.
8. P. Drăgan, Z. Garban, D. Ciubotariu, Șt. Holban, Elena Giurgiulescu, *Baki.Hamaabada - Israel J. Clin. Biochem. and Lab. Sci.*, **1985**, 4, 12.
9. Monica Leal Alcure, P.A. Vargas, J. Jorge Jr., O. di Hipolito Jr., M.A. Lopes, “Clinical and histopathological findings in sialoliths”, *Brazil. J. Oral Sci.*, **2005**, 4, 899.
10. Z. Garban, P. Drăgan, Gisela Nemeș, Gabriela Daranyi, Doina Popeti, Livia Martoni, „Considerations on the metal composition of the calculi in urolithiasis”, p.81, in *Meeting of the Federation of European Biochemical Sciences: Metal Ions, Proteins and Membranes, Abstracts Volume*, Algarve, April 21-26, **1985**.
11. G.H. Nacollas, M.A.S. Johnsson, *Adv. Dent. Res.*, **1994**, 8, 307.
12. A.Teymooatash, Anette Ramamswamy, J.A. Wemer, *J. Oral. Sci.*, **2003**, 45, 233.
13. Gabriela Garban, Unpublished data
14. J. W. Paxton, “Measurement of drugs in saliva: A review”, *Methods and Findings in Experimental and Clinical Pharmacology*. **1979**, 1, 11.
15. B. Caddy, “Saliva as a specimen for drug analysis”. Vol.1, pp 198-254, In *Advances in analytical toxicology* (Ed. R. C. Baselt), Foster City, Biomedical Publications, **1984**.
16. I.D. Mandel, *J. Dent. Res.*, **1974**, 53, 246.
17. I.L. Shannon, R.P. Suddick, F.J. Dowd Jr., “Monographs in oral science. Saliva: composition and secretion”, Vol. 2, Basel, Karger S., **1974**.
18. C. Lentner (Ed.), “Geigy scientific tables”, Vol.1, 8th edition, Basel, Ciba Geigy, **1981**.
19. Gertrude E. Glock, Margaret M. Murray, *J. Dent. Res.*, **1938**, 17, 257.
20. H.W. Davenport, “Salivary secretion”, pp. 85-94, In *Physiology textbook series. Physiology of the digestive tract: an introductory text* (Ed. H. W. Davenport), 4th edition, Chicag, Year Book Medical Publishers, **1977**.
21. E. D. Jacobson, “Salivary secretion”, pp. 46-54, in *Gastrointestinal physiology* (Ed. L. R. Johnson), 2nd edition, St. Louis, C.V. Mosby Co., **1981**.
22. P.L. Altman, Dorothy S. Dittmer (Eds.), “Biological Handbooks-Metabolism”, Federation of American Societies for Experimental Biology, Bethesda, Maryland, **1968**.
23. P.L. Altman, Dittmer S.Dorothy (Eds.), “Biological Handbooks – Biology Data Book”, Vol. III, 2nd edition, Federation of American Societies for Experimental Biology, Bethesda, Maryland, 1974.
24. I.Yamamoto, M. Itoh, S. Tszukada, I. Arimatsu, M. Kitawo, *Med. Biol.*, **1984**, 108, 361.
25. F. Grases, C. Santiago, B.M.Simonet, A. Costa-Bauza, *Clin Chim Acta*, **2003**, 334, 131.
26. Z. Garban, “Biochimie: Tratat comprehensiv”, Vol. 1, ediția 2-a, Ed. Didactică și Pedagogică R.A., București, **1999**.
27. T. Austin, J. Davis, T. Chan, “Sialolithiasis of submandibular gland”, *J. Emerg. Med.*, **2004**, 26, 221.

28. F. Ottaviani, P. Capaccio, R. Rivolta, P. Cosmacini, L. Pignataro, D. Castagnone, *Radiology*, **1997**, *204*, 437.
29. J.A. Harrill, J.S. King, W.H. Boyce, *Laryngoscope*, **1959**, *69*, 481-492
30. S. Rauch, "Die Speicheldrüsen des Menschen", Georg Thieme Verlag, Stuttgart, **1959**.
31. I.M. Blatt, "Studies in Sialolithiasis: III. Pathogenesis, diagnosis and treatment", *South. Med. J.*, **1964**, *57*, 723.
32. W.J. Marshall, S.K. Bangert, „Clinical Biochemistry – metabolic and clinical aspects“; Churchill – Livingstone-New York–Edinburgh–London–Madrid–Melbourne–San Francisco–Tokyo, **1995**.
33. W. Kater, R. Rahn, W.W. Meyer, D. Liernan, T. Wehrmann, „Ambulante excorporale Stosswellenlithotripsie von Speichelsteinen als neues nichinvasives Behandlungskonzept“, *Dtsch. Z. Mund Kiefer Gesicht Chir.* **1990**, *14*, 216
34. J Rabinowitz, E. Korostoff, D.W. Cohen, S. Orlean, *J Dent Res* 1969, *48*, 1216-1218.